Relaxation-induced flow in a smooth fracture for Ellis rheology

Advances in Water Resources

Relaxation-induced flow in a smooth fracture for Ellis rheology

--Manuscript Draft--

Manuscript Number:	ADWR-D-21-00036R1
Article Type:	Research Paper
Keywords:	hydraulic fracturing; Non-Newtonian; Ellis rheology; elastic wall; backflow
Corresponding Author:	Valentina Ciriello, Prof. University of Bologna Bologna, ITALY
First Author:	Valentina Ciriello, Prof.
Order of Authors:	Valentina Ciriello, Prof.
	Alessandro Lenci
	Sandro Longo, Prof.
	Vittorio Di Federico, Prof.
Abstract:	Hydraulic fracturing is a process aimed at improving the productivity of oil, gas or geothermal reservoirs. During hydrofracturing, backflow follows injection and represents the second phase of the process, when part of the fracturing fluid returns from fractures to well, and from well to surface. A conceptual model is presented to grasp the essential features of the phenomenon, conceiving the draining subsurface domain as a planar and rigid fracture. Backflow against an outlet pressure in the injection well is induced by the relaxation of the fracture wall, exerting a force on the fluid proportional to h^λ, with h the time-variable aperture and λ a non-negative exponent; an overload on the fracture may contribute to slowing or accelerating the closure process. The fluid rheology is described by the three-parameter Ellis constitutive equation, well representing the shear-thinning rheology typical of hydrofracturing fluids and coupling Newtonian and power-law behaviour. The interplay between these tendencies is modulated by a dimensionless number N encapsulating most problem parameters; the range of variation of N is discussed and found to vary around unity. The time-variable aperture and discharge rate, the space-time variable pressure field, and the time to drain a specified fraction of the fracture volume are derived as functions of geometry (length and initial aperture), wall elastic parameters, fluid properties, outlet pressure p_e and overload f_0. The late-time behaviour of the system is practically independent from rheology as the Newtonian nature of the fluid prevails at low shear stress. In particular, aperture and discharge scale asymptotically with time as $t^{-1/(\lambda+2)}$ and $t^{-1/(\lambda+3)}$ for $p_e-f_0=0$; else, the aperture tends to a constant, residual value proportional to $(p_e-f_0)^\lambda$. A case study with equally spaced fractures adopting realistic geometric, mechanical and rheological parameters is examined: two fluids normally used in fracking technology show completely different behaviours, with backflow dynamics and drainage times initially not dissimilar, later varying by orders of magnitude.
Suggested Reviewers:	Ivan C. Christov Purdue University School of Mechanical Engineering christov@purdue.edu
	Daniel M. Tartakovsky Stanford University tartakovsky@stanford.edu
	Clément Roques Université Rennes 1 clement.roques@univ-rennes1.fr
	Xiuyu Liang SUSTECH liangxy@sustc.edu.cn

	Walter Illman University of Waterloo willman@uwaterloo.ca
Response to Reviewers:	Dear Editor: We would like to thank you, the anonymous Reviewer and the Associate Editor for the positive assessment of our work and for the suggestions, which have helped us to further improve the presentation. Our detailed response to the Reviewer is given in a separate file. Her/his comments are reproduced in italic. The corresponding changes in the manuscript are typeset in blue. Sincerely yours, Valentina Ciriello Alessandro Lenci Sandro Longo Vittorio Di Federico

Relaxation-induced flow in a smooth fracture for Ellis rheology

Valentina Ciriello[a], Alessandro Lenci[a], Sandro Longo[b], Vittorio Di Federico[a]

[a] *Dipartimento di Ingegneria Civile, Chimica, Ambientale e dei Materiali (DICAM), Università di Bologna, Bologna (Italy)*
[b] *Dipartimento di Ingegneria e Architettura (DIA), Università di Parma, Parma, Italy*

Abstract

Hydraulic fracturing is a process aimed at improving the productivity of oil, gas or geothermal reservoirs. During hydrofracturing, backflow follows injection and represents the second phase of the process, when part of the fracturing fluid returns from fractures to well, and from well to surface. A conceptual model is presented to grasp the essential features of the phenomenon, conceiving the draining subsurface domain as a planar and rigid fracture. Backflow against an outlet pressure in the injection well is induced by the relaxation of the fracture wall, exerting a force on the fluid proportional to h^λ, with h the time-variable aperture and λ a non-negative exponent; an overload on the fracture may contribute to slowing or accelerating the closure process. The fluid rheology is described by the three-parameter Ellis constitutive equation, well representing the shear-thinning rheology typical of hydrofracturing fluids and coupling Newtonian and power-law behaviour. The interplay between these tendencies is modulated by a dimensionless number N encapsulating most problem parameters; the range of variation of N is discussed and found to vary around unity. The time-variable aperture and discharge rate, the space-time variable pressure field, and the time to drain a specified fraction of the fracture volume are derived as functions of geometry (length and initial aperture), wall elastic parameters, fluid properties, outlet pressure p_e and overload f_0. The late-time behaviour of the system is practically independent from rheology as the Newtonian nature of the fluid prevails at low shear stress. In particular, aperture and discharge scale asymptotically with time as $t^{-1/(\lambda+2)}$ and $t^{-1/(\lambda+3)}$ for $p_e - f_0 = 0$; else, the aperture tends to a constant, residual value proportional to $(p_e - f_0)^\lambda$. A case study with equally spaced fractures adopting realistic geometric, me-

chanical and rheological parameters is examined: two fluids normally used in fracking technology show completely different behaviours, with backflow dynamics and drainage times initially not dissimilar, later varying by orders of magnitude.

Keywords:
Hydraulic fracturing, Non-Newtonian, Ellis rheology, elastic wall, backflow

---

1. Introduction

Hydraulic fracturing is a process aimed at improving the productivity of oil, gas or geothermal reservoirs. Analysis of the different phases of hydraulic fracturing is of particular modeling and experimental interest [e.g. 1, 2].

An understanding of fractured media flow induced by the relaxation of elastic fracture walls is crucial in modeling fracturing fluid backflow, a complicated phenomenon involving hydrodynamic, mechanical and chemical processes. Backflow is typically the final phase of the hydraulic fracturing process: in the first one, fracturing fluid is injected at high pressure in a rock mass, forming new fractures and enlarging existing ones; in the second phase, proppant is introduced in the subsurface environment to prop fractures open; then when the injection ceases, the pressure drops, existing and new fractures tend to close, and a portion of the injected fracturing fluid, often mixed with proppant [3], flows back towards the injection well and interact with the relaxing walls of the fractures. As the retention of fracturing fluid in the fracture network impairs the fracture conductivity reducing the wellbore productivity [4], and favours migration in the subsurface environment along different pathways [5], it is of utmost interest to optimize the amount of fluid recovered, irrespective of the reservoir product, be it oil [6], gas [7] or heat [8].

The scientific literature offers two main approaches to modeling backflow: (i) detailed numerical simulations involving single fractures [9], fracture networks [10] or dual or triple porosity models [11], or (ii) conceptual models capturing the main features of the interaction between fracture flow and wall relaxation [12], including the effects of branching networks described at different degrees of complexity [13, 14]. A recent addition to the modeling effort is the influence of fluid rheology, following the notion that the backflow fluid is non-Newtonian in the widest sense [15], as not only the relationship between shear stress and shear rate is nonlinear, but also exhibits normal

stress and temperature dependency, as well as viscoelasticity, thixotropy, and nonzero yield stress [16]. At the same time, non-Newtonian fluids allow achieving several engineering objectives, such as (i) minimize the pressure-drop in the entire process; (ii) carry suspended proppant; (iii) minimize the leak-off within the formation; (iv) adapt their characteristics to different environments in terms of temperature and chemical composition; and (v) flow back easily towards the wellbore. Given their versatility and economic value, these fluids are typically treated for reuse once recovered, removing contaminants they may have transported to the surface [17]. The recovery ratios of backflow fluid vary between 2% and 48% according to Ipatova and Chuprakov [18], with considerable economic value.

Modeling non Newtonian backflow is in its early stage, in variance with the injection and fracture formation stage, for which several conceptualizations and models are available: see Detournay [19] for a review and the recent work by Wrobel [20] comparing different rheological models for fracturing fluids. To the best of our knowledge, only Chiapponi et al. [21] considered non-Newtonian fluids in the context of backflow modeling: these authors examined flow of a power-law fluid towards a wellbore in a single fracture of annular geometry, supporting their theoretical findings with laboratory experiments. The present paper develops the analysis of non-Newtonian backflow for a smooth fracture, common in field applications [22], and adds realism by employing a three-parameter Ellis model, that well represents the rheology of hydrofracturing [23] and drilling fluids [24]. The Ellis model tends to Newtonian for low shear rates, to power-law for high shear rates and allows avoiding the unphysical effect of infinite apparent viscosity at zero shear rate that is typical of the power-law model [25]. We note in passing that our results are of a general nature for Newtonian pressurized flow in ducts of variable width and may be of interest for, and be applied also to, deformable microfluidic [26] and biological [27] systems.

The plan of the paper is as follows. Section 2 formulates the problem of relaxation-induced backflow of an Ellis fluid in a fracture with nonlinear wall reaction and subject to overload. Numerical results obtained are presented and discussed in Section 3 as a function of dimensionless groups characterizing the system: the indicial exponent α quantifying the degree of shear-thinning behaviour of the Ellis fluid, the non-negative exponent λ modulating the fracture wall reaction, and a further group N encapsulating most problem parameters. Section 4 illustrates an hypothetical case study adopting realistic geometric and mechanical parameters and two real hy-

drofracturing fluids decribed by the Ellis model. Section 5 reports the main conclusions and perspectives for future work. In Appendix A the special case of a Newtonian fluid is examined, obtaining results that generalize those of Dana et al. [13] to a nonlinear wall reaction, while Appendix B presents an alternative expression for the dimensionless number N, shown to be a combination of well-known dimensionless groups in fluid mechanics.

2. Material and methods

2.1. Problem statement

A rock fracture produced by hydrofracturing, though of irregular geometry, is often conceptualized for modeling purposes as a 3-D space of length L, width W, and aperture h between two parallel walls [28]; the Cartesian coordinate system x, y, z is illustrated in Figure 1 and the fracture is subject to a pressure gradient $\nabla p' \equiv (\partial p'/\partial x, 0, 0)$ in the x direction. In horizontal fractures, the additional gravity-induced pressure gradient is perpendicular the flow plane and has no effect on the flow field. If the (x, y) plane is not horizontal, the z direction perpendicular to the walls is not vertical and gravity effects can be included in a reduced pressure term p, thus leading to a mathematical treatment with no gravity term to consider. For instance, for the Figure 3 below representing multiple vertical fractures backflowing to an horizontal well, the reduced pressure p is equal to $p = p' + \rho g y$.

The walls are taken to be rigid, so that the aperture $h(t)$ is solely a function of time, and the deformation is concentrated for mathematical convenience in the upper wall, that behaves as a nonlinear elastic foundation exerting a reaction on the fluid. At $t = 0$ the relaxation of the wall induces a backflow in the negative x direction, and the fracture begins to drain subject to a constant outlet pressure p_e at $x = 0$ and to a no-flow boundary condition at the upstream end $x = L$. Three further hypotheses are adopted: i) the flow is quasi-steady, allowing to neglect the time derivative of the velocity in the momentum equation; ii) the fracture aspect ratio is small, $h_0/L \ll 1$, warranting the lubrication approximation, and iii) the flow is essentially one-dimensional along x, $L \gg W$. The latter conceptualization is usually adopted in hydrogeology also when the two dimensions are comparable, as it is often the case for rock fractures [11].

The flowback fluid is taken to be incompressible of density ρ, non-Newtonian shear-thinning [15] and described by the Ellis three-parameter model [29]. Under the above assumptions, the fluid undergoes simple shear flow in the

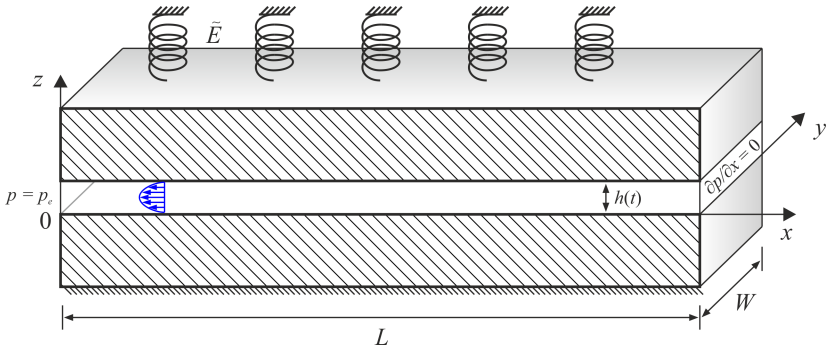

Figure 1: Layout of a plane fracture of variable uniform aperture $h(t)$.

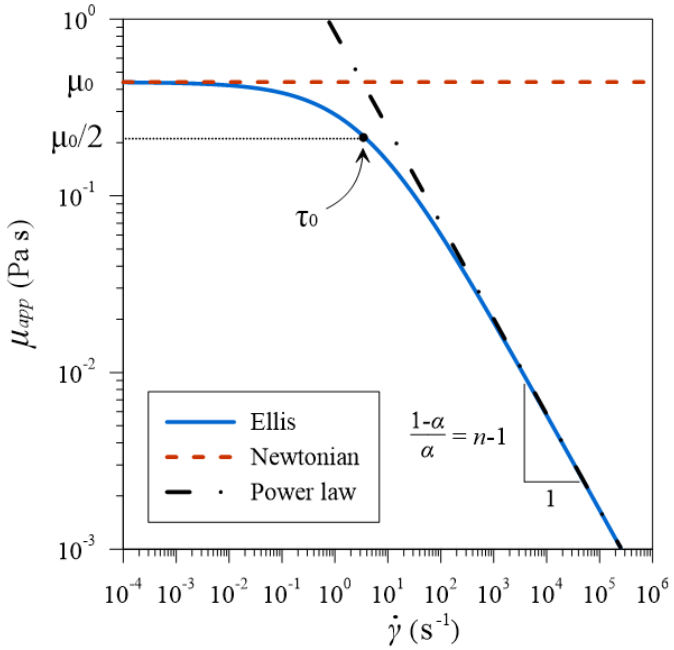

Figure 2: Apparent viscosity for three rheological models: Ellis (blue solid line) of parameters μ_0, τ_0, α; Newtonian (red dashed line) of viscosity μ_0; power-law (black dot-dashed line) of consistency index m and rheological index n. The comparison with the latter is drawn assuming: $\alpha = 1/n$ and $\tau_0 = (m/\mu_0^n)^{n/(1-n)}$.

x direction, and the Ellis rheology is described by the following relationship between shear stress τ_{zx} (hereinafter τ) and shear rate $\dot{\gamma}_{zx}$ (hereinafter simply $\dot{\gamma}$)

$$\tau = \frac{\mu_0}{1 + (\tau/\tau_0)^{\alpha-1}}\dot{\gamma}; \quad \dot{\gamma} = \frac{\partial u}{\partial z}, \tag{1}$$

where u is the velocity in the x direction. The rheological law (1) features a viscosity parameter μ_0, a constant τ_0 defined as the shear stress corresponding to apparent viscosity $\mu_0/2$, and an indicial parameter α, typically larger than one as the fluid is shear-thinning. For $\alpha = 1$, a pseudo-Newtonian behaviour with dynamic viscosity $\mu_0/2$ is recovered, see Figure 2 showing the apparent viscosity $\mu_{app} = \tau/\dot{\gamma}$ for the Ellis model compared to Newtonian and power-law models. Newtonian behaviour in the form of a plateau for low shear rates is also observed for $\gamma \to 0$. For high shear rates the behaviour is power-law, and its two parameters can be determined from the Ellis model parameters, see Appendix A in Balhoff and Thompson [28]; in particular, the rheological index is $n = 1/\alpha$ [30]. Note that when curve fitting is performed on real data, n and $1/\alpha$ may significantly differ [23], as two different models are fitted to the same data set. It is also seen that the Ellis model allows avoiding the unphysical effect of infinite apparent viscosity at zero shear rate that is typical of power-law fluids [25]. In the following, we will consider $\alpha > 1$, dealing with the case $\alpha = 1$ in the Appendix, and the parameters μ_0 and τ_0 to be finite and positive. Couette-Poiseuille slit flow of an Ellis fluid under a constant pressure gradient was studied extensively by Steller [31], listing all combinations of parameters leading to Newtonian or pseudo-Newtonian behaviour. In particular, the negative velocity $u(z)$ under a positive reduced pressure gradient $\partial p/\partial$ in the x direction is

$$\begin{aligned} u(z,t) = -\frac{1}{8\mu_0}\left[h^2 - (2z-h)^2\right]\frac{\partial p}{\partial x} + \\ - \frac{1}{(\alpha+1)2^{\alpha+1}\mu_0\tau_0^{\alpha-1}}\left[h^{\alpha+1} - |2z-h|^{\alpha+1}\right]\frac{\partial p}{\partial x}\left|\frac{\partial p}{\partial x}\right|^{\alpha-1}. \end{aligned} \tag{2}$$

The corresponding average velocity $\overline{u}$ and flow per unit width q_x in the x direction are

$$\overline{u} = -\frac{h^2}{12\mu_0}\frac{\partial p}{\partial x} - \frac{h^{\alpha+1}}{2^{\alpha+1}(\alpha+2)\mu_0\tau_0^{\alpha-1}}\frac{\partial p}{\partial x}\left|\frac{\partial p}{\partial x}\right|^{\alpha-1}; q_x = \overline{u}h. \tag{3}$$

For the Newtonian case ($\alpha = 1$) the latter equation reduces to the classical "cubic law" [32] written for a fluid with viscosity $\mu_0/2$. The continuity equation reads [13]

$$\frac{\mathrm{d}h}{\mathrm{d}t} + h(t)\frac{\partial \overline{u}}{\partial x} = 0, \tag{4}$$

and substituting eq. (3) in eq. (4) gives

$$\frac{\mathrm{d}h}{\mathrm{d}t} = \frac{h^3}{12\mu_0}\frac{\partial^2 p}{\partial x^2} + \frac{\alpha h^{\alpha+2}}{2^{\alpha+1}(\alpha+2)\mu_0\tau_0^{\alpha-1}}\left|\frac{\partial p}{\partial x}\right|^{\alpha-1}\frac{\partial^2 p}{\partial x^2}. \tag{5}$$

The problem formulation is completed by the force balance, expressed per unit width of fracture, among the fluid pressure and the elastic reaction of the upper wall, taken to be proportional to aperture h; an overload at the upper wall f_0 (a force per unit width) is included in the balance for generality [21]; the overload represents an additional force exerted by the walls and usually opposing the fracture opening due, e.g., to a residual stress state generated by the load history of the rocks. It is assumed constant and independent from the fracture aperture. The balance reads

$$\int_0^L p(x,t)\,\mathrm{d}x = \tilde{E}Lh(t) + f_0, \tag{6}$$

where the constant of proportionality $\tilde{E}$ has dimensions $[ML^{-2}T^{-2}]$; for a linear elastic foundation, called a Winkler soil in geotechnical applications, $\tilde{E}$ is equal, for a thin elastic layer of thickness l, to the ratio between the Young modulus of the layer's material E $[ML^{-1}T^{-2}]$ and l, $\tilde{E} = E/l$. In the context of hydraulic fracturing, l may be identified with the fracture spacing [13, 21], a design parameter that depends, among others, on the type of rock; in hydraulically fractured shales, values of l/L equal to 0.057, 0.28, and 0.029 are reported, respectively, by Ghanbari and Dehghanpour [7], Wang et al. [11], and Wang et al. [33]. In the case of vertical/sub-vertical fractures perpendicular to a horizontal/sub-horizontal well or borehole, the geometry of the idealized system is described by Figure 3, showing the two wings of equally spaced planar fractures of half-length L, width W, aperture h and spacing l. Albeit the flow very close to the well is radial, the influence of the boundary condition at the well decreases rapidly with distance, and flow in most of the fracture half-length L is uniform, consistently with the assumption $L \gg W$. Hence, as an approximation the boundary condition of assigned pressure p_e at the well is extended to a segment of height W. In the

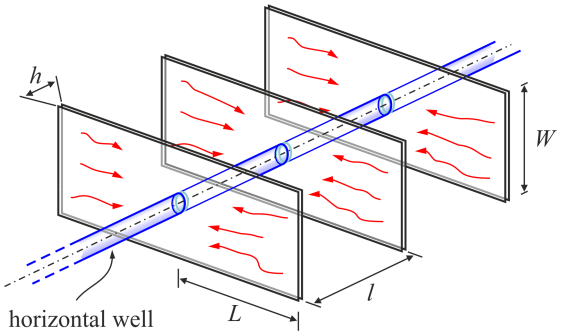

Figure 3: Typical scheme for bi-wing planar fractures around a horizontal borehole; L, W and h are the fracture length, width and aperture, l is the fracture spacing.

case of planar vertical fractures parallel to, and propagating from, a vertical well, the geometry of the flow is plane without using this approximation.

A further issue deserving investigation is the linearity of the relationship between the wall reaction and the fracture aperture. In fact, a nonlinear elastic behaviour can be the result of the pervasive damage of rocks by microcracks and voids, which determines nonlinearity even for infinitesimal strain, also with an incremental jump in the elastic modulus from tension to compression [34, 35]. In this case the Young modulus of the material is a function of the strain rate, $E = E_0(h/l)$, and assuming that the latter dependence is expressed with a power-law function one has

$$E = E_0 \left(\frac{h}{l}\right)^{\lambda-1}, \tag{7}$$

where λ is a non-negative exponent modulating the nature of the reaction: for $\lambda = 1$ a constant Young modulus is recovered, while $0 < \lambda < 1$ is associated to a softening behaviour, and $\lambda > 1$ to a stiffening one. The assumption results in

$$\tilde{E} = \frac{E_0}{l}\left(\frac{h}{l}\right)^{\lambda-1} \equiv \hat{E}h^{\lambda-1}, \tag{8}$$

and eq. (6) is modified as

$$\int_0^L p(x,t)\,\mathrm{d}x = \hat{E}Lh^{\lambda}(t) + f_0, \tag{9}$$

with $\hat{E} = E_0 l^{-\lambda}$ of dimensions $[ML^{-1-\lambda}T^{-2}]$.

Equations (5) and (9) are subject to the following initial and boundary conditions

$$h(0) = h_0, \quad \frac{\partial p(x,t)}{\partial x}(L,t) = 0, \quad p(0,t) = p_e, \tag{10}$$

h_0 being the initial fracture aperture, and p_e the exit pressure at the well.

The solution to the above problem yields two relevant quantities expressed per unit width, the flowrate exiting the fracture at the well, $q(t)$, and the residual volume of the fracture at a given time, $v(t)$; these are easily derivable as

$$q(t) = L\frac{\mathrm{d}h(t)}{\mathrm{d}t}, \quad v(t) = Lh(t). \tag{11}$$

2.2. Dimensionless form

Dimensionless quantities are defined as

$$\begin{aligned} X = x/L,\, H = h/h_0, T = t/t_c,\, P = (p - p_e)/p_c,\, P_e = p_e/p_c, \\ Q = qt_c/(h_0 L) = q/(u_0 h_0),\, V = v/(h_0 L), \end{aligned} \tag{12}$$

where the scales for pressure and time are

$$p_c = \hat{E} h_0^{\lambda}, \quad t_c = \frac{(2+\alpha)}{\alpha}\left(\frac{2L}{h_0}\right)^{1+\alpha} \frac{1}{h_0^{\alpha\lambda}} \frac{\mu_0 \tau_0^{\alpha-1}}{\hat{E}^{\alpha}}, \tag{13}$$

and $u_0 = L/t_c$ is a velocity scale. This leads to the dimensionless counterpart of eq. (5)

$$\frac{\mathrm{d}H}{\mathrm{d}T} = NH^3 \frac{\partial^2 P}{\partial X^2} + H^{\alpha+2}\left(\frac{\partial P}{\partial X}\right)^{\alpha-1} \frac{\partial^2 P}{\partial X^2}, \tag{14}$$

where the pure number

$$N = \frac{2+\alpha}{3\alpha}\left(\frac{2\tau_0 L}{\hat{E} {h_0}^{\lambda+1}}\right)^{\alpha-1} = \frac{2+\alpha}{3\alpha}\left[\frac{2\tau_0}{p_c(h_0/L)}\right]^{\alpha-1} \tag{15}$$

modulates the relative importance of the Newtonian behaviour of the Ellis fluid at low shear rate, expressed by the first term on the r.h.s. of eq. (14), with respect to the second term, the power-law behaviour at high shear rate. For a Newtonian fluid ($\alpha = 1$) N reduces to unity; for a shear-thinning fluid ($\alpha > 1$), N is zero for $\tau_0 = 0$ and/or a rigid wall ($\hat{E} = E_0/l^{\lambda} \to \infty$), but the latter case renders the scales (13) meaningless. In eq. (15) defining N,

the quantity within brackets represents the ratio between the characteristic shear stress τ_0 of the Ellis fluid and the pressure scale $p_c = \hat{E}{h_0}^{\lambda}$ associated with the elastic reaction of the fracture wall; the ratio is in turn corrected by the initial aspect ratio of the fracture h_0/L. This formulation of N includes only parameters defined at the single fracture scale. Note that if the scheme of multiple fractures with spacing l depicted in Figure 3 is considered, eq. (15) may be rewritten as

$$N = \frac{2+\alpha}{3\alpha}\left[\frac{2\left(\frac{\tau_0}{E_0}\right)\left(\frac{l}{L}\right)}{\left(\frac{h_0}{L}\right)^2}\frac{\left(\frac{l}{L}\right)^{\lambda-1}}{\left(\frac{h_0}{L}\right)^{\lambda-1}}\right]^{\alpha-1}, \tag{16}$$

where τ_0/E_0 is the ratio between the representative shear stress of the fluid and the Young modulus of the host rock, and l/L is the dimensionless fracture spacing. The terms to the power $(\lambda - 1)$ represent the contribution due to non-linear elastic behaviour of the walls, and disappear for $\lambda = 1$. An alternative formulation of N as a function of Cauchy, Reynolds, and Ellis dimensionless groups is reported in Appendix B. To grasp the order of magnitude of N, we recall that l/L may be taken to vary between 0.03 and 0.3 (with $l/L \approx 0.1$ being appropriate for an order of magnitude analysis), while the initial fracture aspect ratio h_0/L, a number much smaller than 1, may be considered of order $10^{-3} - 10^{-5}$ [7, 11, 33]. The latter reference also reports $E_0 = 2.5 \cdot 10^{10}$ Pa for the rock elastic modulus in fractured shales; quite close values, $E_0 = 3 \cdot 10^{10}$ Pa and $E_0 = 2.76 \cdot 10^{10}$ Pa are reported in [19] and [36], hence reference values $E_0 = 2.5 - 3.0 \cdot 10^{10}$ Pa are considered.

Actual values of rheological parameters for Ellis fluids are quite scarce in the literature. A reference specific to fracking is [23], where the Ellis parameters are reported for two fracturing fluids, HPG (Hydroxypropylguar) and VES (viscoelastic surfactant). For the first, $\mu_0 = 0.44$ Pa $\cdot$ s, $\tau_0 = 2.01$ Pa, and $\alpha = 1.22$; for the second, $\mu_0 = 49$ Pa $\cdot$ s, $\tau_0 = 8.836$ Pa, and $\alpha = 12$. Adopting as reference geometrical parameters $l/L = 0.1$ and $h_0/L = 10^{-4}$, and a young modulus of $E_0 = 2.75 \cdot 10^{10}$ Pa for the host rock, one obtains $N = 0.209$ for HPG and $N \simeq 0$ for VES, indicating that for the latter fluid the Newtonian component of rheological behaviour is negligible. A further consideration is that VES is very strongly shear-thinning ($\alpha \gg 1$), therefore the value of N is extremely sensitive to variations in parameters: adopting for example $l/L = 0.125$, $h_0/L = 10^{-5}$, and $E_0 = 2.5 \cdot 10^{10}$ Pa, again realistic

values, one obtains $N = 0.100$ for VES and $N = 0.618$ for HPG. This second set of parameters is adopted for later reference in Section 4 describing a case study and is shown there in dimensional form (see Table 1). Trying further combinations of realistic values for fluid and rock properties, it is seen that N may take values smaller or larger than unity, the former case being more frequent. This indicates a certain prevalence of the power-law component of rheology over the Newtonian one, although the asymptotic system behaviour is dominated by the latter, as will be shown in the next section. We bear in mind that a large variety of combinations is possible for the two parameters N and α depending on geometry and properties of fluid and rock, but with the constraint from the definition (15) that for $\alpha = 1$ it must be $N = 1$.

The dynamic boundary condition (9) and the boundary conditions (10) transform as

$$\int_0^1 P(X,T)\,\mathrm{d}X = H^\lambda - P_e + F_0, \tag{17}$$

$$H(0) = 1, \quad \frac{\partial P}{\partial X}(1,T) = 0, \quad P(0,T) = 0. \tag{18}$$

2.3. Solution

A solution to eq. (14) is sought by integrating in two steps the pressure of the fluid and the fracture aperture. Posing

$$U(X,T) = \frac{\partial P}{\partial X}, \quad \dot{H} = \frac{\mathrm{d}H}{\mathrm{d}T}, \tag{19}$$

eq. (14) can be written as

$$B\left(1 + AU^{\alpha-1}\right)\frac{\partial U}{\partial X} = \dot{H} \tag{20}$$

where

$$A = A(T) = \frac{(H)^{\alpha-1}}{N}, \quad B = B(T) = NH^3, \tag{21}$$

while the second boundary condition in eq. (18) becomes

$$U(1,T) = 0. \tag{22}$$

Separating variables in eq. (20), and integrating with the boundary condition (22) leads to

$$\frac{BU\left(AU^{\alpha-1} + \alpha\right)}{\alpha} = -\dot{H}(1 - X). \tag{23}$$

Eq. (23) can be rewritten as

$$U^\alpha + CU + D(1 - X) = 0 \tag{24}$$

where

$$C = C(T) = \frac{\alpha N}{H^{\alpha-1}}, \quad D = D(T) = \frac{\alpha \dot{H}}{H^{2+\alpha}}. \tag{25}$$

Eq. (25) is algebraic in U and admits an analytical solution for $\alpha = 1, 2, 3$ and for $\alpha = 1/2, 1/3$ in the form of a combination of functions of H and $\dot{H}$. This solution can be integrated once in space, with the boundary condition $P(0, T) = 0$, obtaining the pressure field. The pressure field is finally integrated in $X \in [0, 1]$ and the integral in eq. (17) is computed as a function of H and $\dot{H}$. Then eq. (17) is transformed in a nonlinear ODE which is numerically integrated with the initial condition $H(0) = 1$.

These solutions are analytical in the x coordinate and numerical in the time domain and seem quite cumbersome, while their accuracy is comparable to that of a fully numerical solution in space and time; the latter also has the advantage of a free selection of the indicial parameter α. Among the many possible numerical schemes, we adopt a finite difference in time and an implicit resolver in space, with a step size reduction to track solution accurately.

The code is written in Mathematica, introducing a parametric solver for the function $U(X, T)$ as a function of $N, \alpha, H_{i+1}, H_i, \Delta t$, where H_{i+1} and H_i are the values at time $(i + 1)\Delta t$ and $i\Delta t$, respectively; the only free parameter is H_{i+1}, all the other parameters are given.

Each time iteration includes the following steps:

- The function $U(X)_{i+1}$ is estimated by solving eq. (20) in parametric form, with $\dot{H} \approx (H_{i+1} - H_i)/\Delta t$, with the term H taken to be the average between H_{i+1} and H_i and with the b.c. $U(1)_{i+1} = 0$, where H_{i+1} is the free parameter; $H_0 = 1$ is assumed at the first step.

- The space values of U, known in parametric form, are used to solve the differential problem $\partial P(X)_{i+1}/\partial X = U(X)_{i+1}$, with $P(0)_{i+1} = 0$, obtaining the pressure $P(X)_{i+1}$.

- The pressure field is numerically integrated (in parametric form) in the domain $[0, 1]$.

- The parametric integral is inserted in eq. (17), and the equality is forced with a Newton method for finding the value of the parameter H_{i+1}.
- The procedure is repeated for the next time step, shifting the values H_{i+1}.

Once the pressure $P(X,T)$ and aperture $H(T)$ fields are known, the dimensionless flowrate and fracture volume are given by

$$Q(T) = \frac{\mathrm{d}H(T)}{\mathrm{d}T} = \dot{H}, \quad V(T) = H(T). \tag{26}$$

Hence at late-time the fracture volume and flowrate behave like the aperture and its time derivative, respectively; for zero borehole pressure and overload the corresponding time scalings are $T^{-1/(\lambda+2)}$ and $T^{-1/(\lambda+3)}$.

3. Results and discussion

Figure 4 shows the results of the numerical computation for the fracture aperture and different α values, with the analytical solution $H = (1+9T)^{-1/3}$ valid for the Newtonian case and a linearly elastic fracture [13], corresponding to $\alpha = 1$, $N = 1$, and $\lambda = 1$. Note that the values $\alpha = 1$, $N = 1$ imply Newtonian behaviour but with a viscosity equal to $\mu_0/2$, thus halving the time scale t_c in eq. (13); this requires doubling the dimensionless time T in eq. (12) to compare results of equations having a different time scale. The time integration was performed with a time step $\Delta t = 0.01$. Since the results of the numerical integration using this fully explicit scheme fit exceedingly well the analytical solution, it was not necessary to adopt higher order schemes, even considering that the solution has no singularity and behaves rather smoothly.

The asymptotic behaviour of the solution $H(T)$ is dictated by the interplay between the two terms on the r.h.s. of eq. (14): the second term scales with the gradient pressure (decaying in time) and with a power of H always larger than 3, since $\alpha > 1$, whereas the first term scales with the third power of H and has N as a coefficient. Since $H \leq 1$ and the gradient pressure quickly decays to values less than unity, the dominant term is the first one, which entails the asymptotic behaviour $H \sim T^{-1/(2+\lambda)}$, see Figure 5 where different values of α, for $N = 1$ and $P_e = 0$, produce almost parallel curves for large T. Figure 5 also shows how variations in λ significantly affect the

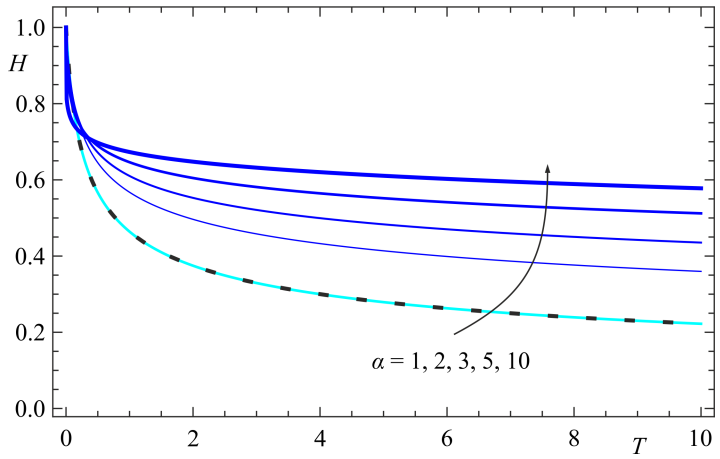

Figure 4: Time variation of the fracture aperture H for $N = 0$, $\lambda = 1$, $P_e - F_0 = 0$ and different α values. The black dotted curve refers to the analytical solution for a Newtonian fluid, $H = (1 + 9T)^{-1/3}$. Due to the different time scales adopted for a Newtonian fluid and for the present model, comparison is feasible if the dimensionless time T in the solution for the Newtonian fluid is doubled.

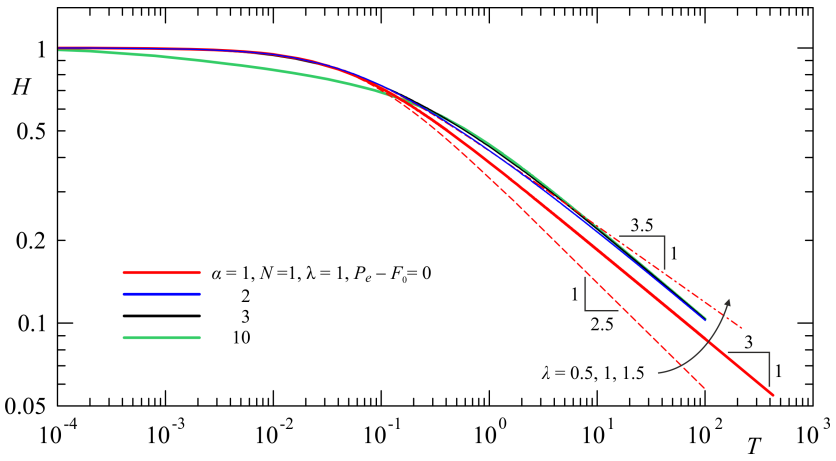

Figure 5: Time variation of the fracture aperture H for $N = 1$, $\lambda = 1$ and different α values. For one case ($\alpha = 1$) the effects of a softening/stiffening wall is explored, see the dashed and dash-dotted thin curves for $\lambda = 0.5 - 1.5$, respectively. The asymptotic behaviour is $H \sim T^{-1/(2+\lambda)}$, independent on α.

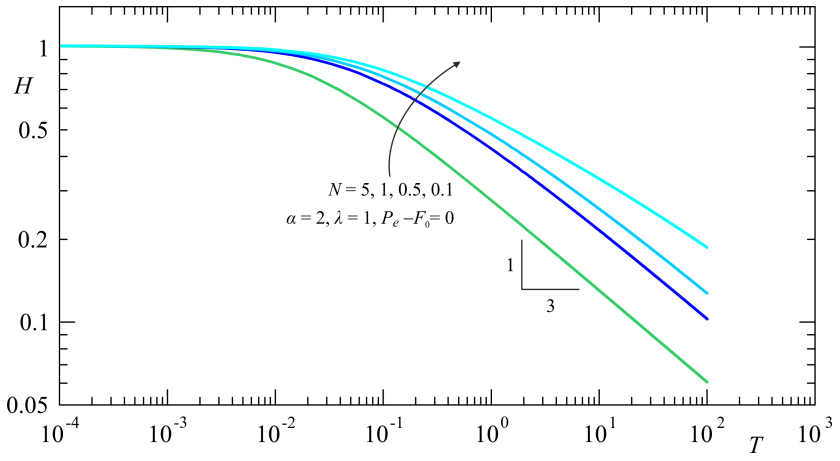

Figure 6: Time variation of the fracture aperture H for $\alpha = 2$, $\lambda = 1$ and different N.

late-time behaviour for fixed α: a stiffening ($\lambda > 1$)/softening ($\lambda < 1$) elastic reaction of the walls delays/facilitates the drainage. It is also seen that the parameter α mainly controls the early stage, the parameter λ the late stage of the backflow process. Figure 6 shows results for a fixed $\alpha = 2$, $\lambda = 1$, and different N values; the asymptote is reached much faster for larger N. In sum, the early time behaviour for zero external pressure at the well is in general dominated by the second term in eq. (14) unless the coefficient $N \gg 1$; in the latter case both terms substantially contribute to the time evolution of H.

In presence of a non-zero external pressure ($P_e > 0$) or a negative overload F_0 (an additional force per unit of wall surface acting in the same direction of the internal pressure), the asymptotic residual aperture is equal to $(P_e - F_0)^{1/\lambda}$, see Figure 7 where both effects are included. The curves coalesce to the asymptote faster for larger N values, implying a dominance of the Newtonian behaviour, while for small N the power-law behaviour prevails and the asymptote is reached for larger dimensionless times. Upon plotting results for $\alpha = 3$ (not shown) the main curves for $\lambda = 1$ and the secondary curves for $\lambda \neq 1$ are very similar to those for $\alpha = 2$.

Figure 8 shows the pressure distribution for two different combinations of the parameters and a shear-thinning fluid with $\alpha = 2$. Results for other combinations are similar (and thus not shown), with a pressure decay in space/time quicker or slower depending on the parameter values; at all times

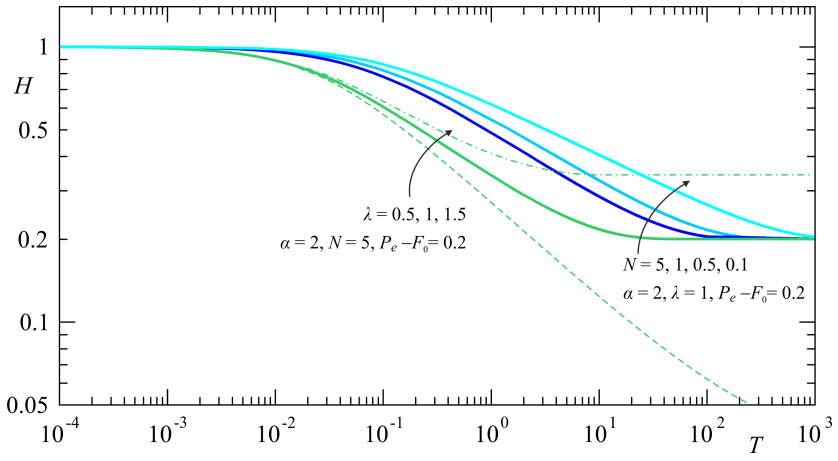

Figure 7: Time variation of the fracture aperture H for $\alpha = 2$ and different N values, with given difference between external pressure and overload $P_e - F_0 = 0.2$. For one case ($N = 5$) the effects of a stiffening/softening elastic reaction of the walls is explored, see the dashed and dash-dotted thin curves for $\lambda = 0.5 - 1.5$, respectively.

the residual pressure within the fracture increases with smaller N values, implying a behaviour closer to Newtonian, and with smaller λ values, i.e. a softening wall; however when the fluid is closer to Newtonian the effect of a λ variation is irrelevant.

An important quantity characterizing the performance of the backflow process is the time required to recover the fluid injected in the fracture network and not lost in the form of leakoff. Here the network is conceptualized as a single fracture and fluid losses are not explicitly represented (they are assumed to take place in the upstream network), however the time T_Y needed to recover $Y\%$ of the fracture volume provides an indication of how rapid the recovery is. Contour maps in the (α, N) space of the dimensionless time T_{90} needed to recover 90% of the fluid are depicted in Figure 9 for a linear wall reaction ($\lambda = 1$). As the degree of shear-thinning behaviour rises with α for constant N, there is a sharp increase in dimensionless T_Y for $N < 0.5$, while T_Y is almost independent on α for $N > 2$. Conversely, T_Y for costant α decreases with larger N values, i.e. as the fluid behaviour is closer to Newtonian; this effect is more evident for larger α. Highest values of T_Y are attained for large α and low N, lowest values for small α and large N, the two combinations farthest and closest to Newtonian behaviour. The effect

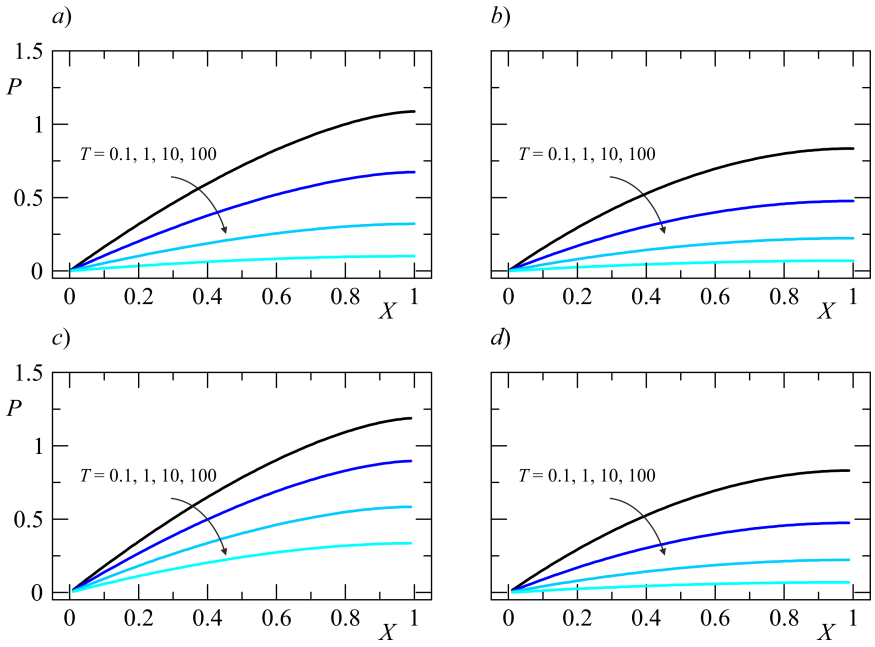

Figure 8: Pressure along the fracture at different times for $P_e - F_0 = 0.2$ and a shear-thinning fluid with $\alpha = 2$. Results for *a*) $N = 0.1$ and $\lambda = 1$; *b*) $N = 5$ and $\lambda = 1$; *c*) $N = 0.1$ and $\lambda = 0.5$; *d*) $N = 5$, $\lambda = 0.5$.

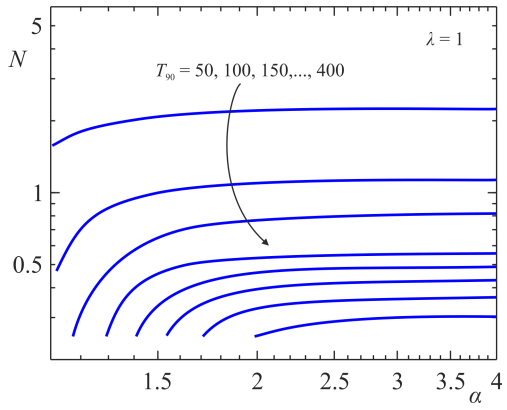

Figure 9: Time to recover 90% of the fluid as a function of α and N, with $\lambda = 1$ and $P_e - F_0 = 0$.

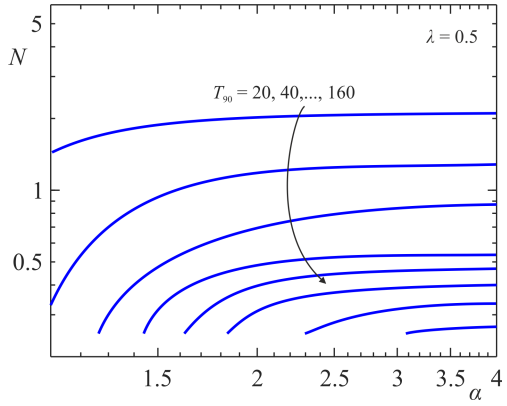

Figure 10: Time to recover 90% of the fluid as a function of α and N, with $\lambda = 0.5$ and $P_e - F_0 = 0$.

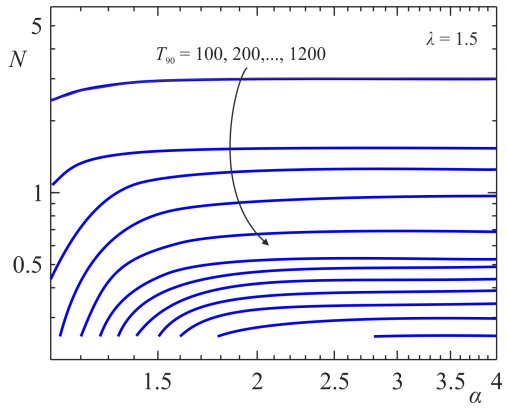

Figure 11: Time to recover 90% of the fluid as a function of α and N, with $\lambda = 1.5$ and $P_e - F_0 = 0$.

Fluid	μ_0 (Pa s)	τ_0 (Pa)	α	L (m)	l (m)	h_0 (mm)	E (Pa)	λ	N
HPG	0.44	2.01	1.22	100	12.5	1.00	$2.5 \cdot 10^{10}$	1.00	0.618
VES	49.00	8.836	12.00	100	12.5	1.00	$2.5 \cdot 10^{10}$	1.00	0.100

Table 1: Reference parameters for case study: μ_0, τ_0 and α are the reference viscosity, shear stress and indicial exponent of the Ellis fluid, L is the fracture length, l is the fracture spacing, h_0 is the fracture initial height, E is the rock modulus of elasticity, λ is the exponent of the rock wall reaction, N is the dimensionless number governing the interplay between Newtonian and power-law behaviour in an Ellis fluid.

of a sublinear wall reaction ($\lambda = 0.5$) is depicted in Figure 10, that of a supralinear wall reaction in Figure 11. The dimensionless time to recover the bulk of the stored fluid is decidedly faster or slower with a softening or stiffening wall, demonstrating once again the decisive influence of the parameter λ modulating the wall reaction at late time.

A word of caution is needed when drawing comparisons between non-Newtonian fluids with different rheology as the models are semi-empirical and the time scale used for the dimensionless formulation depends upon the rheological parameters of the Ellis model and is particularly sensitive to the value of the indicial exponent α. Hence model outputs are best compared in dimensional coordinates when quantitative results are needed.

4. A case study

A case study is illustrated by comparing the performance of two real hydrofracturing fluids [23], HPG (Hydroxypropylguar) and VES (viscoelastic surfactant) in a realistic setting. The rheological parameters according with the Ellis model are reported for both fluids in Table 1, together with realistic geometric and mechanical parameters within plausible ranges deduced from the literature, see the earlier discussion in Section 2.2. It is seen that HPG is relatively close to Newtonian in behaviour, while VES is extremely shear-thinning, with an equivalent rheological index n less than 0.1 when expressed according to the power-law model.

Figure 12 shows the relaxation of the fracture aperture for the two fluids:

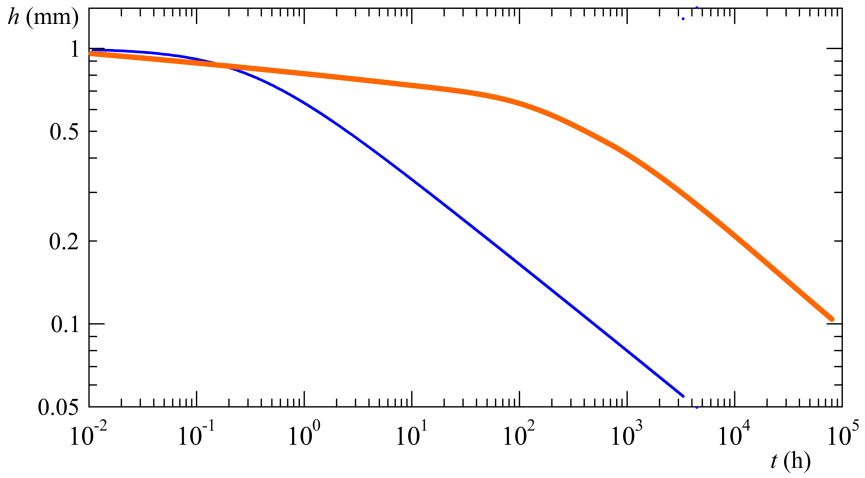

Figure 12: Time variation of the fracture aperture h for the HPG (thin line) and VES (thick line) fluids.

the aperture for the HPG is only initially slightly larger than for the VES, but then closes more rapidly, reaching one tenth of the initial value at a time around 500 hours. The closure is much more gradual for the VES, requiring about a year to reach the same stage. The difference between corresponding pressure profiles, illustrated in Figure 13, shows a decidedly sharper pressure decrease for HPG than for VES in the initial stage.

Figure 14 shows the time to recover the volume stored in the fracture for the two fluids. Following the same trend manifested for the evolution of

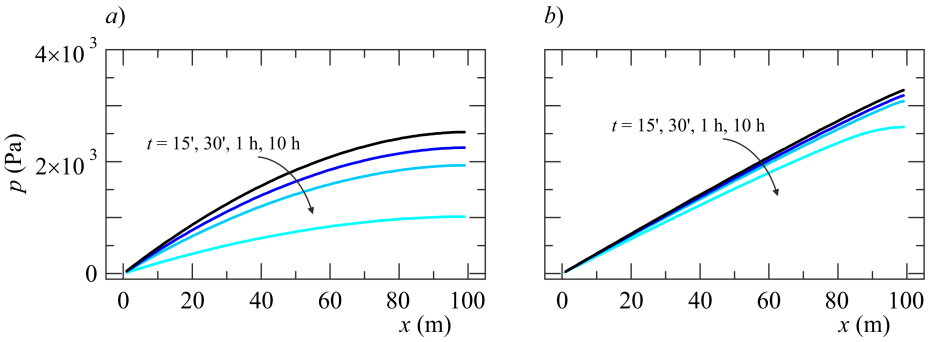

Figure 13: Pressure distribution at different time a) for HPG fluid, and b) for VES.

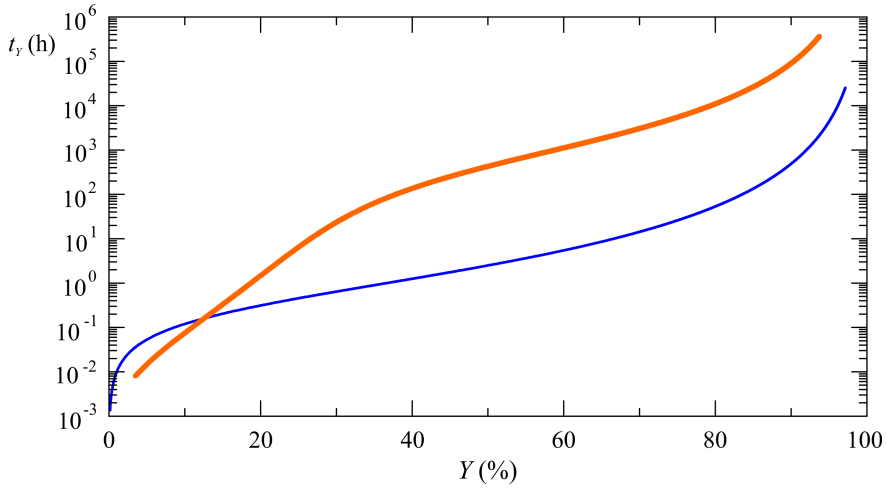

Figure 14: Time to recover the fracture volume $Y\%$ for the HPG (thin line) and VES (thick line) fluids.

fracture opening, VES demonstrates a higher drainage capacity than HPG in the very early phase, for $Y < 15\%$; subsequently it is much less efficient, and requires an extra time at least three orders of magnitude larger to drain the same percentage of fluid than HPG. Overall the large difference in rheology, mainly encapsulated in the α value, translates into corresponding wide differences in terms of aperture, pressure, and drainage time. This is so because the value of the dimensionless group N is very low for VES, thus allowing the fluid to manifest its essentially power-law nature. We tried a number of other combinations of parameters and found that for very shear thinning fluids like VES the results are very sensitive to relatively small changes in parameters: slightly increasing the modulus of elasticity E to $3 \cdot 10^{10}$ and increasing the spacing to 20 m, leaving the other parameters in Table 1 unchanged, leads to $N(HPG) = 0.659$ and $N(VES) = 2.360$. While the change in the N value associated to HPG is modest (6.6%) and implies the system behaviour is essentially unchanged with respecto to the reference case, the increase in N for the VES is dramatic (2260%) and entails a fluid behaviour closer to Newtonian despite the exceedingly high value of α. Upon plotting the aperture variation over time for this case (not shown) the two fluids exhibit a similar behaviour, with only modest differences (less than 10%) in the fracture aperture at early times and an almost identical behaviour later on. The pressure profiles do not show any significant differences.

5. Conclusions

A conceptual model for backflow of non-Newtonian fluid from a closing rock fracture was presented in this paper. Under the assumption of Ellis rheology and elastic, but non-deformable wall, the problem in plane geometry is tractable in semi-analytical form to yield the time-variable fracture aperture $h(t)$, pressure field $p(x,t)$ and discharge rate $q(t)$, as well as the drainage time t_Y for a specified recovery rate Y, outlet pressure p_e and overload f_0.

Our results lead to the following specific conclusions:

- The Ellis model adopted herein to describe shear-thinning rheology couples Newtonian and power-law behaviour. When an Ellis fluid backflows from a relaxating fracture the interplay between the two natures is modulated by a dimensionless group N encapsulating the main problem parameters. N can be expressed in terms of i) the indicial exponent α of the Ellis rheology, ii) the parameter λ governing the wall relaxation process, iii) the ratio between the characteristic shear stress of the Ellis fluid τ_0 and the rock modulus of elasticity E, iv) two geometric ratios, the fracture initial aspect ratio h_0/L and dimensionless spacing l/L. An alternative format of N is a modified ratio between the Cauchy number and the product of Reynolds and Ellis numbers.

- The factors N and α mostly influence the early and intermediate time evolution of the system: when $N < 1$ the power-law behaviour prevails; for $N = 1$ the pure Newtonian case is recovered ($\alpha = 1$ entails $N = 1$), while for $N \gg 1$ the behaviour is mixed.

- For late-time the system behaviour tends to Newtonian, is independent of N and is governed by the wall relaxation parameter λ: aperture and discharge scale asymptotically with time as $t^{-1/(\lambda+2)}$ and $t^{-1/(\lambda+3)}$ for $p_e - f_0 = 0$; else, the aperture tends asymptotically to a constant value proportional to $(p_e - f_0)^{1/\lambda}$.

- Very shear-thinning fluids (larger α) and reactive walls (larger λ) are associated with a more gradual closure of the aperture.

- The residual pressure within the fracture increases with smaller N values and with a softening wall ($\lambda < 1$); when the fluid is close to Newtonian the effect of a λ variation is almost irrelevant.

- The dimensionless drainage time T_Y attains the largest values for large α and low N, the lowest values for small α and large N, the two combinations farthest and closest to Newtonian behaviour. A non-linear reaction of the walls result in a faster/slower recovery for $\lambda < 1$ (softening) and $\lambda > 1$ (stiffening). For recovery values close to 100%, T_Y is very sensitive to variations of model parameters.

- Results are discussed in dimensional form for a case study to reinforce the notion that dimensionless results need to be compared with caution as scales include fluid rheological parameters. Realistic geometric and mechanical parameters are adopted for a system of equally spaced fractures, and results are compared for two fluids, HPG and VES, normally used in fracking technology. The time evolution of the aperture and the dependence of the drainage time upon the recovery ratio are similar at early times, then differ by orders of magnitude at intermediate and late times.

The developments presented, together with earlier results [13, 21], provide an overview of the backflow phenomenon in the two basic geometric configurations for a single fracture, plane and radial, and for three rheological models of increasing complexity: Newtonian, power-law, and Ellis. Further improvements of the model remain open in several directions, e.g.: i) a more complex geometry, considering nonplanar fractures with non-negligible curvature; ii) the combination of non-Newtonian rheology with multiple fracture systems, adopting the asymptotic viewpoint of Dana et al. [14]; iii) the incorporation of particle transport to simulate the settling of solid proppant.

Acknowledgments

This work was supported in part by Università di Bologna Almaidea 2017 Linea Senior grant awarded to Vittorio Di Federico. The authors have no conflicts of interest to declare. There are no data sharing issues since all of the numerical information is provided in the figures produced by solving the equations in the paper.

Appendix A. The Newtonian case ($n = 1$)

For $\alpha = 1$ and $N = 1$ eq. (25) reduces to

$$C = 1, \quad D = \frac{\dot{H}}{H^3}, \tag{A.1}$$

and integrating eq. (24) using these expressions yields

$$P(X,T) = \frac{\dot{H}}{4H^3}[(X-1)^2 - 1]. \tag{A.2}$$

Substituting in eq. (17) and integrating $P(X,T)$ over X gives

$$-\frac{\dot{H}}{3H^3} = H^\lambda - P_e + F_0, \tag{A.3}$$

generalizing eq. (2.14) of Dana et al. [13], where $\lambda = 1$ and $F_0 = 0$, to non-linear wall reaction and non-zero overload. Now define an effective pressure $\tilde{P}_e = P_e - F_0$ at the fracture outflow: this symbol will be used for brevity in the sequel. Consider first the case $\tilde{P}_e = 0$. Integration of eq. (A.3) over time T yields, with the first b.c. in eq. (18),

$$H(T) = [1 + 3(2+\lambda)T]^{-\frac{1}{2+\lambda}}, \tag{A.4}$$

that for $\lambda = 1$ gives back eq. (2.15) of [13].

Consider now the case $\tilde{P}_e > 0$. Integration with the help of Mathematica and using transformation formulae for the analytic continuation of hypergeometric functions [37] yields for generic λ the following implicit equation

$$T = \frac{1}{3(\lambda+2)}\left[\frac{1}{H^{\lambda+2}}\,{}_2F_1\left(1, \frac{\lambda+2}{\lambda}; \frac{2(\lambda+1)}{\lambda}; \frac{\tilde{P}_e}{H^\lambda}\right) + \right.$$
$$\left. - {}_2F_1\left(1, \frac{\lambda+2}{\lambda}; \frac{2(\lambda+1)}{\lambda}; \tilde{P}_e\right)\right], \tag{A.5}$$

where ${}_2F_1(\alpha, \beta; \gamma; z)$ is the hypergeometric function of parameters α, β, γ, and argument z. Specific results for $\lambda = 1/2$, $\lambda = 1$, $\lambda = 2$, i.e. a sublinear, linear or supralinear wall reaction, can be obtained as

$$T = \frac{1}{18\tilde{P}_e^{\,5}}\left[12\ln\left(\frac{H^{1/2}(1-\tilde{P}_e)}{H-\tilde{P}_e}\right) - \frac{12\tilde{P}_e}{H^{1/2}} - \frac{6\tilde{P}_e^{\,2}}{H} - \frac{4\tilde{P}_e^{\,3}}{H^{3/2}} - \frac{3\tilde{P}_e^{\,4}}{H^2} + \right.$$
$$\left. + 12\tilde{P}_e + 6\tilde{P}_e^{\,2} + 4\tilde{P}_e^{\,3} + 3\tilde{P}_e^{\,4}\right], \tag{A.6}$$

$$T = \frac{1}{6\tilde{P}_e^{\,3}}\left[2\ln\left(\frac{H(1-\tilde{P}_e)}{H-\tilde{P}_e}\right) - \frac{2\tilde{P}_e}{H} - \frac{\tilde{P}_e^{\,2}}{H^2} + 2\tilde{P}_e + \tilde{P}_e^{\,2}\right], \tag{A.7}$$

$$T = \frac{1}{6\tilde{P}_e^{\,2}}\left[\ln\left(\frac{H^2(1-\tilde{P}_e)}{H^2-\tilde{P}_e}\right) - \frac{\tilde{P}_e}{H^2} + \tilde{P}_e\right], \tag{A.8}$$

either by direct integration of eq. (A.5) or using transformations involving the hypergeometric functions [37]. Eq. (A.7) valid for $\lambda = 1$ is identical to Eq. (2.18) of Dana et al. [13]. Other results in terms of trascendental and algebraic functions can be obtained for other special values of $\lambda \in \mathbb{N}$ or $1/\lambda \in \mathbb{N}$ but are too cumbersome to report and/or of little technical interest.

Expressions (A.5)-(A.8), when evaluated for for given $\tilde{P}_e$, allow deriving $H(T)$ and the drainage time T_Y needed to drain $Y\%$ of the fracture volume. As the latter quantity is given in dimensionless form by H according to (26), to derive T_Y it is sufficient to evaluate (A.5) and its special cases (15)-(A.8) for $H = (100 - Y)/100$.

Finally, it is wortwhile to derive the asymptotic behaviour of the general equation (A.5) for the limit case $\lambda \to 0$. According to eq. (9), $\lambda = 0$ implies a wall reaction constant over time rather than dependent from the fracture aperture. Integrating (A.3) for $H^\lambda = 1$ gives

$$H = \frac{1}{[1 + 6(1-\tilde{P}_e)T]^{1/2}}, \tag{A.9}$$

a result that can be simplified for large time to $H = 1/[6(1-\tilde{P}_e)T]^{1/2}$ and further for $\tilde{P}_e = 0$ to $H = 1/(6T)^{1/2}$. Equation (A.9) can be also obtained directly from eq. (A.5) for $\lambda \to 0$ on the basis of eq. (9.121.1) in [37]. The late-time scaling for a Newtonian fluid and a wall with constant reaction ($\lambda = 0$) is therefore $H \propto T^{-1/2}$, a result coinciding with the scaling $H \propto T^{-1/(2+\lambda)}$ implied by Figure 5 for a Newtonian fluid with $N = 1$, $\alpha = 1$.

Appendix B. The dimensionless group N

The pure number N may be expressed as a function of well-known dimensionless groups in fluid mechanics [see, e.g., 38]. Multiplying and dividing eq. (16) by $\rho\mu_0 h_0 u_0^3$, where u_0 is the reference velocity defined in (12), yields

$$N = K\left(\frac{\mathrm{Ca}}{\mathrm{Re}\cdot\mathrm{El}}\right)^{\alpha-1};\quad \mathrm{Ca}=\frac{\rho u_0^2}{E};\quad \mathrm{Re}=\frac{2\rho u_0 h_0}{\mu_0};\quad \mathrm{El}=\frac{\mu_0 u_0}{\tau_0 h_0}, \tag{B.1}$$

$$K = K\left(\alpha,\lambda,l/L,h_0/L\right)=\frac{2+\alpha}{3\alpha}\left[\frac{4\left(\frac{l}{L}\right)^{\lambda}}{\left(\frac{h_0}{L}\right)^{\lambda+1}}\right]^{\alpha-1} \tag{B.2}$$

where Ca, Re, and El are the Cauchy, Reynolds, and Ellis numbers, and K a geometric factor correcting the ratio $\mathrm{Ca}/(\mathrm{Re}\cdot\mathrm{El})$. In turn, Ca is the ratio between inertial forces and elastic forces transmitted by solid walls, Re is the ratio between inertial and viscous forces, while El is the ratio between the viscous stress associated with the low shear rate Newtonian behaviour and the shear stress τ_0 associated with high shear rate non-Newtonian (power-law) behaviour.

References

[1] N. Dutler, B. Valley, V. Gischig, M. Jalali, B. Brixel, H. Krietsch, C. Roques, F. Amann, Hydromechanical insight of fracture opening and closure during in-situ hydraulic fracturing in crystalline rock, International Journal of Rock Mechanics and Mining Sciences 135 (2020) 104450.

[2] Y. Wu, L. Cheng, S. Fang, S. Huang, P. Jia, A green element method-based discrete fracture model for simulation of the transient flow in heterogeneous fractured porous media, Advances in Water Resources 136 (2020) 103489.

[3] O. Ezulike, H. Dehghanpour, C. Virues, R. V. Hawkes, J. Jones, R. Steven, Flowback fracture closure: A key factor for estimating effective pore volume, SPE Reservoir Evaluation & Engineering 19 (04) (2016) 567–582. doi:10.2118/175143-PA.

[4] M. T. Balhoff, M. J. Miller, An analytical model for cleanup of yield-stress fluids in hydraulic fractures, SPE Journal 10 (01) (2005) 5–12. doi:10.2118/77596-PA.

[5] D. Birdsell, H. Rajaram, D. D. H. Viswanathan, Hydraulic fracturing fluid migration in the subsurface: a review and expanded modeling results, Water Resources Research 37 (2015) 1–30. doi:10.1002/2015WR017810.

[6] B. Zanganeh, M. Ahmadi, C. Hanks, O. Awoleke, The role of hydraulic fracture geometry and conductivity profile, unpropped zone conductivity and fracturing fluid flowback on production performance of shale oil wells, Journal of Unconventional Oil and Gas Resources 9 (2015) 103–113. doi:10.1016/J.JUOGR.2014.11.006.

[7] E. Ghanbari, H. Dehghanpour, The fate of fracturing water: A field and simulation study, Fuel 163 (2016) 282–294. doi:10.1016/j.fuel.2015.09.040.

[8] J. McLennan, I. Walton, J. Moore, D. Brinton, J. Lund, Proppant backflow: Mechanical and flow considerations, Geothermics 57 (2015) 224 – 237. doi:10.1016/j.geothermics.2015.06.006.

[9] J. Zeng, H. Li, D. Zhang, Numerical simulation of proppant transport in hydraulic fracture with the upscaling cfd-dem method, Journal of Natural Gas Science and Engineering 33 (2016) 264 – 277. doi:10.1016/j.jngse.2016.05.030.

[10] J. Hyman, J. Jiménez-Martínez, H. Viswanathan, J. Carey, M. Porter, E. Rougier, S. Karra, Q. Kang, L. Frash, L. Chen, Z. Lei, D. O'Malley, N. Makedonska, Understanding hydraulic fracturing: a multi-scale problem, Philosophical Transactions of the Royal Society A: Mathematical, Physical and Engineering Sciences 374 (2016) 20150426. doi:doi:10.1098/rsta.2015.0426.

[11] F. Wang, Z. Pan, Y. Zhang, S. Zhang, Simulation of coupled hydro-mechanical-chemical phenomena in hydraulically fractured gas shale during fracturing-fluid flowback, Journal of Petroleum Science and Engineering 163 (2018) 16 – 26. doi:10.1016/j.petrol.2017.12.029.

[12] J. Huang, J. Hu, W. Zeng, Y. Zhang, Investigation of a critical choke during hydraulic-fracture flowback for a tight sandstone gas reservoir, Journal of Geophysics and Engineering 16 (6) (2019) 1178–1190. doi:10.1093/jge/gxz088.

[13] A. Dana, Z. Zheng, G. G. Peng, H. A. Stone, H. E. Huppert, G. Z. Ramon, Dynamics of viscous backflow from a model fracture network, Journal of Fluid Mechanics 836 (2018) 828–849. doi:10.1017/jfm.2017.778.

[14] A. Dana, G. G. Peng, H. A. Stone, H. E. Huppert, G. Z. Ramon, Backflow from a model fracture network: an asymptotic investigation, Journal of Fluid Mechanics 864 (2019) 899–924. doi:10.1017/jfm.2019.39.

[15] A. Barbati, J. Desroches, A. Robisson, G. McKinley, Complex Fluids and Hydraulic Fracturing, Annu. Rev. Chem. Biomol. Eng. 7 (2016) 415–453. doi:10.1146/annurev-chembioeng-080615-033630.

[16] S. Hormozi, I. A. Frigaard, Dispersion of solids in fracturing flows of yield stress fluids, Journal of Fluid Mechanics 830 (2017) 93–137. doi:10.1017/jfm.2017.465.

[17] Y. Lester, T. Yacob, I. Morrissey, K. G. Linden, Can we treat hydraulic fracturing flowback with a conventional biological process? the case of guar gum, Environ. Sci. Technol. Lett. 1 (1) (2014) 133–136. doi:10.1021/ez4000115.

[18] A. Ipatova, D. Chuprakov, Role of preexisting rock discontinuities in fracturing fluid leakoff and flowback, Transport in Porous Media 135 (1) (2020) 137–180. doi:10.1007/s11242-020-01472-3.

[19] E. Detournay, Mechanics of hydraulic fractures, Annu. Rev. Fluid Mech. 48 (2016) 311–339. doi:10.1146/annurev-fluid-010814-014736.

[20] M. Wrobel, On the application of simplified rheological models of fluid in the hydraulic fracture problems, International Journal of Engineering Science 150 (2020) 103275. doi:10.1016/j.ijengsci.2020.103275.

[21] L. Chiapponi, V. Ciriello, S. Longo, V. Di Federico, Non-newtonian backflow in an elastic fracture, Water Resources Research 55 (12) (2019) 10144–10158. doi:10.1029/2019WR026071.

[22] A. Osiptov, Fluid mechanics of hydraulic fracturing: a review, Journal of Petroleum Science and Engineering 156 (2017) 513–535. doi:10.1016/j.petrol.2017.05.019.

[23] F.-E. Moukhtari, B. Lecampion, A semi-infinite hydraulic fracture driven by a shear-thinning fluid, Journal of Fluid Mechanics 838 (2018) 573–605. doi:10.1017/jfm.2017.900.

[24] S. Shah, N. H. Shanker, C. C. Ogugbue, Future challenges of drilling fluids and their rheological measurements, in: 2010 AADE Fluids Conference and Exhibition, Vol. AADE-10-DF-HO-41, Houston, Texas, 2010.

[25] T. G. Myers, Application of non-newtonian models to thin film flow, PRE 72 (6) (2005) 066302. doi:10.1103/PhysRevE.72.066302.

[26] V. Anand, J. David, I. C. Christov, Non-newtonian fluid-structure interactions: Static response of a microchannel due to internal flow of a power-law fluid, Journal of Non-Newtonian Fluid Mechanics 264 (2019) 62–72. doi:10.1016/j.jnnfm.2018.12.008.

[27] N. Ali, S. Hussain, K. Ullah, O. Anwar Beg, Mathematical modeling of two-fluid electro-osmotic peristaltic pumping of an ellis fluid in an axisymmetric tube, The European Physical Journal Plus 134 (4) (2019) 141. doi:10.1140/epjp/i2019-12488-2.

[28] M. Balhoff, K. Thompson, A macroscopic model for shear-thinning flow in packed beds based on network modeling, Chemical Engineering Science 61 (2) (2006) 698–719. doi:10.1016/j.ces.2005.04.030.

[29] A. Skelland, Non-Newtonian Flow and Heat Transfer, Wiley, 1967.

[30] A. Al-Behadili, M. Sellier, J. N. Hewett, R. I. Nokes, M. Moyers-Gonzalez, Identification of ellis rheological law from free surface velocity, Journal of Non-Newtonian Fluid Mechanics 263 (2019) 15 – 23. doi:10.1016/j.jnnfm.2018.10.010.

[31] R. T. Steller, Generalized slit flow of an ellis fluid, Polym Eng Sci 41 (11) (2001) 1859–1870. doi:10.1002/pen.10883.

[32] R. W. Zimmerman, G. S. Bodvarsson, Hydraulic conductivity of rock fractures, Transport in Porous Media 23 (1996) 1–30. doi:10.1007/BF00145263.

[33] J. Wang, D. Elsworth, M. K. Denison, Hydraulic fracturing with leakoff in a pressure-sensitive dual porosity medium, International

Journal of Rock Mechanics and Mining Sciences 107 (2018) 55–68. doi:10.1016/j.ijrmms.2018.04.042.

[34] B. Budiansky, R. J. O'Connell, Elastic moduli of a cracked solid, International Journal of Solids and Structures 12 (2) (1976) 81–97.

[35] V. Lyakhovsky, Z. Reches, R. Weinberger, T. E. Scott, Non-linear elastic behaviour of damaged rocks, Geophysical Journal International 130 (1) (1997) 157–166. doi:10.1111/j.1365-246X.1997.tb00995.x.

[36] M. K. Fisher, N. R. Warpinski, Hydraulic-fracture-height growth: Real data, SPE Production & Operations 27 (01) (2012) 8–19. doi:10.2118/145949-PA.

[37] I. S. Gradshteyn, I. M. Ryzhik, Table of integrals, series, and products, Academic Press, 2014.

[38] B. S. Massey, Units, dimensional analysis and physical similarity, Van Nostrand Reinhold, 1971.

Dear Editor:

We would like to thank you, the anonymous Reviewer and the Associate Editor for the positive assessment of our work and for the suggestions, which have helped us to further improve the presentation. Our detailed response to the Reviewer is given below. Her/his comments are reproduced in italic. The corresponding changes in the manuscript are typeset in blue.

Sincerely yours,

Valentina Ciriello
Alessandro Lenci
Sandro Longo
Vittorio Di Federico

Bologna, April 4th 2021

Reply to Reviewer #1

The manuscript presents an analytical solution for back-flow of a fracking fluid towards a well. The analysis is elegant and relevant to several subsurface applications. It is also innovative and well-described. For these reasons I recommend to publish this manuscript after the following issues are resolved.

We thank the Referee for this succinct summary of our contribution and for the positive assessment of our work. All the minor editorial changes suggested are incorporated in the revision.

The authors argue that "gravity effects are usually neglected when compared to pressure gradients" (page 4). What is a typical range of the Froude number encountered in this application?

We note that the gravity term can be included in a pressure term corrected by adding the hydrostatic pressure; this leads to a mathematical treatment with no gravity term to consider. We do so in the revised manuscript. For instance, for the Figure 3 representing multiple vertical fractures backflowing to an horizontal well, the reduced pressure p is equal to $p = p' + \rho g y$, with p' being pressure. The objection is then mute as no approximation is needed. *The authors assume that "the deformation is concentrated for convenience in the upper wall" (page 4). Convenience is not an adequate justification for the model construction. Perhaps the lower wall can be thought of as a line of symmetry (the middle of a fracture) instead?*

In a real fracture the deformation would be concentrated at both the upper and the lower wall. Under the one-dimensional approximation in the x direction adopted in the model, this makes no real difference as fluid velocities in perpendicular directions are neglected, and considering the squeezing of both walls would only complicate the notation. An alternative formulation is suggested by the reviewer, considering the lower wall as a line of symmetry and the fracture having aperture $2h$. As the word "'convenience"' by itself may appear misleading, for brevity and to maintain consistency of the model formulation with other references, we have changed the wording to ""'mathematical convenience"'"'.

Since the authors are concerned with back-flow towards a well where flow is divergent, treating it as a "planar flow" (do you mean uniform?) requires a better justification than "convenience" (see above).

The refereee is right in asking for a clarification, and the word "'simplicity"' in the original manuscript was misleading. We revised the whole paragraph explaining the approximation adopted for vertical fractures perpendicular to the horizontal borehole axis, and introducing the case of vertical fractures parallel to the borehole axis, where no appximation is needed. We also note that there was a typo in the "'Problem statement"' that read $L \ll W$ while the correct assumption to be listed is $L \gg W$. THe typo has been corrected and may have contributed to the reviewer's remark.

What does "the overload at the upper wall" mean in this context?

We added an additional sentence to better explain its meaning.

Abstract. Replace "independent on rheology" with "independent from rheology".

Done.

The phrase "parallelepide space" (page 4) is suspect.

The word is correct English, we substituted it with "3-D space" for ease of reading.

Replace "following Figure 3" with "Figure 3 below".

Done.

The phrase "shear flow of coordinates" (page 4) doesn't make sense.

We thank the reviewer, we corrected the sentence.

Replace "Figure eq. (2)" (page 6) with "Figure 2"

Done.

Replace "Figure (3)" (page 7) with "Figure 3"

Done.

Remove the indent in the lines following Eqs. 13 and 14.

Done.

What does "pure number" (page 9) mean?

An adimensional quantity in physics, a synonimous is "dimensionless", used elsewhere in the manuscript. We prefer to leave the sentence as is.

What does the phrase "solutions are analytical in space and numerical in time" mean?

We reformulated the sentence for ease of reading.

Highlights

- Our model handles realistic shear-thinning behaviour with upper-bounded apparent viscosity
- A dimensionless number reveals the relative importance of governing parameters during backflow
- Time to recover the fluid is compared for two hydrofracturing fluids showing significant differences

Relaxation-induced flow in a smooth fracture for Ellis rheology

Valentina Ciriello[1], Alessandro Lenci[1], Sandro Longo[1], Vittorio Di Federico[1]

[a]*Dipartimento di Ingegneria Civile, Chimica, Ambientale e dei Materiali (DICAM), Università di Bologna, Bologna (Italy)*
[b]*Dipartimento di Ingegneria e Architettura (DIA), Università di Parma, Parma, Italy*

Abstract

Hydraulic fracturing is a process aimed at improving the productivity of oil, gas or geothermal reservoirs. During hydrofracturing, backflow follows injection and represents the second phase of the process, when part of the fracturing fluid returns from fractures to well, and from well to surface. A conceptual model is presented to grasp the essential features of the phenomenon, conceiving the draining subsurface domain as a planar and rigid fracture. Backflow against an outlet pressure in the injection well is induced by the relaxation of the fracture wall, exerting a force on the fluid proportional to h^λ, with h the time-variable aperture and λ a non-negative exponent; an overload on the fracture may contribute to slowing or accelerating the closure process. The fluid rheology is described by the three-parameter Ellis constitutive equation, well representing the shear-thinning rheology typical of hydrofracturing fluids and coupling Newtonian and power-law behaviour. The interplay between these tendencies is modulated by a dimensionless number N encapsulating most problem parameters; the range of variation of N is discussed and found to vary around unity. The time-variable aperture and discharge rate, the space-time variable pressure field, and the time to drain a specified fraction of the fracture volume are derived as functions of geometry (length and initial aperture), wall elastic parameters, fluid properties, outlet pressure p_e and overload f_0. The late-time behaviour of the system is practically independent from rheology as the Newtonian nature of the fluid prevails at low shear stress. In particular, aperture and discharge scale asymptotically with time as $t^{-1/(\lambda+2)}$ and $t^{-1/(\lambda+3)}$ for $p_e - f_0 = 0$; else, the aperture tends to a constant, residual value proportional to $(p_e - f_0)^\lambda$. A case study with equally spaced fractures adopting realistic geometric, me-

chanical and rheological parameters is examined: two fluids normally used in fracking technology show completely different behaviours, with backflow dynamics and drainage times initially not dissimilar, later varying by orders of magnitude.

Key words:
Hydraulic fracturing, Non-Newtonian, Ellis rheology, elastic wall, backflow

---

1. Introduction

Hydraulic fracturing is a process aimed at improving the productivity of oil, gas or geothermal reservoirs. Analysis of the different phases of hydraulic fracturing is of particular modeling and experimental interest [e.g. **?** **?**].

An understanding of fractured media flow induced by the relaxation of elastic fracture walls is crucial in modeling fracturing fluid backflow, a complicated phenomenon involving hydrodynamic, mechanical and chemical processes. Backflow is typically the final phase of the hydraulic fracturing process: in the first one, fracturing fluid is injected at high pressure in a rock mass, forming new fractures and enlarging existing ones; in the second phase, proppant is introduced in the subsurface environment to prop fractures open; then when the injection ceases, the pressure drops, existing and new fractures tend to close, and a portion of the injected fracturing fluid, often mixed with proppant [**?**], flows back towards the injection well and interact with the relaxing walls of the fractures. As the retention of fracturing fluid in the fracture network impairs the fracture conductivity reducing the wellbore productivity [**?**], and favours migration in the subsurface environment along different pathways [**?**], it is of utmost interest to optimize the amount of fluid recovered, irrespective of the reservoir product, be it oil [**?**], gas [**?**] or heat [**?**].

The scientific literature offers two main approaches to modeling backflow: (i) detailed numerical simulations involving single fractures [**?**], fracture networks [**?**] or dual or triple porosity models [**?**], or (ii) conceptual models capturing the main features of the interaction between fracture flow and wall relaxation [**?**], including the effects of branching networks described at different degrees of complexity [**?** **?**]. A recent addition to the modeling effort is the influence of fluid rheology, following the notion that the backflow fluid is non-Newtonian in the widest sense [**?**], as not only the relationship between shear stress and shear rate is nonlinear, but also exhibits normal

stress and temperature dependency, as well as viscoelasticity, thixotropy, and nonzero yield stress [**?**]. At the same time, non-Newtonian fluids allow achieving several engineering objectives, such as (i) minimize the pressure-drop in the entire process; (ii) carry suspended proppant; (iii) minimize the leak-off within the formation; (iv) adapt their characteristics to different environments in terms of temperature and chemical composition; and (v) flow back easily towards the wellbore. Given their versatility and economic value, these fluids are typically treated for reuse once recovered, removing contaminants they may have transported to the surface [**?**]. The recovery ratios of backflow fluid vary between 2% and 48% according to Ipatova and Chuprakov [**?**], with considerable economic value.

Modeling non Newtonian backflow is in its early stage, in variance with the injection and fracture formation stage, for which several conceptualizations and models are available: see Detournay [**?**] for a review and the recent work by Wrobel [**?**] comparing different rheological models for fracturing fluids. To the best of our knowledge, only Chiapponi et al. [**?**] considered non-Newtonian fluids in the context of backflow modeling: these authors examined flow of a power-law fluid towards a wellbore in a single fracture of annular geometry, supporting their theoretical findings with laboratory experiments. The present paper develops the analysis of non-Newtonian backflow for a smooth fracture, common in field applications [**?**], and adds realism by employing a three-parameter Ellis model, that well represents the rheology of hydrofracturing [**?**] and drilling fluids [**?**]. The Ellis model tends to Newtonian for low shear rates, to power-law for high shear rates and allows avoiding the unphysical effect of infinite apparent viscosity at zero shear rate that is typical of the power-law model [**?**]. We note in passing that our results are of a general nature for Newtonian pressurized flow in ducts of variable width and may be of interest for, and be applied also to, deformable microfluidic [**?**] and biological [**?**] systems.

The plan of the paper is as follows. Section 2 formulates the problem of relaxation-induced backflow of an Ellis fluid in a fracture with nonlinear wall reaction and subject to overload. Numerical results obtained are presented and discussed in Section 3 as a function of dimensionless groups characterizing the system: the indicial exponent α quantifying the degree of shear-thinning behaviour of the Ellis fluid, the non-negative exponent λ modulating the fracture wall reaction, and a further group N encapsulating most problem parameters. Section 4 illustrates an hypothetical case study adopting realistic geometric and mechanical parameters and two real hy-

drofracturing fluids decribed by the Ellis model. Section 5 reports the main conclusions and perspectives for future work. In Appendix A the special case of a Newtonian fluid is examined, obtaining results that generalize those of Dana et al. [**?**] to a nonlinear wall reaction, while Appendix B presents an alternative expression for the dimensionless number N, shown to be a combination of well-known dimensionless groups in fluid mechanics.

2. Material and methods

2.1. Problem statement

A rock fracture produced by hydrofracturing, though of irregular geometry, is often conceptualized for modeling purposes as a 3-D space of length L, width W, and aperture h between two parallel walls [**?**]; the Cartesian coordinate system x, y, z is illustrated in Figure **??** and the fracture is subject to a pressure gradient $\nabla p' \equiv (\partial p'/\partial x, 0, 0)$ in the x direction. In horizontal fractures, the additional gravity-induced pressure gradient is perpendicular the flow plane and has no effect on the flow field. If the (x, y) plane is not horizontal, the z direction perpendicular to the walls is not vertical and gravity effects can be included in a reduced pressure term p, thus leading to a mathematical treatment with no gravity term to consider. For instance, for the Figure **??** below representing multiple vertical fractures backflowing to an horizontal well, the reduced pressure p is equal to $p = p' + \rho g y$.

The walls are taken to be rigid, so that the aperture $h(t)$ is solely a function of time, and the deformation is concentrated for mathematical convenience in the upper wall, that behaves as a nonlinear elastic foundation exerting a reaction on the fluid. At $t = 0$ the relaxation of the wall induces a backflow in the negative x direction, and the fracture begins to drain subject to a constant outlet pressure p_e at $x = 0$ and to a no-flow boundary condition at the upstream end $x = L$. Three further hypotheses are adopted: i) the flow is quasi-steady, allowing to neglect the time derivative of the velocity in the momentum equation; ii) the fracture aspect ratio is small, $h_0/L \ll 1$, warranting the lubrication approximation, and iii) the flow is essentially one-dimensional along x, $L \gg W$. The latter conceptualization is usually adopted in hydrogeology also when the two dimensions are comparable, as it is often the case for rock fractures [**?**].

The flowback fluid is taken to be incompressible of density ρ, non-Newtonian shear-thinning [**?**] and described by the Ellis three-parameter model [**?**]. Under the above assumptions, the fluid undergoes simple shear flow in the

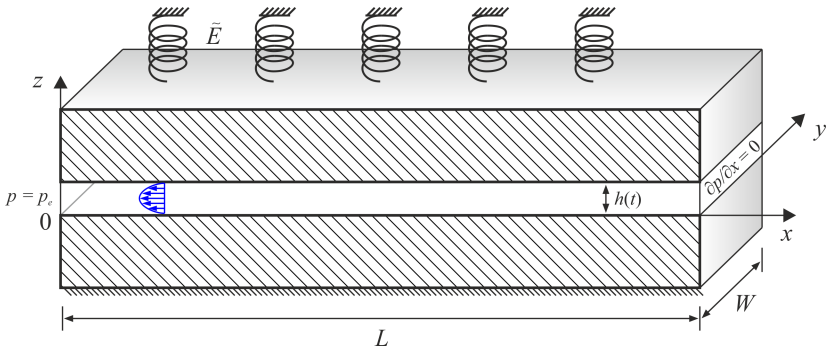

Figure 1: Layout of a plane fracture of variable uniform aperture $h(t)$.

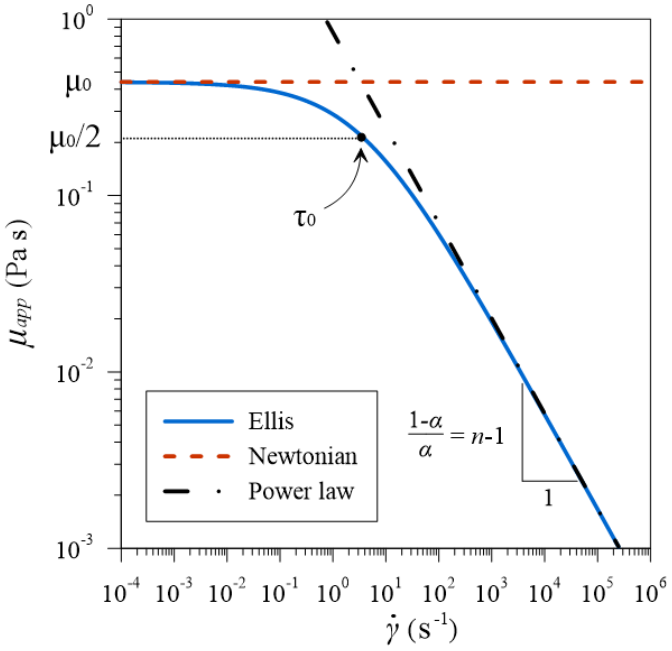

Figure 2: Apparent viscosity for three rheological models: Ellis (blue solid line) of parameters μ_0, τ_0, α; Newtonian (red dashed line) of viscosity μ_0; power-law (black dot-dashed line) of consistency index m and rheological index n. The comparison with the latter is drawn assuming: $\alpha = 1/n$ and $\tau_0 = (m/\mu_0^n)^{n/(1-n)}$.

x direction, and the Ellis rheology is described by the following relationship between shear stress τ_{zx} (hereinafter τ) and shear rate $\dot{\gamma}_{zx}$ (hereinafter simply $\dot{\gamma}$)

$$\tau = \frac{\mu_0}{1 + (\tau/\tau_0)^{\alpha-1}}\dot{\gamma}; \quad \dot{\gamma} = \frac{\partial u}{\partial z}, \tag{1}$$

where u is the velocity in the x direction. The rheological law (**??**) features a viscosity parameter μ_0, a constant τ_0 defined as the shear stress corresponding to apparent viscosity $\mu_0/2$, and an indicial parameter α, typically larger than one as the fluid is shear-thinning. For $\alpha = 1$, a pseudo-Newtonian behaviour with dynamic viscosity $\mu_0/2$ is recovered, see Figure **??** showing the apparent viscosity $\mu_{app} = \tau/\dot{\gamma}$ for the Ellis model compared to Newtonian and power-law models. Newtonian behaviour in the form of a plateau for low shear rates is also observed for $\gamma \to 0$. For high shear rates the behaviour is power-law, and its two parameters can be determined from the Ellis model parameters, see Appendix A in Balhoff and Thompson [**?**]; in particular, the rheological index is $n = 1/\alpha$ [**?**]. Note that when curve fitting is performed on real data, n and $1/\alpha$ may significantly differ [**?**], as two different models are fitted to the same data set. It is also seen that the Ellis model allows avoiding the unphysical effect of infinite apparent viscosity at zero shear rate that is typical of power-law fluids [**?**]. In the following, we will consider $\alpha > 1$, dealing with the case $\alpha = 1$ in the Appendix, and the parameters μ_0 and τ_0 to be finite and positive. Couette-Poiseuille slit flow of an Ellis fluid under a constant pressure gradient was studied extensively by Steller [**?**], listing all combinations of parameters leading to Newtonian or pseudo-Newtonian behaviour. In particular, the negative velocity $u(z)$ under a positive reduced pressure gradient $\partial p/\partial$ in the x direction is

$$\begin{aligned} u(z,t) = -\frac{1}{8\mu_0}\left[h^2 - (2z-h)^2\right]\frac{\partial p}{\partial x} + \\ - \frac{1}{(\alpha+1)2^{\alpha+1}\mu_0\tau_0^{\alpha-1}}\left[h^{\alpha+1} - |2z-h|^{\alpha+1}\right]\frac{\partial p}{\partial x}\left|\frac{\partial p}{\partial x}\right|^{\alpha-1}. \end{aligned} \tag{2}$$

The corresponding average velocity $\overline{u}$ and flow per unit width q_x in the x direction are

$$\overline{u} = -\frac{h^2}{12\mu_0}\frac{\partial p}{\partial x} - \frac{h^{\alpha+1}}{2^{\alpha+1}(\alpha+2)\mu_0\tau_0^{\alpha-1}}\frac{\partial p}{\partial x}\left|\frac{\partial p}{\partial x}\right|^{\alpha-1}; q_x = \overline{u}h. \tag{3}$$

For the Newtonian case ($\alpha = 1$) the latter equation reduces to the classical "cubic law" [**?**] written for a fluid with viscosity $\mu_0/2$. The continuity equation reads [**?**]

$$\frac{\mathrm{d}h}{\mathrm{d}t} + h(t)\frac{\partial \overline{u}}{\partial x} = 0, \tag{4}$$

and substituting eq. (**??**) in eq. (**??**) gives

$$\frac{\mathrm{d}h}{\mathrm{d}t} = \frac{h^3}{12\mu_0}\frac{\partial^2 p}{\partial x^2} + \frac{\alpha h^{\alpha+2}}{2^{\alpha+1}(\alpha+2)\mu_0\tau_0^{\alpha-1}}\left|\frac{\partial p}{\partial x}\right|^{\alpha-1}\frac{\partial^2 p}{\partial x^2}. \tag{5}$$

The problem formulation is completed by the force balance, expressed per unit width of fracture, among the fluid pressure and the elastic reaction of the upper wall, taken to be proportional to aperture h; an overload at the upper wall f_0 (a force per unit width) is included in the balance for generality [**?**]; the overload represents an additional force exerted by the walls and usually opposing the fracture opening due, e.g., to a residual stress state generated by the load history of the rocks. It is assumed constant and independent from the fracture aperture. The balance reads

$$\int_0^L p(x,t)\,\mathrm{d}x = \tilde{E}Lh(t) + f_0, \tag{6}$$

where the constant of proportionality $\tilde{E}$ has dimensions $[ML^{-2}T^{-2}]$; for a linear elastic foundation, called a Winkler soil in geotechnical applications, $\tilde{E}$ is equal, for a thin elastic layer of thickness l, to the ratio between the Young modulus of the layer's material E $[ML^{-1}T^{-2}]$ and l, $\tilde{E} = E/l$. In the context of hydraulic fracturing, l may be identified with the fracture spacing [**?** **?**], a design parameter that depends, among others, on the type of rock; in hydraulically fractured shales, values of l/L equal to 0.057, 0.28, and 0.029 are reported, respectively, by Ghanbari and Dehghanpour [**?**], Wang et al. [**?**], and Wang et al. [**?**]. In the case of vertical/sub-vertical fractures perpendicular to a horizontal/sub-horizontal well or borehole, the geometry of the idealized system is described by Figure **??**, showing the two wings of equally spaced planar fractures of half-length L, width W, aperture h and spacing l. Albeit the flow very close to the well is radial, the influence of the boundary condition at the well decreases rapidly with distance, and flow in most of the fracture half-length L is uniform, consistently with the assumption $L \gg W$. Hence, as an approximation the boundary condition of assigned pressure p_e at the well is extended to a segment of height W. In the

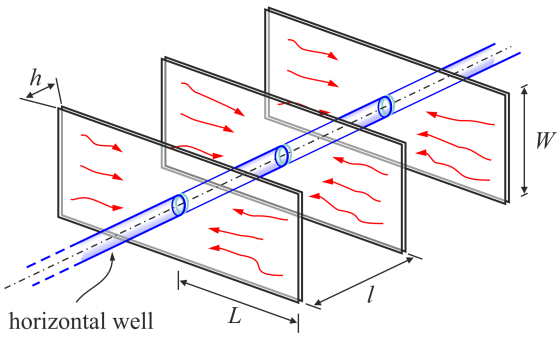

Figure 3: Typical scheme for bi-wing planar fractures around a horizontal borehole; L, W and h are the fracture length, width and aperture, l is the fracture spacing.

case of planar vertical fractures parallel to, and propagating from, a vertical well, the geometry of the flow is plane without using this approximation.

A further issue deserving investigation is the linearity of the relationship between the wall reaction and the fracture aperture. In fact, a nonlinear elastic behaviour can be the result of the pervasive damage of rocks by micro-cracks and voids, which determines nonlinearity even for infinitesimal strain, also with an incremental jump in the elastic modulus from tension to compression [**? ?**]. In this case the Young modulus of the material is a function of the strain rate, $E = E_0(h/l)$, and assuming that the latter dependence is expressed with a power-law function one has

$$E = E_0 \left(\frac{h}{l}\right)^{\lambda-1}, \tag{7}$$

where λ is a non-negative exponent modulating the nature of the reaction: for $\lambda = 1$ a constant Young modulus is recovered, while $0 < \lambda < 1$ is associated to a softening behaviour, and $\lambda > 1$ to a stiffening one. The assumption results in

$$\tilde{E} = \frac{E_0}{l}\left(\frac{h}{l}\right)^{\lambda-1} \equiv \hat{E}h^{\lambda-1}, \tag{8}$$

and eq. (**??**) is modified as

$$\int_0^L p(x,t)\,\mathrm{d}x = \hat{E}Lh^{\lambda}(t) + f_0, \tag{9}$$

with $\hat{E} = E_0 l^{-\lambda}$ of dimensions $[ML^{-1-\lambda}T^{-2}]$.

Equations (??) and (??) are subject to the following initial and boundary conditions

$$h(0) = h_0, \quad \frac{\partial p(x,t)}{\partial x}(L,t) = 0, \quad p(0,t) = p_e, \tag{10}$$

h_0 being the initial fracture aperture, and p_e the exit pressure at the well.

The solution to the above problem yields two relevant quantities expressed per unit width, the flowrate exiting the fracture at the well, $q(t)$, and the residual volume of the fracture at a given time, $v(t)$; these are easily derivable as

$$q(t) = L\frac{\mathrm{d}h(t)}{\mathrm{d}t}, \quad v(t) = Lh(t). \tag{11}$$

2.2. Dimensionless form

Dimensionless quantities are defined as

$$\begin{aligned} X = x/L,\, H = h/h_0, T = t/t_c,\, P = (p - p_e)/p_c,\, P_e = p_e/p_c, \\ Q = qt_c/(h_0 L) = q/(u_0 h_0),\, V = v/(h_0 L), \end{aligned} \tag{12}$$

where the scales for pressure and time are

$$p_c = \hat{E} h_0^{\lambda}, \quad t_c = \frac{(2+\alpha)}{\alpha}\left(\frac{2L}{h_0}\right)^{1+\alpha} \frac{1}{h_0^{\alpha\lambda}} \frac{\mu_0 \tau_0^{\alpha-1}}{\hat{E}^{\alpha}}, \tag{13}$$

and $u_0 = L/t_c$ is a velocity scale. This leads to the dimensionless counterpart of eq. (??)

$$\frac{\mathrm{d}H}{\mathrm{d}T} = NH^3 \frac{\partial^2 P}{\partial X^2} + H^{\alpha+2}\left(\frac{\partial P}{\partial X}\right)^{\alpha-1} \frac{\partial^2 P}{\partial X^2}, \tag{14}$$

where the pure number

$$N = \frac{2+\alpha}{3\alpha}\left(\frac{2\tau_0 L}{\hat{E} {h_0}^{\lambda+1}}\right)^{\alpha-1} = \frac{2+\alpha}{3\alpha}\left[\frac{2\tau_0}{p_c(h_0/L)}\right]^{\alpha-1} \tag{15}$$

modulates the relative importance of the Newtonian behaviour of the Ellis fluid at low shear rate, expressed by the first term on the r.h.s. of eq. (??), with respect to the second term, the power-law behaviour at high shear rate. For a Newtonian fluid ($\alpha = 1$) N reduces to unity; for a shear-thinning fluid ($\alpha > 1$), N is zero for $\tau_0 = 0$ and/or a rigid wall ($\hat{E} = E_0/l^{\lambda} \to \infty$), but the latter case renders the scales (??) meaningless. In eq. (??) defining N, the quantity within brackets represents the ratio between the characteristic

shear stress τ_0 of the Ellis fluid and the pressure scale $p_c = \hat{E} {h_0}^{\lambda}$ associated with the elastic reaction of the fracture wall; the ratio is in turn corrected by the initial aspect ratio of the fracture h_0/L. This formulation of N includes only parameters defined at the single fracture scale. Note that if the scheme of multiple fractures with spacing l depicted in Figure **??** is considered, eq. (**??**) may be rewritten as

$$N = \frac{2+\alpha}{3\alpha} \left[\frac{2\left(\frac{\tau_0}{E_0}\right)\left(\frac{l}{L}\right)}{\left(\frac{h_0}{L}\right)^2} \frac{\left(\frac{l}{L}\right)^{\lambda-1}}{\left(\frac{h_0}{L}\right)^{\lambda-1}} \right]^{\alpha-1} , \tag{16}$$

where τ_0/E_0 is the ratio between the representative shear stress of the fluid and the Young modulus of the host rock, and l/L is the dimensionless fracture spacing. The terms to the power $(\lambda - 1)$ represent the contribution due to non-linear elastic behaviour of the walls, and disappear for $\lambda = 1$. An alternative formulation of N as a function of Cauchy, Reynolds, and Ellis dimensionless groups is reported in **??**. To grasp the order of magnitude of N, we recall that l/L may be taken to vary between 0.03 and 0.3 (with $l/L \approx 0.1$ being appropriate for an order of magnitude analysis), while the initial fracture aspect ratio h_0/L, a number much smaller than 1, may be considered of order $10^{-3} - 10^{-5}$ [**?** **?** **?**]. The latter reference also reports $E_0 = 2.5 \cdot 10^{10}$ Pa for the rock elastic modulus in fractured shales; quite close values, $E_0 = 3 \cdot 10^{10}$ Pa and $E_0 = 2.76 \cdot 10^{10}$ Pa are reported in [**?**] and [**?**], hence reference values $E_0 = 2.5 - 3.0 \cdot 10^{10}$ Pa are considered.

Actual values of rheological parameters for Ellis fluids are quite scarce in the literature. A reference specific to fracking is [**?**], where the Ellis parameters are reported for two fracturing fluids, HPG (Hydroxypropylguar) and VES (viscoelastic surfactant). For the first, $\mu_0 = 0.44$ Pa $\cdot$ s, $\tau_0 = 2.01$ Pa, and $\alpha = 1.22$; for the second, $\mu_0 = 49$ Pa $\cdot$ s, $\tau_0 = 8.836$ Pa, and $\alpha = 12$. Adopting as reference geometrical parameters $l/L = 0.1$ and $h_0/L = 10^{-4}$, and a young modulus of $E_0 = 2.75 \cdot 10^{10}$ Pa for the host rock, one obtains $N = 0.209$ for HPG and $N \simeq 0$ for VES, indicating that for the latter fluid the Newtonian component of rheological behaviour is negligible. A further consideration is that VES is very strongly shear-thinning ($\alpha \gg 1$), therefore the value of N is extremely sensitive to variations in parameters: adopting for example $l/L = 0.125$, $h_0/L = 10^{-5}$, and $E_0 = 2.5 \cdot 10^{10}$ Pa, again realistic values, one obtains $N = 0.100$ for VES and $N = 0.618$ for HPG. This second

set of parameters is adopted for later reference in Section **??** describing a case study and is shown there in dimensional form (see Table **??**). Trying further combinations of realistic values for fluid and rock properties, it is seen that N may take values smaller or larger than unity, the former case being more frequent. This indicates a certain prevalence of the power-law component of rheology over the Newtonian one, although the asymptotic system behaviour is dominated by the latter, as will be shown in the next section. We bear in mind that a large variety of combinations is possible for the two parameters N and α depending on geometry and properties of fluid and rock, but with the constraint from the definition (**??**) that for $\alpha = 1$ it must be $N = 1$.

The dynamic boundary condition (**??**) and the boundary conditions (**??**) transform as

$$\int_0^1 P(X,T)\,\mathrm{d}X = H^\lambda - P_e + F_0, \tag{17}$$

$$H(0) = 1, \quad \frac{\partial P}{\partial X}(1,T) = 0, \quad P(0,T) = 0. \tag{18}$$

2.3. Solution

A solution to eq. (**??**) is sought by integrating in two steps the pressure of the fluid and the fracture aperture. Posing

$$U(X,T) = \frac{\partial P}{\partial X}, \quad \dot{H} = \frac{\mathrm{d}H}{\mathrm{d}T}, \tag{19}$$

eq. (**??**) can be written as

$$B\left(1 + AU^{\alpha-1}\right)\frac{\partial U}{\partial X} = \dot{H} \tag{20}$$

where

$$A = A(T) = \frac{(H)^{\alpha-1}}{N}, \quad B = B(T) = NH^3, \tag{21}$$

while the second boundary condition in eq. (**??**) becomes

$$U(1,T) = 0. \tag{22}$$

Separating variables in eq. (**??**), and integrating with the boundary condition (**??**) leads to

$$\frac{BU\left(AU^{\alpha-1} + \alpha\right)}{\alpha} = -\dot{H}(1 - X). \tag{23}$$

Eq. (**??**) can be rewritten as

$$U^\alpha + CU + D(1-X) = 0 \tag{24}$$

where

$$C = C(T) = \frac{\alpha N}{H^{\alpha-1}}, \quad D = D(T) = \frac{\alpha \dot{H}}{H^{2+\alpha}}. \tag{25}$$

Eq. (**??**) is algebraic in U and admits an analytical solution for $\alpha = 1, 2, 3$ and for $\alpha = 1/2, 1/3$ in the form of a combination of functions of H and $\dot{H}$. This solution can be integrated once in space, with the boundary condition $P(0,T) = 0$, obtaining the pressure field. The pressure field is finally integrated in $X \in [0,1]$ and the integral in eq. (**??**) is computed as a function of H and $\dot{H}$. Then eq. (**??**) is transformed in a nonlinear ODE which is numerically integrated with the initial condition $H(0) = 1$.

These solutions are analytical in the x coordinate and numerical in the time domain and seem quite cumbersome, while their accuracy is comparable to that of a fully numerical solution in space and time; the latter also has the advantage of a free selection of the indicial parameter α. Among the many possible numerical schemes, we adopt a finite difference in time and an implicit resolver in space, with a step size reduction to track solution accurately.

The code is written in Mathematica, introducing a parametric solver for the function $U(X,T)$ as a function of $N, \alpha, H_{i+1}, H_i, \Delta t$, where H_{i+1} and H_i are the values at time $(i+1)\Delta t$ and $i\Delta t$, respectively; the only free parameter is H_{i+1}, all the other parameters are given.

Each time iteration includes the following steps:

- The function $U(X)_{i+1}$ is estimated by solving eq. (**??**) in parametric form, with $\dot{H} \approx (H_{i+1} - H_i)/\Delta t$, with the term H taken to be the average between H_{i+1} and H_i and with the b.c. $U(1)_{i+1} = 0$, where H_{i+1} is the free parameter; $H_0 = 1$ is assumed at the first step.

- The space values of U, known in parametric form, are used to solve the differential problem $\partial P(X)_{i+1}/\partial X = U(X)_{i+1}$, with $P(0)_{i+1} = 0$, obtaining the pressure $P(X)_{i+1}$.

- The pressure field is numerically integrated (in parametric form) in the domain $[0,1]$.

- The parametric integral is inserted in eq. (**??**), and the equality is forced with a Newton method for finding the value of the parameter H_{i+1}.

- The procedure is repeated for the next time step, shifting the values H_{i+1}.

Once the pressure $P(X,T)$ and aperture $H(T)$ fields are known, the dimensionless flowrate and fracture volume are given by

$$Q(T) = \frac{\mathrm{d}H(T)}{\mathrm{d}T} = \dot{H}, \quad V(T) = H(T). \tag{26}$$

Hence at late-time the fracture volume and flowrate behave like the aperture and its time derivative, respectively; for zero borehole pressure and overload the corresponding time scalings are $T^{-1/(\lambda+2)}$ and $T^{-1/(\lambda+3)}$.

3. Results and discussion

Figure **??** shows the results of the numerical computation for the fracture aperture and different α values, with the analytical solution $H = (1+9T)^{-1/3}$ valid for the Newtonian case and a linearly elastic fracture [**?**], corresponding to $\alpha = 1$, $N = 1$, and $\lambda = 1$. Note that the values $\alpha = 1$, $N = 1$ imply Newtonian behaviour but with a viscosity equal to $\mu_0/2$, thus halving the time scale t_c in eq. (**??**); this requires doubling the dimensionless time T in eq. (**??**) to compare results of equations having a different time scale. The time integration was performed with a time step $\Delta t = 0.01$. Since the results of the numerical integration using this fully explicit scheme fit exceedingly well the analytical solution, it was not necessary to adopt higher order schemes, even considering that the solution has no singularity and behaves rather smoothly.

The asymptotic behaviour of the solution $H(T)$ is dictated by the interplay between the two terms on the r.h.s. of eq. (**??**): the second term scales with the gradient pressure (decaying in time) and with a power of H always larger than 3, since $\alpha > 1$, whereas the first term scales with the third power of H and has N as a coefficient. Since $H \leq 1$ and the gradient pressure quickly decays to values less than unity, the dominant term is the first one, which entails the asymptotic behaviour $H \sim T^{-1/(2+\lambda)}$, see Figure **??** where different values of α, for $N = 1$ and $P_e = 0$, produce almost parallel curves for large T. Figure **??** also shows how variations in λ significantly affect the

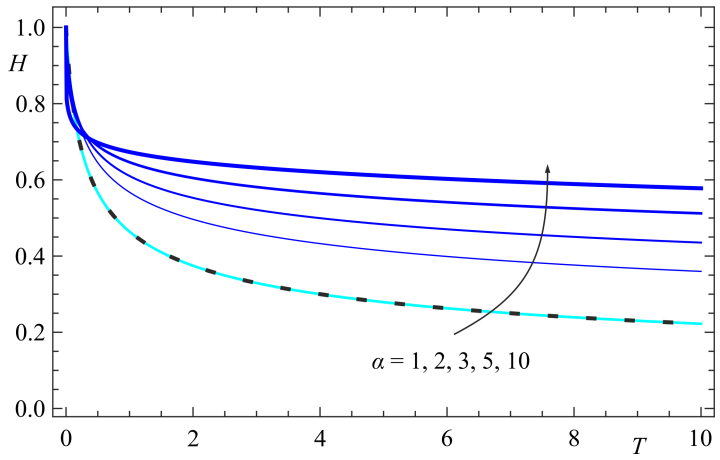

Figure 4: Time variation of the fracture aperture H for $N = 0$, $\lambda = 1$, $P_e - F_0 = 0$ and different α values. The black dotted curve refers to the analytical solution for a Newtonian fluid, $H = (1+9T)^{-1/3}$. Due to the different time scales adopted for a Newtonian fluid and for the present model, comparison is feasible if the dimensionless time T in the solution for the Newtonian fluid is doubled.

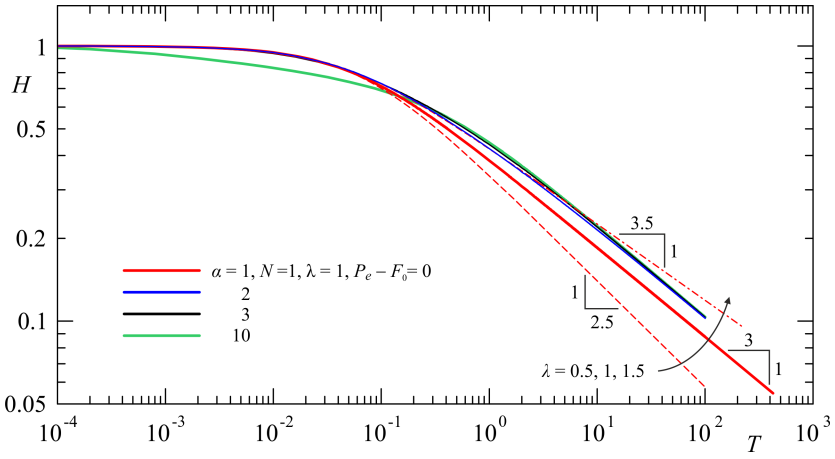

Figure 5: Time variation of the fracture aperture H for $N = 1$, $\lambda = 1$ and different α values. For one case ($\alpha = 1$) the effects of a softening/stiffening wall is explored, see the dashed and dash-dotted thin curves for $\lambda = 0.5 - 1.5$, respectively. The asymptotic behaviour is $H \sim T^{-1/(2+\lambda)}$, independent on α.

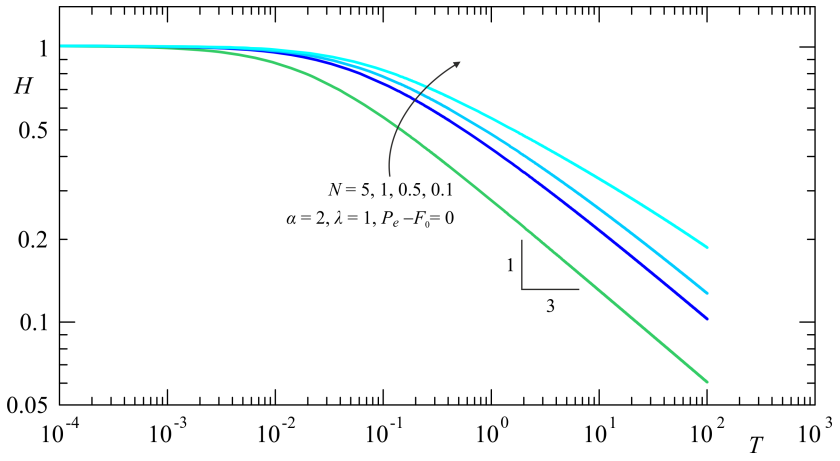

Figure 6: Time variation of the fracture aperture H for $\alpha = 2$, $\lambda = 1$ and different N.

late-time behaviour for fixed α: a stiffening ($\lambda > 1$)/softening ($\lambda < 1$) elastic reaction of the walls delays/facilitates the drainage. It is also seen that the parameter α mainly controls the early stage, the parameter λ the late stage of the backflow process. Figure **??** shows results for a fixed $\alpha = 2$, $\lambda = 1$, and different N values; the asymptote is reached much faster for larger N. In sum, the early time behaviour for zero external pressure at the well is in general dominated by the second term in eq. (**??**) unless the coefficient $N \gg 1$; in the latter case both terms substantially contribute to the time evolution of H.

In presence of a non-zero external pressure ($P_e > 0$) or a negative overload F_0 (an additional force per unit of wall surface acting in the same direction of the internal pressure), the asymptotic residual aperture is equal to $(P_e - F_0)^{1/\lambda}$, see Figure **??** where both effects are included. The curves coalesce to the asymptote faster for larger N values, implying a dominance of the Newtonian behaviour, while for small N the power-law behaviour prevails and the asymptote is reached for larger dimensionless times. Upon plotting results for $\alpha = 3$ (not shown) the main curves for $\lambda = 1$ and the secondary curves for $\lambda \neq 1$ are very similar to those for $\alpha = 2$.

Figure **??** shows the pressure distribution for two different combinations of the parameters and a shear-thinning fluid with $\alpha = 2$. Results for other combinations are similar (and thus not shown), with a pressure decay in space/time quicker or slower depending on the parameter values; at all times the residual pressure within the fracture increases with smaller N values,

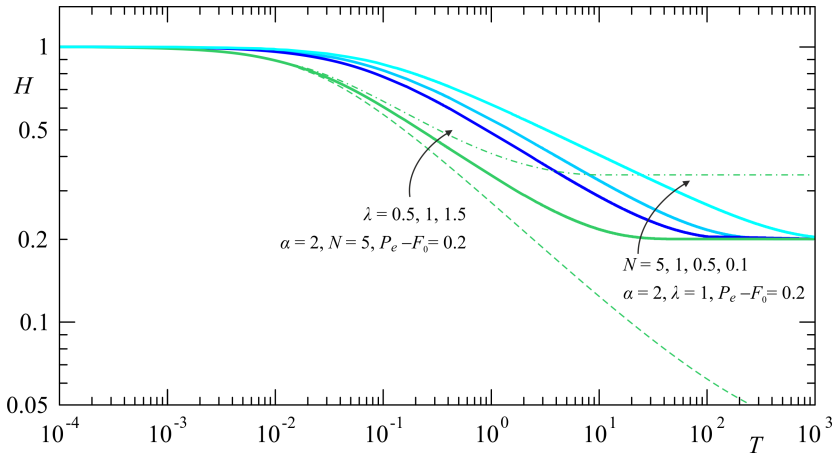

Figure 7: Time variation of the fracture aperture H for $\alpha = 2$ and different N values, with given difference between external pressure and overload $P_e - F_0 = 0.2$. For one case ($N = 5$) the effects of a stiffening/softening elastic reaction of the walls is explored, see the dashed and dash-dotted thin curves for $\lambda = 0.5 - 1.5$, respectively.

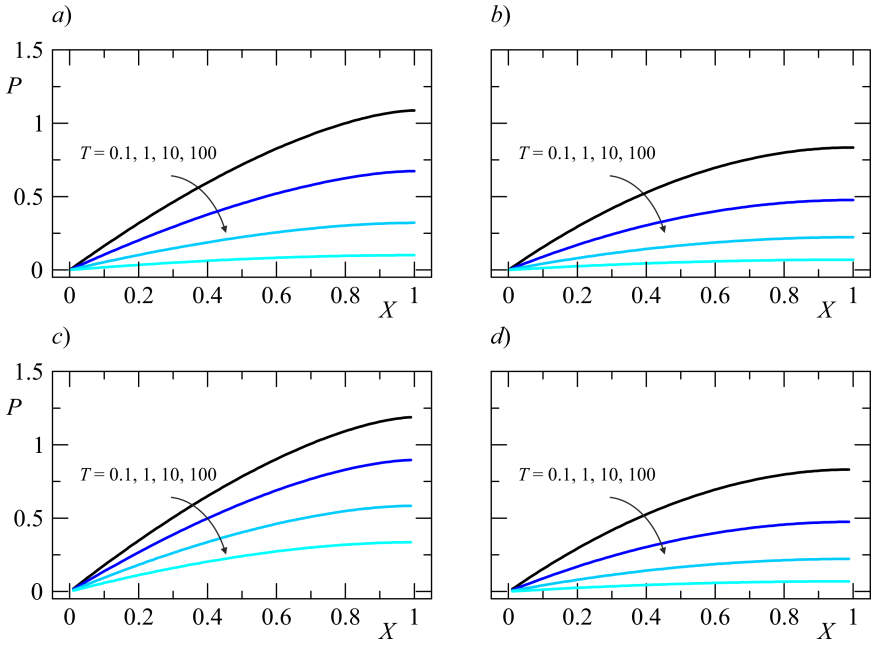

Figure 8: Pressure along the fracture at different times for $P_e - F_0 = 0.2$ and a shear-thinning fluid with $\alpha = 2$. Results for *a*) $N = 0.1$ and $\lambda = 1$; *b*) $N = 5$ and $\lambda = 1$; *c*) $N = 0.1$ and $\lambda = 0.5$; *d*) $N = 5$, $\lambda = 0.5$.

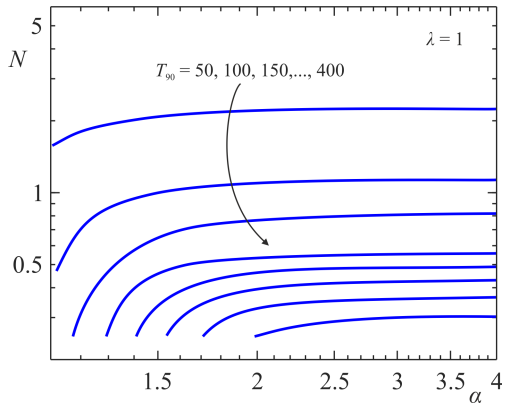

Figure 9: Time to recover 90% of the fluid as a function of α and N, with $\lambda = 1$ and $P_e - F_0 = 0$.

implying a behaviour closer to Newtonian, and with smaller λ values, i.e. a softening wall; however when the fluid is closer to Newtonian the effect of a λ variation is irrelevant.

An important quantity characterizing the performance of the backflow process is the time required to recover the fluid injected in the fracture network and not lost in the form of leakoff. Here the network is conceptualized as a single fracture and fluid losses are not explicitly represented (they are assumed to take place in the upstream network), however the time T_Y needed to recover Y% of the fracture volume provides an indication of how rapid the recovery is. Contour maps in the (α, N) space of the dimensionless time T_{90} needed to recover 90% of the fluid are depicted in Figure **??** for a linear wall reaction ($\lambda = 1$). As the degree of shear-thinning behaviour rises with α for constant N, there is a sharp increase in dimensionless T_Y for $N < 0.5$, while T_Y is almost independent on α for $N > 2$. Conversely, T_Y for costant α decreases with larger N values, i.e. as the fluid behaviour is closer to Newtonian; this effect is more evident for larger α. Highest values of T_Y are attained for large α and low N, lowest values for small α and large N, the two combinations farthest and closest to Newtonian behaviour. The effect of a sublinear wall reaction ($\lambda = 0.5$) is depicted in Figure **??**, that of a supralinear wall reaction in Figure **??**. The dimensionless time to recover the bulk of the stored fluid is decidedly faster or slower with a softening or stiffening wall, demonstrating once again the decisive influence of the parameter λ modulating the wall reaction at late time.

A word of caution is needed when drawing comparisons between non-

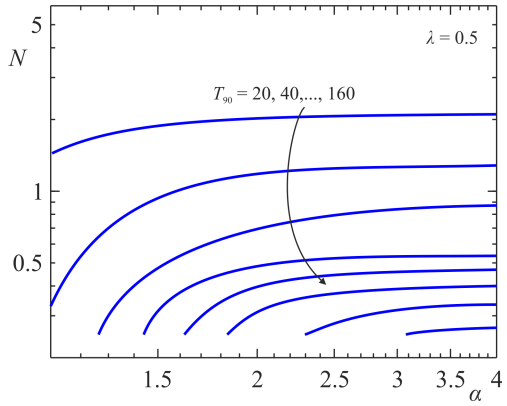

Figure 10: Time to recover 90% of the fluid as a function of α and N, with $\lambda = 0.5$ and $P_e - F_0 = 0$.

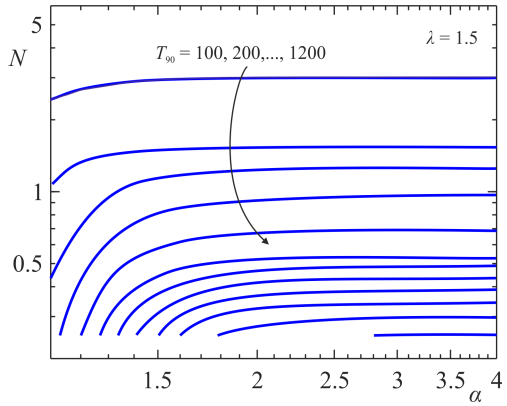

Figure 11: Time to recover 90% of the fluid as a function of α and N, with $\lambda = 1.5$ and $P_e - F_0 = 0$.

Fluid	μ_0 (Pa s)	τ_0 (Pa)	α	L (m)	l (m)	h_0 (mm)	E (Pa)	λ	N
HPG	0.44	2.01	1.22	100	12.5	1.00	$2.5 \cdot 10^{10}$	1.00	0.618
VES	49.00	8.836	12.00	100	12.5	1.00	$2.5 \cdot 10^{10}$	1.00	0.100

Table 1: Reference parameters for case study: μ_0, τ_0 and α are the reference viscosity, shear stress and indicial exponent of the Ellis fluid, L is the fracture length, l is the fracture spacing, h_0 is the fracture initial height, E is the rock modulus of elasticity, λ is the exponent of the rock wall reaction, N is the dimensionless number governing the interplay between Newtonian and power-law behaviour in an Ellis fluid.

Newtonian fluids with different rheology as the models are semi-empirical and the time scale used for the dimensionless formulation depends upon the rheological parameters of the Ellis model and is particularly sensitive to the value of the indicial exponent α. Hence model outputs are best compared in dimensional coordinates when quantitative results are needed.

4. A case study

A case study is illustrated by comparing the performance of two real hydrofracturing fluids [**?**], HPG (Hydroxypropylguar) and VES (viscoelastic surfactant) in a realistic setting. The rheological parameters according with the Ellis model are reported for both fluids in Table **??**, together with realistic geometric and mechanical parameters within plausible ranges deduced from the literature, see the earlier discussion in Section **??**. It is seen that HPG is relatively close to Newtonian in behaviour, while VES is extremely shear-thinning, with an equivalent rheological index n less than 0.1 when expressed according to the power-law model.

Figure **??** shows the relaxation of the fracture aperture for the two fluids: the aperture for the HPG is only initially slightly larger than for the VES, but then closes more rapidly, reaching one tenth of the initial value at a time around 500 hours. The closure is much more gradual for the VES, requiring about a year to reach the same stage. The difference between corresponding pressure profiles, illustrated in Figure **??**, shows a decidedly sharper pressure decrease for HPG than for VES in the initial stage.

Figure **??** shows the time to recover the volume stored in the fracture for the two fluids. Following the same trend manifested for the evolution of

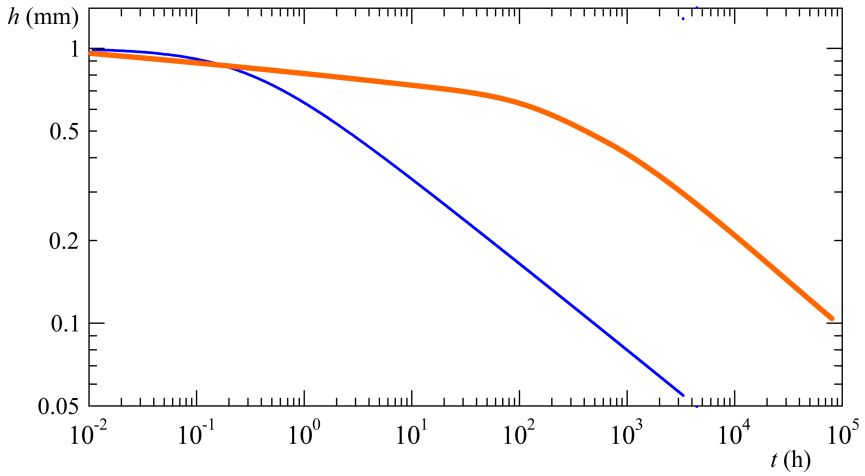

Figure 12: Time variation of the fracture aperture h for the HPG (thin line) and VES (thick line) fluids.

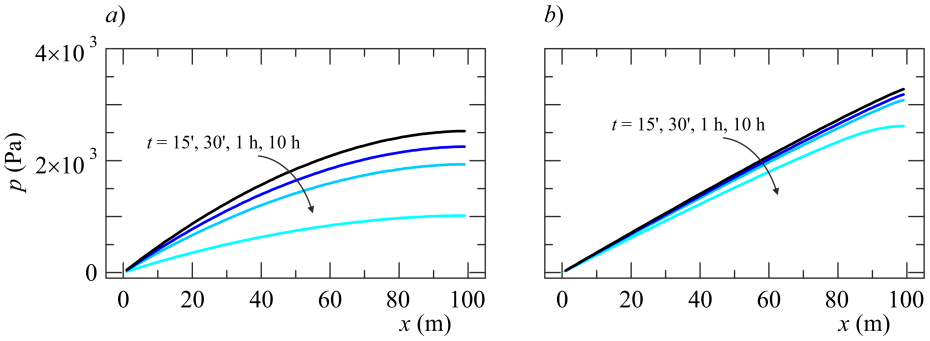

Figure 13: Pressure distribution at different time a) for HPG fluid, and b) for VES.

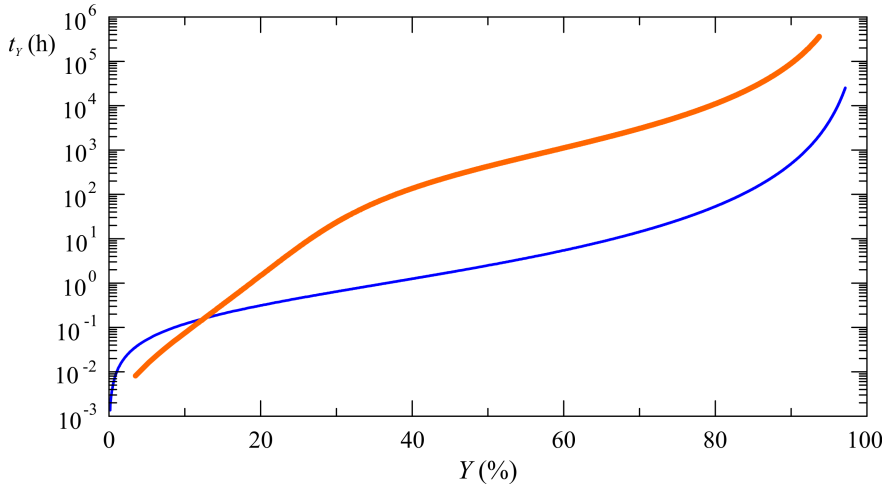

Figure 14: Time to recover the fracture volume $Y\%$ for the HPG (thin line) and VES (thick line) fluids.

fracture opening, VES demonstrates a higher drainage capacity than HPG in the very early phase, for $Y < 15\%$; subsequently it is much less efficient, and requires an extra time at least three orders of magnitude larger to drain the same percentage of fluid than HPG. Overall the large difference in rheology, mainly encapsulated in the α value, translates into corresponding wide differences in terms of aperture, pressure, and drainage time. This is so because the value of the dimensionless group N is very low for VES, thus allowing the fluid to manifest its essentially power-law nature. We tried a number of other combinations of parameters and found that for very shear thinning fluids like VES the results are very sensitive to relatively small changes in parameters: slightly increasing the modulus of elasticity E to $3 \cdot 10^{10}$ and increasing the spacing to 20 m, leaving the other parameters in Table **??** unchanged, leads to $N(HPG) = 0.659$ and $N(VES) = 2.360$. While the change in the N value associated to HPG is modest (6.6%) and implies the system behaviour is essentially unchanged with respecto to the reference case, the increase in N for the VES is dramatic (2260%) and entails a fluid behaviour closer to Newtonian despite the exceedingly high value of α. Upon plotting the aperture variation over time for this case (not shown) the two fluids exhibit a similar behaviour, with only modest differences (less than 10%) in the fracture aperture at early times and an almost identical behaviour later on. The pressure profiles do not show any significant differences.

5. Conclusions

A conceptual model for backflow of non-Newtonian fluid from a closing rock fracture was presented in this paper. Under the assumption of Ellis rheology and elastic, but non-deformable wall, the problem in plane geometry is tractable in semi-analytical form to yield the time-variable fracture aperture $h(t)$, pressure field $p(x,t)$ and discharge rate $q(t)$, as well as the drainage time t_Y for a specified recovery rate Y, outlet pressure p_e and overload f_0.

Our results lead to the following specific conclusions:

- The Ellis model adopted herein to describe shear-thinning rheology couples Newtonian and power-law behaviour. When an Ellis fluid backflows from a relaxating fracture the interplay between the two natures is modulated by a dimensionless group N encapsulating the main problem parameters. N can be expressed in terms of i) the indicial exponent α of the Ellis rheology, ii) the parameter λ governing the wall relaxation process, iii) the ratio between the characteristic shear stress of the Ellis fluid τ_0 and the rock modulus of elasticity E, iv) two geometric ratios, the fracture initial aspect ratio h_0/L and dimensionless spacing l/L. An alternative format of N is a modified ratio between the Cauchy number and the product of Reynolds and Ellis numbers.

- The factors N and α mostly influence the early and intermediate time evolution of the system: when $N < 1$ the power-law behaviour prevails; for $N = 1$ the pure Newtonian case is recovered ($\alpha = 1$ entails $N = 1$), while for $N \gg 1$ the behaviour is mixed.

- For late-time the system behaviour tends to Newtonian, is independent of N and is governed by the wall relaxation parameter λ: aperture and discharge scale asymptotically with time as $t^{-1/(\lambda+2)}$ and $t^{-1/(\lambda+3)}$ for $p_e - f_0 = 0$; else, the aperture tends asymptotically to a constant value proportional to $(p_e - f_0)^{1/\lambda}$.

- Very shear-thinning fluids (larger α) and reactive walls (larger λ) are associated with a more gradual closure of the aperture.

- The residual pressure within the fracture increases with smaller N values and with a softening wall ($\lambda < 1$); when the fluid is close to Newtonian the effect of a λ variation is almost irrelevant.

- The dimensionless drainage time T_Y attains the largest values for large α and low N, the lowest values for small α and large N, the two combinations farthest and closest to Newtonian behaviour. A non-linear reaction of the walls result in a faster/slower recovery for $\lambda < 1$ (softening) and $\lambda > 1$ (stiffening). For recovery values close to 100%, T_Y is very sensitive to variations of model parameters.

- Results are discussed in dimensional form for a case study to reinforce the notion that dimensionless results need to be compared with caution as scales include fluid rheological parameters. Realistic geometric and mechanical parameters are adopted for a system of equally spaced fractures, and results are compared for two fluids, HPG and VES, normally used in fracking technology. The time evolution of the aperture and the dependence of the drainage time upon the recovery ratio are similar at early times, then differ by orders of magnitude at intermediate and late times.

The developments presented, together with earlier results [**?** **?**], provide an overview of the backflow phenomenon in the two basic geometric configurations for a single fracture, plane and radial, and for three rheological models of increasing complexity: Newtonian, power-law, and Ellis. Further improvements of the model remain open in several directions, e.g.: i) a more complex geometry, considering nonplanar fractures with non-negligible curvature; ii) the combination of non-Newtonian rheology with multiple fracture systems, adopting the asymptotic viewpoint of Dana et al. [**?**]; iii) the incorporation of particle transport to simulate the settling of solid proppant.

Acknowledgments

This work was supported in part by Università di Bologna Almaidea 2017 Linea Senior grant awarded to Vittorio Di Federico. The authors have no conflicts of interest to declare. There are no data sharing issues since all of the numerical information is provided in the figures produced by solving the equations in the paper.

Appendix A. The Newtonian case ($n = 1$)

For $\alpha = 1$ and $N = 1$ eq. (**??**) reduces to

$$C = 1, \quad D = \frac{\dot{H}}{H^3}, \tag{A.1}$$

and integrating eq. (**??**) using these expressions yields

$$P(X,T) = \frac{\dot{H}}{4H^3}[(X-1)^2 - 1]. \tag{A.2}$$

Substituting in eq. (**??**) and integrating $P(X,T)$ over X gives

$$-\frac{\dot{H}}{3H^3} = H^\lambda - P_e + F_0, \tag{A.3}$$

generalizing eq. (2.14) of Dana et al. [**?**], where $\lambda = 1$ and $F_0 = 0$, to nonlinear wall reaction and non-zero overload. Now define an effective pressure $\tilde{P}_e = P_e - F_0$ at the fracture outflow: this symbol will be used for brevity in the sequel. Consider first the case $\tilde{P}_e = 0$. Integration of eq. (**??**) over time T yields, with the first b.c. in eq. (**??**),

$$H(T) = [1 + 3(2+\lambda)T]^{-\frac{1}{2+\lambda}}, \tag{A.4}$$

that for $\lambda = 1$ gives back eq. (2.15) of [**?**].

Consider now the case $\tilde{P}_e > 0$. Integration with the help of Mathematica and using transformation formulae for the analytic continuation of hypergeometric functions [**?**] yields for generic λ the following implicit equation

$$T = \frac{1}{3(\lambda+2)}\left[\frac{1}{H^{\lambda+2}}{}_2F_1\left(1, \frac{\lambda+2}{\lambda}; \frac{2(\lambda+1)}{\lambda}; \frac{\tilde{P}_e}{H^\lambda}\right) + \right.$$
$$\left. - {}_2F_1\left(1, \frac{\lambda+2}{\lambda}; \frac{2(\lambda+1)}{\lambda}; \tilde{P}_e\right)\right], \tag{A.5}$$

where ${}_2F_1(\alpha, \beta; \gamma; z)$ is the hypergeometric function of parameters α, β, γ, and argument z. Specific results for $\lambda = 1/2$, $\lambda = 1$, $\lambda = 2$, i.e. a sublinear, linear or supralinear wall reaction, can be obtained as

$$T = \frac{1}{18\tilde{P}_e^{\,5}}\left[12\ln\left(\frac{H^{1/2}(1-\tilde{P}_e)}{H - \tilde{P}_e}\right) - \frac{12\tilde{P}_e}{H^{1/2}} - \frac{6\tilde{P}_e^{\,2}}{H} - \frac{4\tilde{P}_e^{\,3}}{H^{3/2}} - \frac{3\tilde{P}_e^{\,4}}{H^2} + \right.$$
$$\left. + 12\tilde{P}_e + 6\tilde{P}_e^{\,2} + 4\tilde{P}_e^{\,3} + 3\tilde{P}_e^{\,4}\right], \tag{A.6}$$

$$T = \frac{1}{6\tilde{P}_e{}^3}\left[2\ln\left(\frac{H(1-\tilde{P}_e)}{H-\tilde{P}_e}\right) - \frac{2\tilde{P}_e}{H} - \frac{\tilde{P}_e{}^2}{H^2} + 2\tilde{P}_e + \tilde{P}_e{}^2\right], \tag{A.7}$$

$$T = \frac{1}{6\tilde{P}_e{}^2}\left[\ln\left(\frac{H^2(1-\tilde{P}_e)}{H^2-\tilde{P}_e}\right) - \frac{\tilde{P}_e}{H^2} + \tilde{P}_e\right], \tag{A.8}$$

either by direct integration of eq. (**??**) or using transformations involving the hypergeometric functions [**?**]. Eq. (**??**) valid for $\lambda = 1$ is identical to Eq. (2.18) of Dana et al. [**?**]. Other results in terms of trascendental and algebraic functions can be obtained for other special values of $\lambda \in \mathbb{N}$ or $1/\lambda \in \mathbb{N}$ but are too cumbersome to report and/or of little technical interest.

Expressions (**??**)-(**??**), when evaluated for for given $\tilde{P}_e$, allow deriving $H(T)$ and the drainage time T_Y needed to drain $Y\%$ of the fracture volume. As the latter quantity is given in dimensionless form by H according to (**??**), to derive T_Y it is sufficient to evaluate (**??**) and its special cases (**??**)-(**??**) for $H = (100 - Y)/100$.

Finally, it is wortwhile to derive the asymptotic behaviour of the general equation (**??**) for the limit case $\lambda \to 0$. According to eq. (**??**), $\lambda = 0$ implies a wall reaction constant over time rather than dependent from the fracture aperture. Integrating (**??**) for $H^\lambda = 1$ gives

$$H = \frac{1}{[1 + 6(1-\tilde{P}_e)T]^{1/2}}, \tag{A.9}$$

a result that can be simplified for large time to $H = 1/[6(1-\tilde{P}_e)T]^{1/2}$ and further for $\tilde{P}_e = 0$ to $H = 1/(6T)^{1/2}$. Equation (**??**) can be also obtained directly from eq. (**??**) for $\lambda \to 0$ on the basis of eq. (9.121.1) in [**?**]. The late-time scaling for a Newtonian fluid and a wall with constant reaction ($\lambda = 0$) is therefore $H \propto T^{-1/2}$, a result coinciding with the scaling $H \propto T^{-1/(2+\lambda)}$ implied by Figure **??** for a Newtonian fluid with $N = 1$, $\alpha = 1$.

Appendix B. The dimensionless group N

The pure number N may be expressed as a function of well-known dimensionless groups in fluid mechanics [see, e.g., **?**]. Multiplying and dividing eq. (**??**) by $\rho\mu_0 h_0 u_0^3$, where u_0 is the reference velocity defined in (**??**), yields

$$N = K\left(\frac{\mathrm{Ca}}{\mathrm{Re}\cdot\mathrm{El}}\right)^{\alpha-1};\quad \mathrm{Ca}=\frac{\rho u_0^2}{E};\quad \mathrm{Re}=\frac{2\rho u_0 h_0}{\mu_0};\quad \mathrm{El}=\frac{\mu_0 u_0}{\tau_0 h_0},\quad \text{(B.1)}$$

$$K = K\left(\alpha,\lambda,l/L,h_0/L\right)=\frac{2+\alpha}{3\alpha}\left[\frac{4\left(\frac{l}{L}\right)^{\lambda}}{\left(\frac{h_0}{L}\right)^{\lambda+1}}\right]^{\alpha-1}\quad \text{(B.2)}$$

where Ca, Re, and El are the Cauchy, Reynolds, and Ellis numbers, and K a geometric factor correcting the ratio $\mathrm{Ca}/(\mathrm{Re}\cdot\mathrm{El})$. In turn, Ca is the ratio between inertial forces and elastic forces transmitted by solid walls, Re is the ratio between inertial and viscous forces, while El is the ratio between the viscous stress associated with the low shear rate Newtonian behaviour and the shear stress τ_0 associated with high shear rate non-Newtonian (power-law) behaviour.

Relaxation-induced flow in a smooth fracture for Ellis rheology

Valentina Ciriello[a], Alessandro Lenci[a], Sandro Longo[b], Vittorio Di Federico[a]

[a] *Dipartimento di Ingegneria Civile, Chimica, Ambientale e dei Materiali (DICAM), Università di Bologna, Bologna (Italy)*
[b] *Dipartimento di Ingegneria e Architettura (DIA), Università di Parma, Parma, Italy*

Abstract

Hydraulic fracturing is a process aimed at improving the productivity of oil, gas or geothermal reservoirs. During hydrofracturing, backflow follows injection and represents the second phase of the process, when part of the fracturing fluid returns from fractures to well, and from well to surface. A conceptual model is presented to grasp the essential features of the phenomenon, conceiving the draining subsurface domain as a planar and rigid fracture. Backflow against an outlet pressure in the injection well is induced by the relaxation of the fracture wall, exerting a force on the fluid proportional to h^λ, with h the time-variable aperture and λ a non-negative exponent; an overload on the fracture may contribute to slowing or accelerating the closure process. The fluid rheology is described by the three-parameter Ellis constitutive equation, well representing the shear-thinning rheology typical of hydrofracturing fluids and coupling Newtonian and power-law behaviour. The interplay between these tendencies is modulated by a dimensionless number N encapsulating most problem parameters; the range of variation of N is discussed and found to vary around unity. The time-variable aperture and discharge rate, the space-time variable pressure field, and the time to drain a specified fraction of the fracture volume are derived as functions of geometry (length and initial aperture), wall elastic parameters, fluid properties, outlet pressure p_e and overload f_0. The late-time behaviour of the system is practically independent from rheology as the Newtonian nature of the fluid prevails at low shear stress. In particular, aperture and discharge scale asymptotically with time as $t^{-1/(\lambda+2)}$ and $t^{-1/(\lambda+3)}$ for $p_e - f_0 = 0$; else, the aperture tends to a constant, residual value proportional to $(p_e - f_0)^\lambda$. A case study with equally spaced fractures adopting realistic geometric, me-

chanical and rheological parameters is examined: two fluids normally used in fracking technology show completely different behaviours, with backflow dynamics and drainage times initially not dissimilar, later varying by orders of magnitude.

Key words:
Hydraulic fracturing, Non-Newtonian, Ellis rheology, elastic wall, backflow

---

1. Introduction

Hydraulic fracturing is a process aimed at improving the productivity of oil, gas or geothermal reservoirs. Analysis of the different phases of hydraulic fracturing is of particular modeling and experimental interest [e.g. 1, 2].

An understanding of fractured media flow induced by the relaxation of elastic fracture walls is crucial in modeling fracturing fluid backflow, a complicated phenomenon involving hydrodynamic, mechanical and chemical processes. Backflow is typically the final phase of the hydraulic fracturing process: in the first one, fracturing fluid is injected at high pressure in a rock mass, forming new fractures and enlarging existing ones; in the second phase, proppant is introduced in the subsurface environment to prop fractures open; then when the injection ceases, the pressure drops, existing and new fractures tend to close, and a portion of the injected fracturing fluid, often mixed with proppant [3], flows back towards the injection well and interact with the relaxing walls of the fractures. As the retention of fracturing fluid in the fracture network impairs the fracture conductivity reducing the wellbore productivity [4], and favours migration in the subsurface environment along different pathways [5], it is of utmost interest to optimize the amount of fluid recovered, irrespective of the reservoir product, be it oil [6], gas [7] or heat [8].

The scientific literature offers two main approaches to modeling backflow: (i) detailed numerical simulations involving single fractures [9], fracture networks [10] or dual or triple porosity models [11], or (ii) conceptual models capturing the main features of the interaction between fracture flow and wall relaxation [12], including the effects of branching networks described at different degrees of complexity [13, 14]. A recent addition to the modeling effort is the influence of fluid rheology, following the notion that the backflow fluid is non-Newtonian in the widest sense [15], as not only the relationship between shear stress and shear rate is nonlinear, but also exhibits normal

stress and temperature dependency, as well as viscoelasticity, thixotropy, and nonzero yield stress [16]. At the same time, non-Newtonian fluids allow achieving several engineering objectives, such as (i) minimize the pressure-drop in the entire process; (ii) carry suspended proppant; (iii) minimize the leak-off within the formation; (iv) adapt their characteristics to different environments in terms of temperature and chemical composition; and (v) flow back easily towards the wellbore. Given their versatility and economic value, these fluids are typically treated for reuse once recovered, removing contaminants they may have transported to the surface [17]. The recovery ratios of backflow fluid vary between 2% and 48% according to Ipatova and Chuprakov [18], with considerable economic value.

Modeling non Newtonian backflow is in its early stage, in variance with the injection and fracture formation stage, for which several conceptualizations and models are available: see Detournay [19] for a review and the recent work by Wrobel [20] comparing different rheological models for fracturing fluids. To the best of our knowledge, only Chiapponi et al. [21] considered non-Newtonian fluids in the context of backflow modeling: these authors examined flow of a power-law fluid towards a wellbore in a single fracture of annular geometry, supporting their theoretical findings with laboratory experiments. The present paper develops the analysis of non-Newtonian backflow for a smooth fracture, common in field applications [22], and adds realism by employing a three-parameter Ellis model, that well represents the rheology of hydrofracturing [23] and drilling fluids [24]. The Ellis model tends to Newtonian for low shear rates, to power-law for high shear rates and allows avoiding the unphysical effect of infinite apparent viscosity at zero shear rate that is typical of the power-law model [25]. We note in passing that our results are of a general nature for Newtonian pressurized flow in ducts of variable width and may be of interest for, and be applied also to, deformable microfluidic [26] and biological [27] systems.

The plan of the paper is as follows. Section 2 formulates the problem of relaxation-induced backflow of an Ellis fluid in a fracture with nonlinear wall reaction and subject to overload. Numerical results obtained are presented and discussed in Section 3 as a function of dimensionless groups characterizing the system: the indicial exponent α quantifying the degree of shear-thinning behaviour of the Ellis fluid, the non-negative exponent λ modulating the fracture wall reaction, and a further group N encapsulating most problem parameters. Section 4 illustrates an hypothetical case study adopting realistic geometric and mechanical parameters and two real hy-

drofracturing fluids decribed by the Ellis model. Section 5 reports the main conclusions and perspectives for future work. In Appendix A the special case of a Newtonian fluid is examined, obtaining results that generalize those of Dana et al. [13] to a nonlinear wall reaction, while Appendix B presents an alternative expression for the dimensionless number N, shown to be a combination of well-known dimensionless groups in fluid mechanics.

2. Material and methods

2.1. Problem statement

A rock fracture produced by hydrofracturing, though of irregular geometry, is often conceptualized for modeling purposes as a 3-D space of length L, width W, and aperture h between two parallel walls [28]; the Cartesian coordinate system x, y, z is illustrated in Figure 1 and the fracture is subject to a pressure gradient $\nabla p' \equiv (\partial p'/\partial x, 0, 0)$ in the x direction. In horizontal fractures, the additional gravity-induced pressure gradient is perpendicular the flow plane and has no effect on the flow field. If the (x, y) plane is not horizontal, the z direction perpendicular to the walls is not vertical and gravity effects can be included in a reduced pressure term p, thus leading to a mathematical treatment with no gravity term to consider. For instance, for the Figure 3 below representing multiple vertical fractures backflowing to an horizontal well, the reduced pressure p is equal to $p = p' + \rho g y$.

The walls are taken to be rigid, so that the aperture $h(t)$ is solely a function of time, and the deformation is concentrated for mathematical convenience in the upper wall, that behaves as a nonlinear elastic foundation exerting a reaction on the fluid. At $t = 0$ the relaxation of the wall induces a backflow in the negative x direction, and the fracture begins to drain subject to a constant outlet pressure p_e at $x = 0$ and to a no-flow boundary condition at the upstream end $x = L$. Three further hypotheses are adopted: i) the flow is quasi-steady, allowing to neglect the time derivative of the velocity in the momentum equation; ii) the fracture aspect ratio is small, $h_0/L \ll 1$, warranting the lubrication approximation, and iii) the flow is essentially one-dimensional along x, $L \gg W$. The latter conceptualization is usually adopted in hydrogeology also when the two dimensions are comparable, as it is often the case for rock fractures [11].

The flowback fluid is taken to be incompressible of density ρ, non-Newtonian shear-thinning [15] and described by the Ellis three-parameter model [29]. Under the above assumptions, the fluid undergoes simple shear flow in the

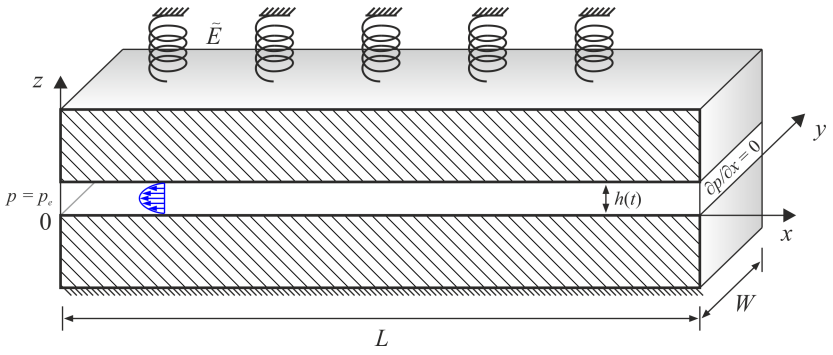

Figure 1: Layout of a plane fracture of variable uniform aperture $h(t)$.

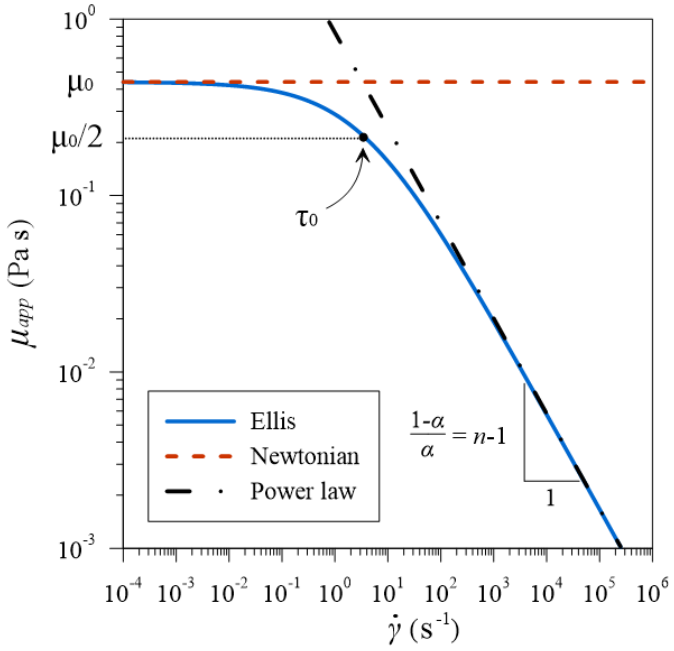

Figure 2: Apparent viscosity for three rheological models: Ellis (blue solid line) of parameters μ_0, τ_0, α; Newtonian (red dashed line) of viscosity μ_0; power-law (black dot-dashed line) of consistency index m and rheological index n. The comparison with the latter is drawn assuming: $\alpha = 1/n$ and $\tau_0 = (m/\mu_0^n)^{n/(1-n)}$.

x direction, and the Ellis rheology is described by the following relationship between shear stress τ_{zx} (hereinafter τ) and shear rate $\dot{\gamma}_{zx}$ (hereinafter simply $\dot{\gamma}$)

$$\tau = \frac{\mu_0}{1 + (\tau/\tau_0)^{\alpha-1}}\dot{\gamma}; \quad \dot{\gamma} = \frac{\partial u}{\partial z}, \tag{1}$$

where u is the velocity in the x direction. The rheological law (1) features a viscosity parameter μ_0, a constant τ_0 defined as the shear stress corresponding to apparent viscosity $\mu_0/2$, and an indicial parameter α, typically larger than one as the fluid is shear-thinning. For $\alpha = 1$, a pseudo-Newtonian behaviour with dynamic viscosity $\mu_0/2$ is recovered, see Figure 2 showing the apparent viscosity $\mu_{app} = \tau/\dot{\gamma}$ for the Ellis model compared to Newtonian and power-law models. Newtonian behaviour in the form of a plateau for low shear rates is also observed for $\gamma \to 0$. For high shear rates the behaviour is power-law, and its two parameters can be determined from the Ellis model parameters, see Appendix A in Balhoff and Thompson [28]; in particular, the rheological index is $n = 1/\alpha$ [30]. Note that when curve fitting is performed on real data, n and $1/\alpha$ may significantly differ [23], as two different models are fitted to the same data set. It is also seen that the Ellis model allows avoiding the unphysical effect of infinite apparent viscosity at zero shear rate that is typical of power-law fluids [25]. In the following, we will consider $\alpha > 1$, dealing with the case $\alpha = 1$ in the Appendix, and the parameters μ_0 and τ_0 to be finite and positive. Couette-Poiseuille slit flow of an Ellis fluid under a constant pressure gradient was studied extensively by Steller [31], listing all combinations of parameters leading to Newtonian or pseudo-Newtonian behaviour. In particular, the negative velocity $u(z)$ under a positive reduced pressure gradient $\partial p/\partial$ in the x direction is

$$\begin{aligned} u(z,t) = -\frac{1}{8\mu_0}\left[h^2 - (2z-h)^2\right]\frac{\partial p}{\partial x} + \\ - \frac{1}{(\alpha+1)2^{\alpha+1}\mu_0\tau_0^{\alpha-1}}\left[h^{\alpha+1} - |2z-h|^{\alpha+1}\right]\frac{\partial p}{\partial x}\left|\frac{\partial p}{\partial x}\right|^{\alpha-1}. \end{aligned} \tag{2}$$

The corresponding average velocity $\overline{u}$ and flow per unit width q_x in the x direction are

$$\overline{u} = -\frac{h^2}{12\mu_0}\frac{\partial p}{\partial x} - \frac{h^{\alpha+1}}{2^{\alpha+1}(\alpha+2)\mu_0\tau_0^{\alpha-1}}\frac{\partial p}{\partial x}\left|\frac{\partial p}{\partial x}\right|^{\alpha-1}; q_x = \overline{u}h. \tag{3}$$

For the Newtonian case ($\alpha = 1$) the latter equation reduces to the classical "cubic law" [32] written for a fluid with viscosity $\mu_0/2$. The continuity equation reads [13]

$$\frac{\mathrm{d}h}{\mathrm{d}t} + h(t)\frac{\partial \overline{u}}{\partial x} = 0, \tag{4}$$

and substituting eq. (3) in eq. (4) gives

$$\frac{\mathrm{d}h}{\mathrm{d}t} = \frac{h^3}{12\mu_0}\frac{\partial^2 p}{\partial x^2} + \frac{\alpha h^{\alpha+2}}{2^{\alpha+1}(\alpha+2)\mu_0\tau_0^{\alpha-1}}\left|\frac{\partial p}{\partial x}\right|^{\alpha-1}\frac{\partial^2 p}{\partial x^2}. \tag{5}$$

The problem formulation is completed by the force balance, expressed per unit width of fracture, among the fluid pressure and the elastic reaction of the upper wall, taken to be proportional to aperture h; an overload at the upper wall f_0 (a force per unit width) is included in the balance for generality [21]; the overload represents an additional force exerted by the walls and usually opposing the fracture opening due, e.g., to a residual stress state generated by the load history of the rocks. It is assumed constant and independent from the fracture aperture. The balance reads

$$\int_0^L p(x,t)\,\mathrm{d}x = \tilde{E}Lh(t) + f_0, \tag{6}$$

where the constant of proportionality $\tilde{E}$ has dimensions $[ML^{-2}T^{-2}]$; for a linear elastic foundation, called a Winkler soil in geotechnical applications, $\tilde{E}$ is equal, for a thin elastic layer of thickness l, to the ratio between the Young modulus of the layer's material E $[ML^{-1}T^{-2}]$ and l, $\tilde{E} = E/l$. In the context of hydraulic fracturing, l may be identified with the fracture spacing [13, 21], a design parameter that depends, among others, on the type of rock; in hydraulically fractured shales, values of l/L equal to 0.057, 0.28, and 0.029 are reported, respectively, by Ghanbari and Dehghanpour [7], Wang et al. [11], and Wang et al. [33]. In the case of vertical/sub-vertical fractures perpendicular to a horizontal/sub-horizontal well or borehole, the geometry of the idealized system is described by Figure 3, showing the two wings of equally spaced planar fractures of half-length L, width W, aperture h and spacing l. Albeit the flow very close to the well is radial, the influence of the boundary condition at the well decreases rapidly with distance, and flow in most of the fracture half-length L is uniform, consistently with the assumption $L \gg W$. Hence, as an approximation the boundary condition of assigned pressure p_e at the well is extended to a segment of height W. In the

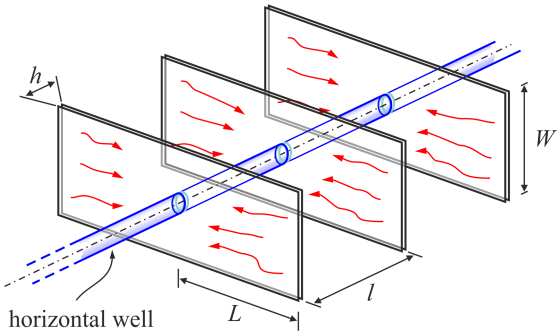

Figure 3: Typical scheme for bi-wing planar fractures around a horizontal borehole; L, W and h are the fracture length, width and aperture, l is the fracture spacing.

case of planar vertical fractures parallel to, and propagating from, a vertical well, the geometry of the flow is plane without using this approximation.

A further issue deserving investigation is the linearity of the relationship between the wall reaction and the fracture aperture. In fact, a nonlinear elastic behaviour can be the result of the pervasive damage of rocks by micro-cracks and voids, which determines nonlinearity even for infinitesimal strain, also with an incremental jump in the elastic modulus from tension to compression [34, 35]. In this case the Young modulus of the material is a function of the strain rate, $E = E_0(h/l)$, and assuming that the latter dependence is expressed with a power-law function one has

$$E = E_0 \left(\frac{h}{l}\right)^{\lambda-1}, \tag{7}$$

where λ is a non-negative exponent modulating the nature of the reaction: for $\lambda = 1$ a constant Young modulus is recovered, while $0 < \lambda < 1$ is associated to a softening behaviour, and $\lambda > 1$ to a stiffening one. The assumption results in

$$\tilde{E} = \frac{E_0}{l}\left(\frac{h}{l}\right)^{\lambda-1} \equiv \hat{E}h^{\lambda-1}, \tag{8}$$

and eq. (6) is modified as

$$\int_0^L p(x,t)\,\mathrm{d}x = \hat{E}Lh^{\lambda}(t) + f_0, \tag{9}$$

with $\hat{E} = E_0 l^{-\lambda}$ of dimensions $[ML^{-1-\lambda}T^{-2}]$.

Equations (5) and (9) are subject to the following initial and boundary conditions

$$h(0) = h_0, \quad \frac{\partial p(x,t)}{\partial x}(L,t) = 0, \quad p(0,t) = p_e, \tag{10}$$

h_0 being the initial fracture aperture, and p_e the exit pressure at the well.

The solution to the above problem yields two relevant quantities expressed per unit width, the flowrate exiting the fracture at the well, $q(t)$, and the residual volume of the fracture at a given time, $v(t)$; these are easily derivable as

$$q(t) = L\frac{\mathrm{d}h(t)}{\mathrm{d}t}, \quad v(t) = Lh(t). \tag{11}$$

2.2. Dimensionless form

Dimensionless quantities are defined as

$$\begin{aligned} X = x/L,\, H = h/h_0, T = t/t_c,\, P = (p-p_e)/p_c,\, P_e = p_e/p_c, \\ Q = qt_c/(h_0 L) = q/(u_0 h_0),\, V = v/(h_0 L), \end{aligned} \tag{12}$$

where the scales for pressure and time are

$$p_c = \hat{E}h_0^{\lambda}, \quad t_c = \frac{(2+\alpha)}{\alpha}\left(\frac{2L}{h_0}\right)^{1+\alpha}\frac{1}{h_0^{\alpha\lambda}}\frac{\mu_0\tau_0^{\alpha-1}}{\hat{E}^{\alpha}}, \tag{13}$$

and $u_0 = L/t_c$ is a velocity scale. This leads to the dimensionless counterpart of eq. (5)

$$\frac{\mathrm{d}H}{\mathrm{d}T} = NH^3\frac{\partial^2 P}{\partial X^2} + H^{\alpha+2}\left(\frac{\partial P}{\partial X}\right)^{\alpha-1}\frac{\partial^2 P}{\partial X^2}, \tag{14}$$

where the pure number

$$N = \frac{2+\alpha}{3\alpha}\left(\frac{2\tau_0 L}{\hat{E}{h_0}^{\lambda+1}}\right)^{\alpha-1} = \frac{2+\alpha}{3\alpha}\left[\frac{2\tau_0}{p_c(h_0/L)}\right]^{\alpha-1} \tag{15}$$

modulates the relative importance of the Newtonian behaviour of the Ellis fluid at low shear rate, expressed by the first term on the r.h.s. of eq. (14), with respect to the second term, the power-law behaviour at high shear rate. For a Newtonian fluid ($\alpha = 1$) N reduces to unity; for a shear-thinning fluid ($\alpha > 1$), N is zero for $\tau_0 = 0$ and/or a rigid wall ($\hat{E} = E_0/l^{\lambda} \to \infty$), but the latter case renders the scales (13) meaningless. In eq. (15) defining N, the quantity within brackets represents the ratio between the characteristic

shear stress τ_0 of the Ellis fluid and the pressure scale $p_c = \hat{E}{h_0}^{\lambda}$ associated with the elastic reaction of the fracture wall; the ratio is in turn corrected by the initial aspect ratio of the fracture h_0/L. This formulation of N includes only parameters defined at the single fracture scale. Note that if the scheme of multiple fractures with spacing l depicted in Figure 3 is considered, eq. (15) may be rewritten as

$$N = \frac{2+\alpha}{3\alpha}\left[\frac{2\left(\frac{\tau_0}{E_0}\right)\left(\frac{l}{L}\right)}{\left(\frac{h_0}{L}\right)^2}\frac{\left(\frac{l}{L}\right)^{\lambda-1}}{\left(\frac{h_0}{L}\right)^{\lambda-1}}\right]^{\alpha-1}, \tag{16}$$

where τ_0/E_0 is the ratio between the representative shear stress of the fluid and the Young modulus of the host rock, and l/L is the dimensionless fracture spacing. The terms to the power $(\lambda-1)$ represent the contribution due to non-linear elastic behaviour of the walls, and disappear for $\lambda = 1$. An alternative formulation of N as a function of Cauchy, Reynolds, and Ellis dimensionless groups is reported in Appendix B. To grasp the order of magnitude of N, we recall that l/L may be taken to vary between 0.03 and 0.3 (with $l/L \approx 0.1$ being appropriate for an order of magnitude analysis), while the initial fracture aspect ratio h_0/L, a number much smaller than 1, may be considered of order $10^{-3}-10^{-5}$ [7, 11, 33]. The latter reference also reports $E_0 = 2.5\cdot10^{10}$ Pa for the rock elastic modulus in fractured shales; quite close values, $E_0 = 3\cdot10^{10}$ Pa and $E_0 = 2.76\cdot10^{10}$ Pa are reported in [19] and [36], hence reference values $E_0 = 2.5 - 3.0 \cdot 10^{10}$ Pa are considered.

Actual values of rheological parameters for Ellis fluids are quite scarce in the literature. A reference specific to fracking is [23], where the Ellis parameters are reported for two fracturing fluids, HPG (Hydroxypropylguar) and VES (viscoelastic surfactant). For the first, $\mu_0 = 0.44$ Pa $\cdot$ s, $\tau_0 = 2.01$ Pa, and $\alpha = 1.22$; for the second, $\mu_0 = 49$ Pa $\cdot$ s, $\tau_0 = 8.836$ Pa, and $\alpha = 12$. Adopting as reference geometrical parameters $l/L = 0.1$ and $h_0/L = 10^{-4}$, and a young modulus of $E_0 = 2.75 \cdot 10^{10}$ Pa for the host rock, one obtains $N = 0.209$ for HPG and $N \simeq 0$ for VES, indicating that for the latter fluid the Newtonian component of rheological behaviour is negligible. A further consideration is that VES is very strongly shear-thinning ($\alpha \gg 1$), therefore the value of N is extremely sensitive to variations in parameters: adopting for example $l/L = 0.125$, $h_0/L = 10^{-5}$, and $E_0 = 2.5\cdot10^{10}$ Pa, again realistic values, one obtains $N = 0.100$ for VES and $N = 0.618$ for HPG. This second

set of parameters is adopted for later reference in Section 4 describing a case study and is shown there in dimensional form (see Table 1). Trying further combinations of realistic values for fluid and rock properties, it is seen that N may take values smaller or larger than unity, the former case being more frequent. This indicates a certain prevalence of the power-law component of rheology over the Newtonian one, although the asymptotic system behaviour is dominated by the latter, as will be shown in the next section. We bear in mind that a large variety of combinations is possible for the two parameters N and α depending on geometry and properties of fluid and rock, but with the constraint from the definition (15) that for $\alpha = 1$ it must be $N = 1$.

The dynamic boundary condition (9) and the boundary conditions (10) transform as

$$\int_0^1 P(X,T)\,\mathrm{d}X = H^\lambda - P_e + F_0, \tag{17}$$

$$H(0) = 1, \quad \frac{\partial P}{\partial X}(1,T) = 0, \quad P(0,T) = 0. \tag{18}$$

2.3. Solution

A solution to eq. (14) is sought by integrating in two steps the pressure of the fluid and the fracture aperture. Posing

$$U(X,T) = \frac{\partial P}{\partial X}, \quad \dot{H} = \frac{\mathrm{d}H}{\mathrm{d}T}, \tag{19}$$

eq. (14) can be written as

$$B\left(1 + AU^{\alpha-1}\right)\frac{\partial U}{\partial X} = \dot{H} \tag{20}$$

where

$$A = A(T) = \frac{(H)^{\alpha-1}}{N}, \quad B = B(T) = NH^3, \tag{21}$$

while the second boundary condition in eq. (18) becomes

$$U(1,T) = 0. \tag{22}$$

Separating variables in eq. (20), and integrating with the boundary condition (22) leads to

$$\frac{BU\left(AU^{\alpha-1} + \alpha\right)}{\alpha} = -\dot{H}(1 - X). \tag{23}$$

Eq. (23) can be rewritten as

$$U^\alpha + CU + D(1 - X) = 0 \tag{24}$$

where

$$C = C(T) = \frac{\alpha N}{H^{\alpha-1}}, \quad D = D(T) = \frac{\alpha \dot{H}}{H^{2+\alpha}}. \tag{25}$$

Eq. (25) is algebraic in U and admits an analytical solution for $\alpha = 1, 2, 3$ and for $\alpha = 1/2, 1/3$ in the form of a combination of functions of H and $\dot{H}$. This solution can be integrated once in space, with the boundary condition $P(0, T) = 0$, obtaining the pressure field. The pressure field is finally integrated in $X \in [0, 1]$ and the integral in eq. (17) is computed as a function of H and $\dot{H}$. Then eq. (17) is transformed in a nonlinear ODE which is numerically integrated with the initial condition $H(0) = 1$.

These solutions are analytical in the x coordinate and numerical in the time domain and seem quite cumbersome, while their accuracy is comparable to that of a fully numerical solution in space and time; the latter also has the advantage of a free selection of the indicial parameter α. Among the many possible numerical schemes, we adopt a finite difference in time and an implicit resolver in space, with a step size reduction to track solution accurately.

The code is written in Mathematica, introducing a parametric solver for the function $U(X, T)$ as a function of $N, \alpha, H_{i+1}, H_i, \Delta t$, where H_{i+1} and H_i are the values at time $(i + 1)\Delta t$ and $i\Delta t$, respectively; the only free parameter is H_{i+1}, all the other parameters are given.

Each time iteration includes the following steps:

- The function $U(X)_{i+1}$ is estimated by solving eq. (20) in parametric form, with $\dot{H} \approx (H_{i+1} - H_i)/\Delta t$, with the term H taken to be the average between H_{i+1} and H_i and with the b.c. $U(1)_{i+1} = 0$, where H_{i+1} is the free parameter; $H_0 = 1$ is assumed at the first step.

- The space values of U, known in parametric form, are used to solve the differential problem $\partial P(X)_{i+1}/\partial X = U(X)_{i+1}$, with $P(0)_{i+1} = 0$, obtaining the pressure $P(X)_{i+1}$.

- The pressure field is numerically integrated (in parametric form) in the domain $[0, 1]$.

- The parametric integral is inserted in eq. (17), and the equality is forced with a Newton method for finding the value of the parameter H_{i+1}.

- The procedure is repeated for the next time step, shifting the values H_{i+1}.

Once the pressure $P(X,T)$ and aperture $H(T)$ fields are known, the dimensionless flowrate and fracture volume are given by

$$Q(T) = \frac{\mathrm{d}H(T)}{\mathrm{d}T} = \dot{H}, \quad V(T) = H(T). \tag{26}$$

Hence at late-time the fracture volume and flowrate behave like the aperture and its time derivative, respectively; for zero borehole pressure and overload the corresponding time scalings are $T^{-1/(\lambda+2)}$ and $T^{-1/(\lambda+3)}$.

3. Results and discussion

Figure 4 shows the results of the numerical computation for the fracture aperture and different α values, with the analytical solution $H = (1+9T)^{-1/3}$ valid for the Newtonian case and a linearly elastic fracture [13], corresponding to $\alpha = 1$, $N = 1$, and $\lambda = 1$. Note that the values $\alpha = 1$, $N = 1$ imply Newtonian behaviour but with a viscosity equal to $\mu_0/2$, thus halving the time scale t_c in eq. (13); this requires doubling the dimensionless time T in eq. (12) to compare results of equations having a different time scale. The time integration was performed with a time step $\Delta t = 0.01$. Since the results of the numerical integration using this fully explicit scheme fit exceedingly well the analytical solution, it was not necessary to adopt higher order schemes, even considering that the solution has no singularity and behaves rather smoothly.

The asymptotic behaviour of the solution $H(T)$ is dictated by the interplay between the two terms on the r.h.s. of eq. (14): the second term scales with the gradient pressure (decaying in time) and with a power of H always larger than 3, since $\alpha > 1$, whereas the first term scales with the third power of H and has N as a coefficient. Since $H \leq 1$ and the gradient pressure quickly decays to values less than unity, the dominant term is the first one, which entails the asymptotic behaviour $H \sim T^{-1/(2+\lambda)}$, see Figure 5 where different values of α, for $N = 1$ and $P_e = 0$, produce almost parallel curves for large T. Figure 5 also shows how variations in λ significantly affect the

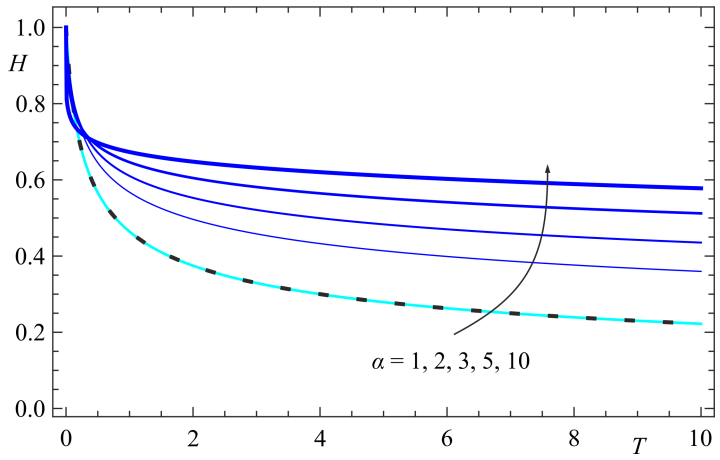

Figure 4: Time variation of the fracture aperture H for $N = 0$, $\lambda = 1$, $P_e - F_0 = 0$ and different α values. The black dotted curve refers to the analytical solution for a Newtonian fluid, $H = (1+9T)^{-1/3}$. Due to the different time scales adopted for a Newtonian fluid and for the present model, comparison is feasible if the dimensionless time T in the solution for the Newtonian fluid is doubled.

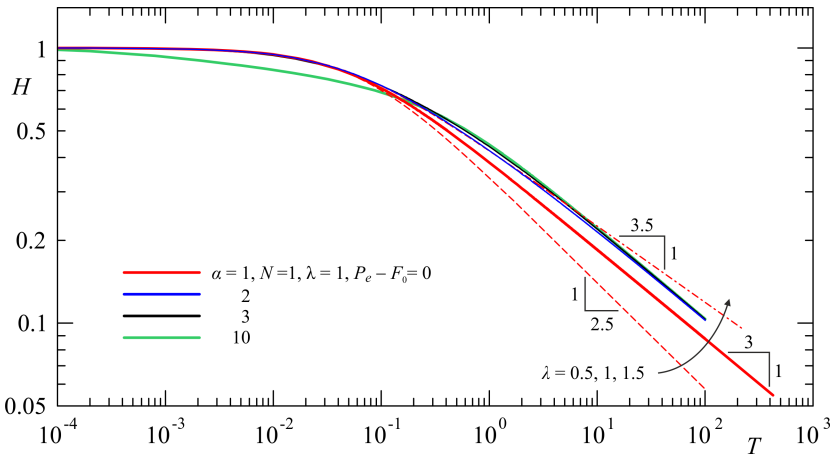

Figure 5: Time variation of the fracture aperture H for $N = 1$, $\lambda = 1$ and different α values. For one case ($\alpha = 1$) the effects of a softening/stiffening wall is explored, see the dashed and dash-dotted thin curves for $\lambda = 0.5 - 1.5$, respectively. The asymptotic behaviour is $H \sim T^{-1/(2+\lambda)}$, independent on α.

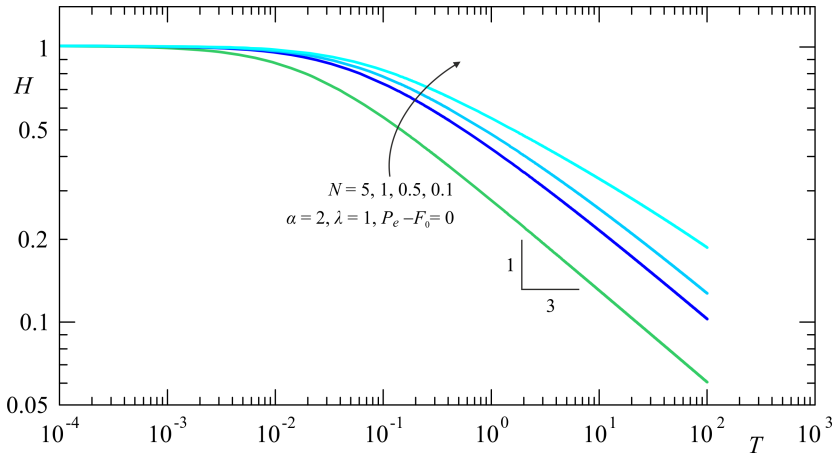

Figure 6: Time variation of the fracture aperture H for $\alpha = 2$, $\lambda = 1$ and different N.

late-time behaviour for fixed α: a stiffening ($\lambda > 1$)/softening ($\lambda < 1$) elastic reaction of the walls delays/facilitates the drainage. It is also seen that the parameter α mainly controls the early stage, the parameter λ the late stage of the backflow process. Figure 6 shows results for a fixed $\alpha = 2$, $\lambda = 1$, and different N values; the asymptote is reached much faster for larger N. In sum, the early time behaviour for zero external pressure at the well is in general dominated by the second term in eq. (14) unless the coefficient $N \gg 1$; in the latter case both terms substantially contribute to the time evolution of H.

In presence of a non-zero external pressure ($P_e > 0$) or a negative overload F_0 (an additional force per unit of wall surface acting in the same direction of the internal pressure), the asymptotic residual aperture is equal to $(P_e - F_0)^{1/\lambda}$, see Figure 7 where both effects are included. The curves coalesce to the asymptote faster for larger N values, implying a dominance of the Newtonian behaviour, while for small N the power-law behaviour prevails and the asymptote is reached for larger dimensionless times. Upon plotting results for $\alpha = 3$ (not shown) the main curves for $\lambda = 1$ and the secondary curves for $\lambda \neq 1$ are very similar to those for $\alpha = 2$.

Figure 8 shows the pressure distribution for two different combinations of the parameters and a shear-thinning fluid with $\alpha = 2$. Results for other combinations are similar (and thus not shown), with a pressure decay in space/time quicker or slower depending on the parameter values; at all times the residual pressure within the fracture increases with smaller N values,

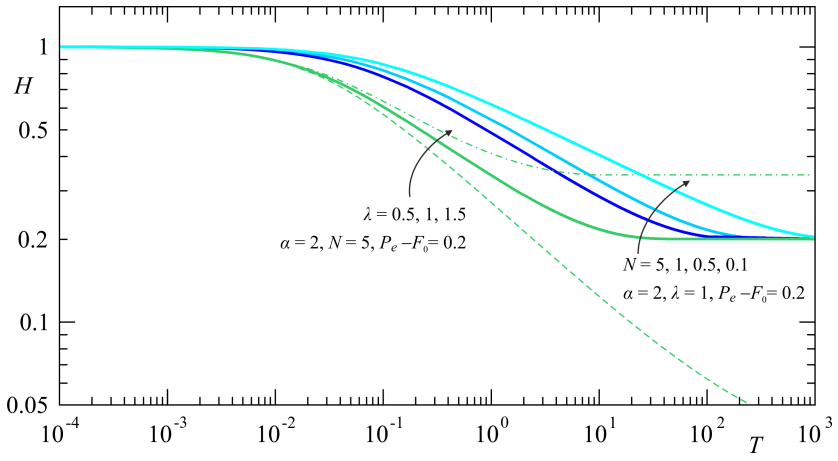

Figure 7: Time variation of the fracture aperture H for $\alpha = 2$ and different N values, with given difference between external pressure and overload $P_e - F_0 = 0.2$. For one case ($N = 5$) the effects of a stiffening/softening elastic reaction of the walls is explored, see the dashed and dash-dotted thin curves for $\lambda = 0.5 - 1.5$, respectively.

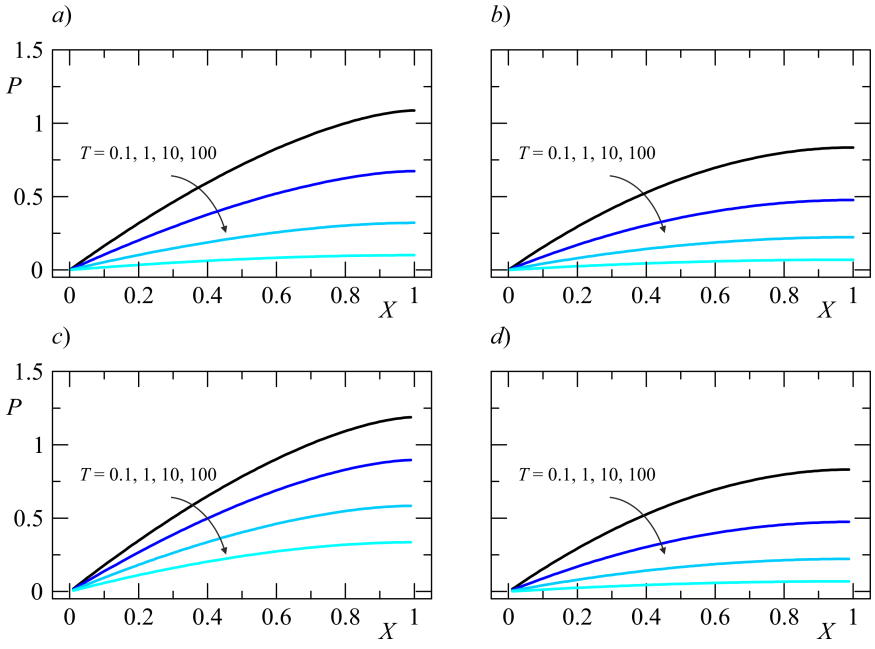

Figure 8: Pressure along the fracture at different times for $P_e - F_0 = 0.2$ and a shear-thinning fluid with $\alpha = 2$. Results for *a*) $N = 0.1$ and $\lambda = 1$; *b*) $N = 5$ and $\lambda = 1$; *c*) $N = 0.1$ and $\lambda = 0.5$; *d*) $N = 5$, $\lambda = 0.5$.

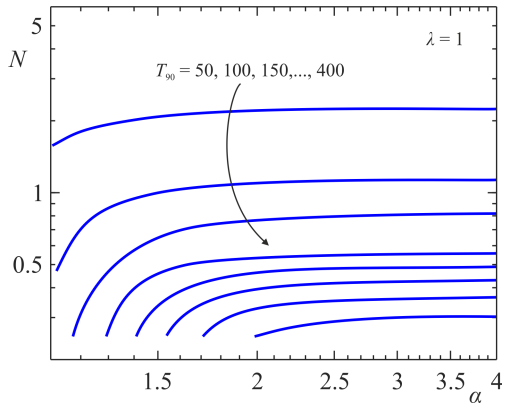

Figure 9: Time to recover 90% of the fluid as a function of α and N, with $\lambda = 1$ and $P_e - F_0 = 0$.

implying a behaviour closer to Newtonian, and with smaller λ values, i.e. a softening wall; however when the fluid is closer to Newtonian the effect of a λ variation is irrelevant.

An important quantity characterizing the performance of the backflow process is the time required to recover the fluid injected in the fracture network and not lost in the form of leakoff. Here the network is conceptualized as a single fracture and fluid losses are not explicitly represented (they are assumed to take place in the upstream network), however the time T_Y needed to recover $Y\%$ of the fracture volume provides an indication of how rapid the recovery is. Contour maps in the (α, N) space of the dimensionless time T_{90} needed to recover 90% of the fluid are depicted in Figure 9 for a linear wall reaction ($\lambda = 1$). As the degree of shear-thinning behaviour rises with α for constant N, there is a sharp increase in dimensionless T_Y for $N < 0.5$, while T_Y is almost independent on α for $N > 2$. Conversely, T_Y for costant α decreases with larger N values, i.e. as the fluid behaviour is closer to Newtonian; this effect is more evident for larger α. Highest values of T_Y are attained for large α and low N, lowest values for small α and large N, the two combinations farthest and closest to Newtonian behaviour. The effect of a sublinear wall reaction ($\lambda = 0.5$) is depicted in Figure 10, that of a supralinear wall reaction in Figure 11. The dimensionless time to recover the bulk of the stored fluid is decidedly faster or slower with a softening or stiffening wall, demonstrating once again the decisive influence of the parameter λ modulating the wall reaction at late time.

A word of caution is needed when drawing comparisons between non-

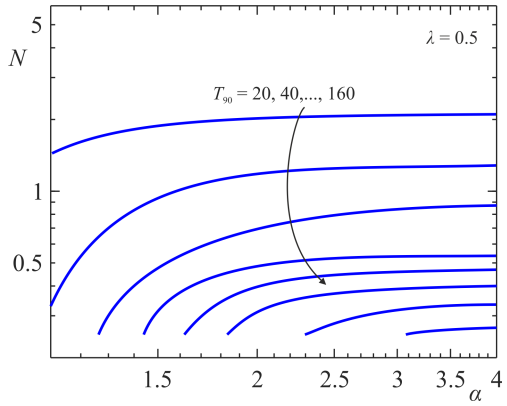

Figure 10: Time to recover 90% of the fluid as a function of α and N, with $\lambda = 0.5$ and $P_e - F_0 = 0$.

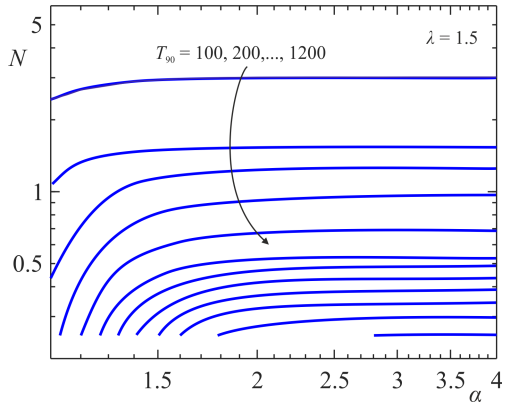

Figure 11: Time to recover 90% of the fluid as a function of α and N, with $\lambda = 1.5$ and $P_e - F_0 = 0$.

Fluid	μ_0 (Pa s)	τ_0 (Pa)	α	L (m)	l (m)	h_0 (mm)	E (Pa)	λ	N
HPG	0.44	2.01	1.22	100	12.5	1.00	$2.5 \cdot 10^{10}$	1.00	0.618
VES	49.00	8.836	12.00	100	12.5	1.00	$2.5 \cdot 10^{10}$	1.00	0.100

Table 1: Reference parameters for case study: μ_0, τ_0 and α are the reference viscosity, shear stress and indicial exponent of the Ellis fluid, L is the fracture length, l is the fracture spacing, h_0 is the fracture initial height, E is the rock modulus of elasticity, λ is the exponent of the rock wall reaction, N is the dimensionless number governing the interplay between Newtonian and power-law behaviour in an Ellis fluid.

Newtonian fluids with different rheology as the models are semi-empirical and the time scale used for the dimensionless formulation depends upon the rheological parameters of the Ellis model and is particularly sensitive to the value of the indicial exponent α. Hence model outputs are best compared in dimensional coordinates when quantitative results are needed.

4. A case study

A case study is illustrated by comparing the performance of two real hydrofracturing fluids [23], HPG (Hydroxypropylguar) and VES (viscoelastic surfactant) in a realistic setting. The rheological parameters according with the Ellis model are reported for both fluids in Table 1, together with realistic geometric and mechanical parameters within plausible ranges deduced from the literature, see the earlier discussion in Section 2.2. It is seen that HPG is relatively close to Newtonian in behaviour, while VES is extremely shear-thinning, with an equivalent rheological index n less than 0.1 when expressed according to the power-law model.

Figure 12 shows the relaxation of the fracture aperture for the two fluids: the aperture for the HPG is only initially slightly larger than for the VES, but then closes more rapidly, reaching one tenth of the initial value at a time around 500 hours. The closure is much more gradual for the VES, requiring about a year to reach the same stage. The difference between corresponding pressure profiles, illustrated in Figure 13, shows a decidedly sharper pressure decrease for HPG than for VES in the initial stage.

Figure 14 shows the time to recover the volume stored in the fracture for the two fluids. Following the same trend manifested for the evolution of

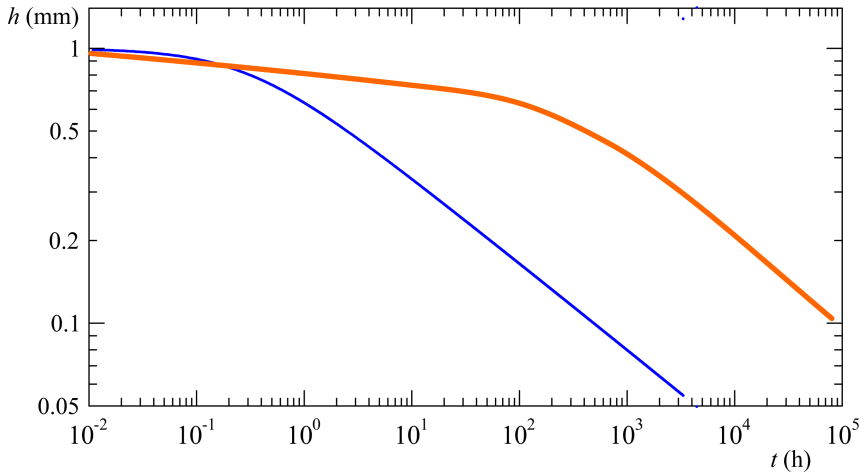

Figure 12: Time variation of the fracture aperture h for the HPG (thin line) and VES (thick line) fluids.

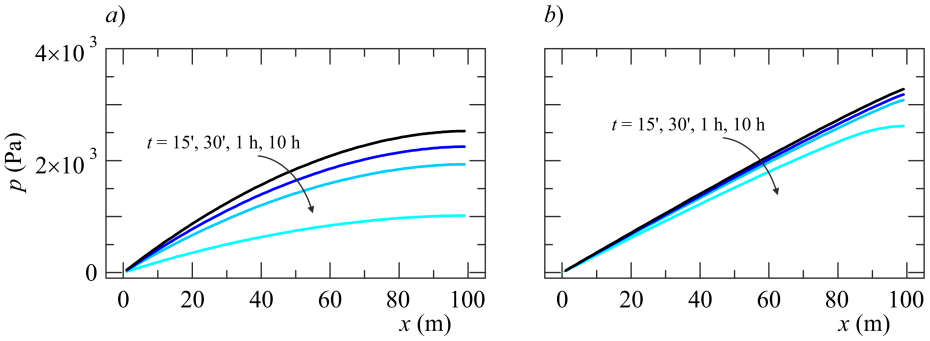

Figure 13: Pressure distribution at different time a) for HPG fluid, and b) for VES.

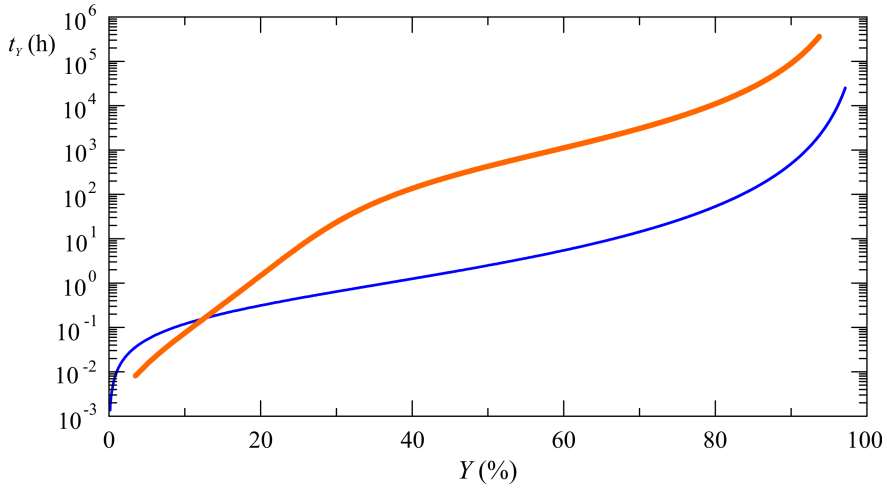

Figure 14: Time to recover the fracture volume $Y\%$ for the HPG (thin line) and VES (thick line) fluids.

fracture opening, VES demonstrates a higher drainage capacity than HPG in the very early phase, for $Y < 15\%$; subsequently it is much less efficient, and requires an extra time at least three orders of magnitude larger to drain the same percentage of fluid than HPG. Overall the large difference in rheology, mainly encapsulated in the α value, translates into corresponding wide differences in terms of aperture, pressure, and drainage time. This is so because the value of the dimensionless group N is very low for VES, thus allowing the fluid to manifest its essentially power-law nature. We tried a number of other combinations of parameters and found that for very shear thinning fluids like VES the results are very sensitive to relatively small changes in parameters: slightly increasing the modulus of elasticity E to $3 \cdot 10^{10}$ and increasing the spacing to 20 m, leaving the other parameters in Table 1 unchanged, leads to $N(HPG) = 0.659$ and $N(VES) = 2.360$. While the change in the N value associated to HPG is modest (6.6%) and implies the system behaviour is essentially unchanged with respecto to the reference case, the increase in N for the VES is dramatic (2260%) and entails a fluid behaviour closer to Newtonian despite the exceedingly high value of α. Upon plotting the aperture variation over time for this case (not shown) the two fluids exhibit a similar behaviour, with only modest differences (less than 10%) in the fracture aperture at early times and an almost identical behaviour later on. The pressure profiles do not show any significant differences.

5. Conclusions

A conceptual model for backflow of non-Newtonian fluid from a closing rock fracture was presented in this paper. Under the assumption of Ellis rheology and elastic, but non-deformable wall, the problem in plane geometry is tractable in semi-analytical form to yield the time-variable fracture aperture $h(t)$, pressure field $p(x,t)$ and discharge rate $q(t)$, as well as the drainage time t_Y for a specified recovery rate Y, outlet pressure p_e and overload f_0.

Our results lead to the following specific conclusions:

- The Ellis model adopted herein to describe shear-thinning rheology couples Newtonian and power-law behaviour. When an Ellis fluid backflows from a relaxating fracture the interplay between the two natures is modulated by a dimensionless group N encapsulating the main problem parameters. N can be expressed in terms of i) the indicial exponent α of the Ellis rheology, ii) the parameter λ governing the wall relaxation process, iii) the ratio between the characteristic shear stress of the Ellis fluid τ_0 and the rock modulus of elasticity E, iv) two geometric ratios, the fracture initial aspect ratio h_0/L and dimensionless spacing l/L. An alternative format of N is a modified ratio between the Cauchy number and the product of Reynolds and Ellis numbers.

- The factors N and α mostly influence the early and intermediate time evolution of the system: when $N < 1$ the power-law behaviour prevails; for $N = 1$ the pure Newtonian case is recovered ($\alpha = 1$ entails $N = 1$), while for $N \gg 1$ the behaviour is mixed.

- For late-time the system behaviour tends to Newtonian, is independent of N and is governed by the wall relaxation parameter λ: aperture and discharge scale asymptotically with time as $t^{-1/(\lambda+2)}$ and $t^{-1/(\lambda+3)}$ for $p_e - f_0 = 0$; else, the aperture tends asymptotically to a constant value proportional to $(p_e - f_0)^{1/\lambda}$.

- Very shear-thinning fluids (larger α) and reactive walls (larger λ) are associated with a more gradual closure of the aperture.

- The residual pressure within the fracture increases with smaller N values and with a softening wall ($\lambda < 1$); when the fluid is close to Newtonian the effect of a λ variation is almost irrelevant.

- The dimensionless drainage time T_Y attains the largest values for large α and low N, the lowest values for small α and large N, the two combinations farthest and closest to Newtonian behaviour. A non-linear reaction of the walls result in a faster/slower recovery for $\lambda < 1$ (softening) and $\lambda > 1$ (stiffening). For recovery values close to 100%, T_Y is very sensitive to variations of model parameters.

- Results are discussed in dimensional form for a case study to reinforce the notion that dimensionless results need to be compared with caution as scales include fluid rheological parameters. Realistic geometric and mechanical parameters are adopted for a system of equally spaced fractures, and results are compared for two fluids, HPG and VES, normally used in fracking technology. The time evolution of the aperture and the dependence of the drainage time upon the recovery ratio are similar at early times, then differ by orders of magnitude at intermediate and late times.

The developments presented, together with earlier results [13, 21], provide an overview of the backflow phenomenon in the two basic geometric configurations for a single fracture, plane and radial, and for three rheological models of increasing complexity: Newtonian, power-law, and Ellis. Further improvements of the model remain open in several directions, e.g.: i) a more complex geometry, considering nonplanar fractures with non-negligible curvature; ii) the combination of non-Newtonian rheology with multiple fracture systems, adopting the asymptotic viewpoint of Dana et al. [14]; iii) the incorporation of particle transport to simulate the settling of solid proppant.

Acknowledgments

This work was supported in part by Università di Bologna Almaidea 2017 Linea Senior grant awarded to Vittorio Di Federico. The authors have no conflicts of interest to declare. There are no data sharing issues since all of the numerical information is provided in the figures produced by solving the equations in the paper.

Appendix A. The Newtonian case ($n = 1$)

For $\alpha = 1$ and $N = 1$ eq. (25) reduces to

$$C = 1, \quad D = \frac{\dot{H}}{H^3}, \tag{A.1}$$

and integrating eq. (24) using these expressions yields

$$P(X,T) = \frac{\dot{H}}{4H^3}[(X-1)^2 - 1]. \tag{A.2}$$

Substituting in eq. (17) and integrating $P(X,T)$ over X gives

$$-\frac{\dot{H}}{3H^3} = H^\lambda - P_e + F_0, \tag{A.3}$$

generalizing eq. (2.14) of Dana et al. [13], where $\lambda = 1$ and $F_0 = 0$, to non-linear wall reaction and non-zero overload. Now define an effective pressure $\tilde{P}_e = P_e - F_0$ at the fracture outflow: this symbol will be used for brevity in the sequel. Consider first the case $\tilde{P}_e = 0$. Integration of eq. (A.3) over time T yields, with the first b.c. in eq. (18),

$$H(T) = [1 + 3(2+\lambda)T]^{-\frac{1}{2+\lambda}}, \tag{A.4}$$

that for $\lambda = 1$ gives back eq. (2.15) of [13].

Consider now the case $\tilde{P}_e > 0$. Integration with the help of Mathematica and using transformation formulae for the analytic continuation of hypergeometric functions [37] yields for generic λ the following implicit equation

$$T = \frac{1}{3(\lambda+2)}\left[\frac{1}{H^{\lambda+2}}\,{}_2F_1\left(1, \frac{\lambda+2}{\lambda}; \frac{2(\lambda+1)}{\lambda}; \frac{\tilde{P}_e}{H^\lambda}\right) + \right.$$
$$\left. - {}_2F_1\left(1, \frac{\lambda+2}{\lambda}; \frac{2(\lambda+1)}{\lambda}; \tilde{P}_e\right)\right], \tag{A.5}$$

where ${}_2F_1(\alpha, \beta; \gamma; z)$ is the hypergeometric function of parameters α, β, γ, and argument z. Specific results for $\lambda = 1/2$, $\lambda = 1$, $\lambda = 2$, i.e. a sublinear, linear or supralinear wall reaction, can be obtained as

$$T = \frac{1}{18\tilde{P}_e^{\,5}}\left[12\ln\left(\frac{H^{1/2}(1-\tilde{P}_e)}{H-\tilde{P}_e}\right) - \frac{12\tilde{P}_e}{H^{1/2}} - \frac{6\tilde{P}_e^{\,2}}{H} - \frac{4\tilde{P}_e^{\,3}}{H^{3/2}} - \frac{3\tilde{P}_e^{\,4}}{H^2} + \right.$$
$$\left. + 12\tilde{P}_e + 6\tilde{P}_e^{\,2} + 4\tilde{P}_e^{\,3} + 3\tilde{P}_e^{\,4}\right], \tag{A.6}$$

$$T = \frac{1}{6\tilde{P}_e^{\,3}}\left[2\ln\left(\frac{H(1-\tilde{P}_e)}{H-\tilde{P}_e}\right) - \frac{2\tilde{P}_e}{H} - \frac{\tilde{P}_e^{\,2}}{H^2} + 2\tilde{P}_e + \tilde{P}_e^{\,2}\right], \tag{A.7}$$

$$T = \frac{1}{6\tilde{P}_e^{\,2}}\left[\ln\left(\frac{H^2(1-\tilde{P}_e)}{H^2-\tilde{P}_e}\right) - \frac{\tilde{P}_e}{H^2} + \tilde{P}_e\right], \tag{A.8}$$

either by direct integration of eq. (A.5) or using transformations involving the hypergeometric functions [37]. Eq. (A.7) valid for $\lambda = 1$ is identical to Eq. (2.18) of Dana et al. [13]. Other results in terms of trascendental and algebraic functions can be obtained for other special values of $\lambda \in \mathbb{N}$ or $1/\lambda \in \mathbb{N}$ but are too cumbersome to report and/or of little technical interest.

Expressions (A.5)-(A.8), when evaluated for for given $\tilde{P}_e$, allow deriving $H(T)$ and the drainage time T_Y needed to drain $Y\%$ of the fracture volume. As the latter quantity is given in dimensionless form by H according to (26), to derive T_Y it is sufficient to evaluate (A.5) and its special cases (15)-(A.8) for $H = (100 - Y)/100$.

Finally, it is wortwhile to derive the asymptotic behaviour of the general equation (A.5) for the limit case $\lambda \to 0$. According to eq. (9), $\lambda = 0$ implies a wall reaction constant over time rather than dependent from the fracture aperture. Integrating (A.3) for $H^\lambda = 1$ gives

$$H = \frac{1}{[1 + 6(1-\tilde{P}_e)T]^{1/2}}, \tag{A.9}$$

a result that can be simplified for large time to $H = 1/[6(1-\tilde{P}_e)T]^{1/2}$ and further for $\tilde{P}_e = 0$ to $H = 1/(6T)^{1/2}$. Equation (A.9) can be also obtained directly from eq. (A.5) for $\lambda \to 0$ on the basis of eq. (9.121.1) in [37]. The late-time scaling for a Newtonian fluid and a wall with constant reaction ($\lambda = 0$) is therefore $H \propto T^{-1/2}$, a result coinciding with the scaling $H \propto T^{-1/(2+\lambda)}$ implied by Figure 5 for a Newtonian fluid with $N = 1$, $\alpha = 1$.

Appendix B. The dimensionless group N

The pure number N may be expressed as a function of well-known dimensionless groups in fluid mechanics [see, e.g., 38]. Multiplying and dividing eq. (16) by $\rho\mu_0 h_0 u_0^3$, where u_0 is the reference velocity defined in (12), yields

$$N = K\left(\frac{\mathrm{Ca}}{\mathrm{Re}\cdot\mathrm{El}}\right)^{\alpha-1};\quad \mathrm{Ca}=\frac{\rho u_0^2}{E};\quad \mathrm{Re}=\frac{2\rho u_0 h_0}{\mu_0};\quad \mathrm{El}=\frac{\mu_0 u_0}{\tau_0 h_0}, \tag{B.1}$$

$$K = K\left(\alpha,\lambda,l/L,h_0/L\right)=\frac{2+\alpha}{3\alpha}\left[\frac{4\left(\frac{l}{L}\right)^{\lambda}}{\left(\frac{h_0}{L}\right)^{\lambda+1}}\right]^{\alpha-1} \tag{B.2}$$

where Ca, Re, and El are the Cauchy, Reynolds, and Ellis numbers, and K a geometric factor correcting the ratio $\mathrm{Ca}/(\mathrm{Re}\cdot\mathrm{El})$. In turn, Ca is the ratio between inertial forces and elastic forces transmitted by solid walls, Re is the ratio between inertial and viscous forces, while El is the ratio between the viscous stress associated with the low shear rate Newtonian behaviour and the shear stress τ_0 associated with high shear rate non-Newtonian (power-law) behaviour.

References

[1] N. Dutler, B. Valley, V. Gischig, M. Jalali, B. Brixel, H. Krietsch, C. Roques, F. Amann, Hydromechanical insight of fracture opening and closure during in-situ hydraulic fracturing in crystalline rock, International Journal of Rock Mechanics and Mining Sciences 135 (2020) 104450.

[2] Y. Wu, L. Cheng, S. Fang, S. Huang, P. Jia, A green element method-based discrete fracture model for simulation of the transient flow in heterogeneous fractured porous media, Advances in Water Resources 136 (2020) 103489.

[3] O. Ezulike, H. Dehghanpour, C. Virues, R. V. Hawkes, J. Jones, R. Steven, Flowback fracture closure: A key factor for estimating effective pore volume, SPE Reservoir Evaluation & Engineering 19 (04) (2016) 567–582. doi:10.2118/175143-PA.

[4] M. T. Balhoff, M. J. Miller, An analytical model for cleanup of yield-stress fluids in hydraulic fractures, SPE Journal 10 (01) (2005) 5–12. doi:10.2118/77596-PA.

[5] D. Birdsell, H. Rajaram, D. D. H. Viswanathan, Hydraulic fracturing fluid migration in the subsurface: a review and expanded modeling results, Water Resources Research 37 (2015) 1–30. doi:10.1002/2015WR017810.

[6] B. Zanganeh, M. Ahmadi, C. Hanks, O. Awoleke, The role of hydraulic fracture geometry and conductivity profile, unpropped zone conductivity and fracturing fluid flowback on production performance of shale oil wells, Journal of Unconventional Oil and Gas Resources 9 (2015) 103–113. doi:10.1016/J.JUOGR.2014.11.006.

[7] E. Ghanbari, H. Dehghanpour, The fate of fracturing water: A field and simulation study, Fuel 163 (2016) 282–294. doi:10.1016/j.fuel.2015.09.040.

[8] J. McLennan, I. Walton, J. Moore, D. Brinton, J. Lund, Proppant backflow: Mechanical and flow considerations, Geothermics 57 (2015) 224 – 237. doi:10.1016/j.geothermics.2015.06.006.

[9] J. Zeng, H. Li, D. Zhang, Numerical simulation of proppant transport in hydraulic fracture with the upscaling cfd-dem method, Journal of Natural Gas Science and Engineering 33 (2016) 264 – 277. doi:10.1016/j.jngse.2016.05.030.

[10] J. Hyman, J. Jiménez-Martínez, H. Viswanathan, J. Carey, M. Porter, E. Rougier, S. Karra, Q. Kang, L. Frash, L. Chen, Z. Lei, D. O'Malley, N. Makedonska, Understanding hydraulic fracturing: a multi-scale problem, Philosophical Transactions of the Royal Society A: Mathematical, Physical and Engineering Sciences 374 (2016) 20150426. doi:doi:10.1098/rsta.2015.0426.

[11] F. Wang, Z. Pan, Y. Zhang, S. Zhang, Simulation of coupled hydro-mechanical-chemical phenomena in hydraulically fractured gas shale during fracturing-fluid flowback, Journal of Petroleum Science and Engineering 163 (2018) 16 – 26. doi:10.1016/j.petrol.2017.12.029.

[12] J. Huang, J. Hu, W. Zeng, Y. Zhang, Investigation of a critical choke during hydraulic-fracture flowback for a tight sandstone gas reservoir, Journal of Geophysics and Engineering 16 (6) (2019) 1178–1190. doi:10.1093/jge/gxz088.

[13] A. Dana, Z. Zheng, G. G. Peng, H. A. Stone, H. E. Huppert, G. Z. Ramon, Dynamics of viscous backflow from a model fracture network, Journal of Fluid Mechanics 836 (2018) 828–849. doi:10.1017/jfm.2017.778.

[14] A. Dana, G. G. Peng, H. A. Stone, H. E. Huppert, G. Z. Ramon, Backflow from a model fracture network: an asymptotic investigation, Journal of Fluid Mechanics 864 (2019) 899–924. doi:10.1017/jfm.2019.39.

[15] A. Barbati, J. Desroches, A. Robisson, G. McKinley, Complex Fluids and Hydraulic Fracturing, Annu. Rev. Chem. Biomol. Eng. 7 (2016) 415–453. doi:10.1146/annurev-chembioeng-080615-033630.

[16] S. Hormozi, I. A. Frigaard, Dispersion of solids in fracturing flows of yield stress fluids, Journal of Fluid Mechanics 830 (2017) 93–137. doi:10.1017/jfm.2017.465.

[17] Y. Lester, T. Yacob, I. Morrissey, K. G. Linden, Can we treat hydraulic fracturing flowback with a conventional biological process? the case of guar gum, Environ. Sci. Technol. Lett. 1 (1) (2014) 133–136. doi:10.1021/ez4000115.

[18] A. Ipatova, D. Chuprakov, Role of preexisting rock discontinuities in fracturing fluid leakoff and flowback, Transport in Porous Media 135 (1) (2020) 137–180. doi:10.1007/s11242-020-01472-3.

[19] E. Detournay, Mechanics of hydraulic fractures, Annu. Rev. Fluid Mech. 48 (2016) 311–339. doi:10.1146/annurev-fluid-010814-014736.

[20] M. Wrobel, On the application of simplified rheological models of fluid in the hydraulic fracture problems, International Journal of Engineering Science 150 (2020) 103275. doi:10.1016/j.ijengsci.2020.103275.

[21] L. Chiapponi, V. Ciriello, S. Longo, V. Di Federico, Non-newtonian backflow in an elastic fracture, Water Resources Research 55 (12) (2019) 10144–10158. doi:10.1029/2019WR026071.

[22] A. Osiptov, Fluid mechanics of hydraulic fracturing: a review, Journal of Petroleum Science and Engineering 156 (2017) 513–535. doi:10.1016/j.petrol.2017.05.019.

[23] F.-E. Moukhtari, B. Lecampion, A semi-infinite hydraulic fracture driven by a shear-thinning fluid, Journal of Fluid Mechanics 838 (2018) 573–605. doi:10.1017/jfm.2017.900.

[24] S. Shah, N. H. Shanker, C. C. Ogugbue, Future challenges of drilling fluids and their rheological measurements, in: 2010 AADE Fluids Conference and Exhibition, Vol. AADE-10-DF-HO-41, Houston, Texas, 2010.

[25] T. G. Myers, Application of non-newtonian models to thin film flow, PRE 72 (6) (2005) 066302. doi:10.1103/PhysRevE.72.066302.

[26] V. Anand, J. David, I. C. Christov, Non-newtonian fluid-structure interactions: Static response of a microchannel due to internal flow of a power-law fluid, Journal of Non-Newtonian Fluid Mechanics 264 (2019) 62–72. doi:10.1016/j.jnnfm.2018.12.008.

[27] N. Ali, S. Hussain, K. Ullah, O. Anwar Beg, Mathematical modeling of two-fluid electro-osmotic peristaltic pumping of an ellis fluid in an axisymmetric tube, The European Physical Journal Plus 134 (4) (2019) 141. doi:10.1140/epjp/i2019-12488-2.

[28] M. Balhoff, K. Thompson, A macroscopic model for shear-thinning flow in packed beds based on network modeling, Chemical Engineering Science 61 (2) (2006) 698–719. doi:10.1016/j.ces.2005.04.030.

[29] A. Skelland, Non-Newtonian Flow and Heat Transfer, Wiley, 1967.

[30] A. Al-Behadili, M. Sellier, J. N. Hewett, R. I. Nokes, M. Moyers-Gonzalez, Identification of ellis rheological law from free surface velocity, Journal of Non-Newtonian Fluid Mechanics 263 (2019) 15 – 23. doi:10.1016/j.jnnfm.2018.10.010.

[31] R. T. Steller, Generalized slit flow of an ellis fluid, Polym Eng Sci 41 (11) (2001) 1859–1870. doi:10.1002/pen.10883.

[32] R. W. Zimmerman, G. S. Bodvarsson, Hydraulic conductivity of rock fractures, Transport in Porous Media 23 (1996) 1–30. doi:10.1007/BF00145263.

[33] J. Wang, D. Elsworth, M. K. Denison, Hydraulic fracturing with leakoff in a pressure-sensitive dual porosity medium, International

Journal of Rock Mechanics and Mining Sciences 107 (2018) 55–68. doi:10.1016/j.ijrmms.2018.04.042.

[34] B. Budiansky, R. J. O'Connell, Elastic moduli of a cracked solid, International Journal of Solids and Structures 12 (2) (1976) 81–97.

[35] V. Lyakhovsky, Z. Reches, R. Weinberger, T. E. Scott, Non-linear elastic behaviour of damaged rocks, Geophysical Journal International 130 (1) (1997) 157–166. doi:10.1111/j.1365-246X.1997.tb00995.x.

[36] M. K. Fisher, N. R. Warpinski, Hydraulic-fracture-height growth: Real data, SPE Production & Operations 27 (01) (2012) 8–19. doi:10.2118/145949-PA.

[37] I. S. Gradshteyn, I. M. Ryzhik, Table of integrals, series, and products, Academic Press, 2014.

[38] B. S. Massey, Units, dimensional analysis and physical similarity, Van Nostrand Reinhold, 1971.

Declaration of interests

☒ The authors declare that they have no known competing financial interests or personal relationships that could have appeared to influence the work reported in this paper.

☐The authors declare the following financial interests/personal relationships which may be considered as potential competing interests:

Author statement

Valentina Ciriello: Methodology, Writing - Original Draft. **Alessandro Lenci**: Methodology, Visualization. **Sandro Longo**: Methodology, Software, Writing - Review & Editing, Visualization. **Vittorio Di Federico**: Conceptualization, Writing - Review & Editing, Project administration, Funding acquisition.